SOME PROPERTIES OF MAGNETOSPHERIC ELECTRONS OBSERVED WEST OF SANAE

BY

JAMES G. GREENER

A thesis submitted in fulfillment of the requirements
for the degree of Master of Science
of Rhodes University.

DECEMBER, 1972.

ACKNOWLEDGEMENTS

Help in the research for and preparation of a thesis is forthcoming in many ways. My sincere thanks goes to all my friends who helped in person and to people and institutions who helped in kind.

To my supervisor, Professor J.A. Gledhill, who always found time between conferences to sort out my problems and listen enthusiastically to my ideas, I extend my thanks and appreciation. To Dr. Chris Goertz who stepped in as an equally enthusiastic supervisor in 'Prof's' absence, thank you as well.

I would also like to single out for thanks Mike Lawrie and Howard Williams for their help in the computations and the physics. For the provision of the Alouette I data, I would like to thank Dr. I.B. McDiarmid of the Canadian Research Council.

I wish to record my appreciation of the role played by the Department of Transport in financing the Antarctic Research Group of which I was a member during part of the time spent on this thesis.

Finally to a few close friends and my parents - thank you very much for encouragement and support.

--- 0 ---

CONTENTS

--- 0 ---

--- 0 ---

INTRODUCTION

The southern hemisphere has always been the neglected twin in the field of geophysical research. The reasons for this are certainly not in the realm of science but in the history of man and his development in the northern half of the globe. Geophysically, however, our southern half provides a wealth of interesting problems and anomalies.

Roederer (1966) explains the use of this word 'anomaly' by showing what some of the oddities of the southern hemisphere are, and by contrasting them with the corresponding regions of the earth across the equator. The principal feature is of course the geomagnetic surface field strength minimum at a point in the South Atlantic ocean very near the coast of Brazil.

Maps of geomagnetic field strength contours for different altitudes (e.g. Roederer et al. (1965)) illustrate how this 'weak spot' is present even at large distances from the earth. Obviously this 'unexpected' minimum has considerable effects on any magnetically influenced geophysical phenomena. The charged particles trapped in the Van Allen radiation belt are one such phenomenon. We shall show, in this thesis, the effects of the anomaly on the fluxes of energetic electrons as they drift eastwards towards this region of low magnetic field strengths.

A good understanding of the distribution of these charged particles in the radiation belt, when they approach the earth's surface is essential to any work concerning their interaction with the upper atmosphere. The effects that the precipitating portion of this distribution have on the different regions of the ionosphere are well recognized (e.g. Gledhill and Torr (1966), Bailey (1968), Tulinov et al. (1969)). A knowledge of the patterns of particle precipitation is therefore of value to the ionospherist.

Data of this nature are generally only obtainable from non earth-based platforms. In the last decade and a half, earth orbiting artificial satellites

2/.....

have proved an essential tool for the collecting of geophysical data. For this dissertation, the data used were obtained by particle detectors on board the Canadian satellite Alouette I.

This thesis contains a detailed analysis of fluxes of electrons with energies greater than 40 keV at a height of one thousand kilometres above the surface of the earth. The survey is restricted to a region over the South Atlantic ocean and South American continent. The variations of these fluxes with geographic longitude, geomagnetic latitude, local time and particle pitch angle are presented and discussed.

--- 0 ---

CHAPTER 1.

DATA ACQUISITION AND INTERPRETATION.

1.1 INTRODUCTION

We have mentioned before that the artificial satellite has become essential to the geoscientist. However, experiments on board such craft generally produce very large quantities of data concerning the phenomena being sampled in real time. These data have to be telemetered back to Earth stations either in real time as well, or else recorded on board for later transmission. Fortunately, electronic data processing has developed alongside of and very much as a result of space research technology.

This chapter will discuss firstly the satellite, its instrumentation and orbital characteristics and finally the format and type of data that was made available from the experiments on board the craft. In addition we shall consider the problem of relating data values on a magnetic tape here on Earth to the actual physical conditions pertaining at the satellite at the time of sampling.

1.2 ALOUETTE I.

Alouette I was launched on 29th September, 1962, and carried four experimental packages into a nearly circular orbit around the Earth. One of these experiments was the energetic particle detector package which provided the data we have analysed. The height of the orbit was nearly constant at 1000 km, apogee and perigee differing by only 35 km. (Data Catalog of Satellite Experiments, 1971).

The satellite was spin stabilised and carried a single fluxgate magnetometer which measured the component ($\bar{B}$mag) of the geomagnetic field ($\bar{B}$) in a plane perpendicular to the spin axis. The spin period was initially 42 seconds, and had a known decay rate (McDiarmid et al. (1963,a)). The attitude of the craft

4/.....

was defined by its pitch angle (α). The diagram illustrates the method of obtaining α through the relation

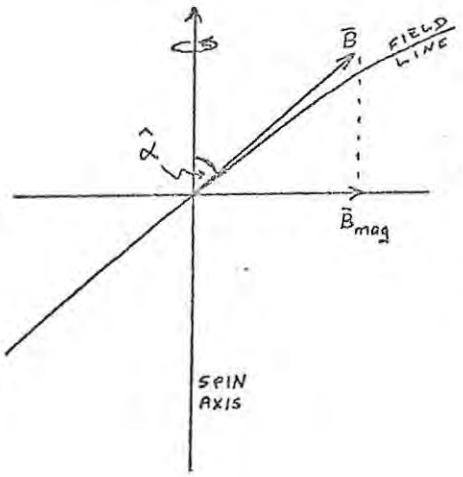

$$\alpha = \sin^{-1} \left(\frac{Bmag}{B} \right)$$

$\bar{B}$, $\bar{B}$mag and the spin axis are co-planar

B is computed from the Jensen & Cain geomagnetic field expression.

Inclination of the orbit was 80.46° and the orbital plane precessed relative to the Sun - Earth line at only 2° per day. As was well illustrated by Thomas and Andrews (1968) this requires three months of continuous data sampling before a full 24 hour local time coverage is obtained. Table 1 shows the periods for which the energetic particle detector data are available for the region in which we are interested. The initial period amply covers the 3 month requirement. Of course, all seasonal variations in the phenomena will be lost if the data is time averaged. All data presented in this thesis have undergone an averaging process, the four periods listed being taken together.

TABLE 1.

INTERVALS DURING WHICH ALOUETTE 1 TRANSMITTED PARTICLE DATA TO SOUTH ATLANTIC STATION

START			FINISH		
Pass No.	Date	Time (U.T.)	Pass No.	Date	Time (U.T.)
0067	2/10/62	04 18 30	1661	29/1/63	10 26 50
2557	2/4/63	14 13 30	2699	13/4/63	01 20 40
3161	16/5/63	21 53 20	3188	18/5/63	21 22 50
4837	16/9/63	16 12 30	4932	23/9/63	15 20 10

Relative to the Earth itself the orbital plane precessed westwards by about 25° between each pass that the satellite made around the globe. Because Alouette I did not have a tape recorder on board, telemetry was in real time and data for any region could only be received when the craft was in sight of a station. The maximum time that any one station could receive the satellite during its pass overhead was about 14 minutes. On relatively few occasions was reception possible on the following pass, although this of course depended on the station latitude. There were 12 stations equipped for reception of the data signals. For our analysis we have used data received at South Atlantic Station in the Falkland Islands.

Latitude	51.7° S	Dip Angle	- 47.0°
Longitude	57.85° W	L Value	1.58

(Data source : Roederer et al. (1965)).

Examination of the data from this station reveals that the extreme geographic ranges for which signals were received from Alouette I were

Longitude	17° West	-	92° West
Latitude	26° South	-	79° South

These extremes, as well as the position of South Atlantic Station, the geomagnetic surface minimum, the South African Antarctic Base (SANAE) and a few other reference points are shown in the map of figure 1.

1.3 THE PARTICLE DETECTORS

Six instruments capable of detecting energetic particles were carried aboard Alouette 1. This experiment (NSSDC 1D 62-049A-02) was called the 'Cosmic Particle Detector' and was initiated by Dr. I.B. McDiarmid of the National Research Council of Canada. Descriptions of these counters and their characteristics have been given by McDiarmid et al. (1963a) and only a summary of the relevant details are given here.

The two counters from which the data discussed in this thesis were obtained were the Anton 302-type geiger counter and the Anton 223-type thin window geiger counter. The 223-type counter was situated at the end of a collimator inclined at 10^{o} to the satellite spin axis and had an angular aperture of 4.5^{o}. The 302-type counter was used only for measurements of omnidirectional flux (Appendix 1). Table 2 adapted from Rose (1966) lists the geometric factors of the counters as well as their responses to the various particles.

TABLE 2.

PROPERTIES OF PARTICLE DETECTORS ABOARD ALOUETTE I.

	ANTON 223-TYPE	ANTON 302-TYPE
DIRECTIONAL		
Geometric factor	5.05×10^{-4} cm^2 sr	-
Particle response	electrons E $>$ 40 keV	-
	protons E $>$500 keV	-
OMNIDIRECTIONAL		
Geometric factor	0.22 cm^2	0.55 cm^2
Particle response	electrons : 2.8 MeV	10% transmission
	3.9 MeV	50% transmission
	protons: $>$ 33 MeV	
Minimum Shielding	$\sim$ 1.4 gm cm^{-2} over 2 sr	$\sim$ 1.4 gm cm^{-2} over 2.4 sr
EFFICIENCY	80% to relativistic electrons	

Although the 223-type counter responded to protons, McDiarmid et al. (1963,b) have shown by using a similar 223-type counter fitted with a magnetic broom, that the response of the 223-type counter was nearly 100% due to electrons and not to protons. We therefore take the counts of the 223-type counter to refer only to electrons of energy greater than 40 keV. Electrons and protons with

7/....

energies greater than 3 MeV and 33 Mev respectively could penetrate the side shielding of the 223-type counter and give rise to background counts. It is possible to correct for these by using the counts from the 302-type counter as suggested by McDiarmid (private communication). Data from each detector consisted of a count rate obtained as an average over 10 seconds. The counting rate in the 223-type counter due to particles which had penetrated the side shielding is given by the rate in the 302-type counter multiplied by the ratio of the omnidirectional geometric factors and by the ratio of the solid angles for which the shielding was a minimum. i.e.

$$\text{corrected 223 count rate} = \text{223 count rate} - \text{302 count rate} \times \frac{0.22}{0.55} \times \frac{2.0}{2.4}$$

$$= \text{223 count rate} - \text{302 count rate} \times .333$$

This corrected 223-type count rate was then converted to directional flux density by dividing by the directional geometric factor and the counting efficiency ($\sim .9$ for non-relativistic electrons) of the detector (McDiarmid, private communication) i.e.

$$\text{directional flux density} = \frac{\text{corrected 223 count rate}}{5.05 \times 10^{-4} \times .9}$$

$$= 2200 \times \text{corrected 223 count rate.}$$

Units of directional flux density are electrons cm^{-2} sr^{-1} $s.^{-1}$ We estimate that the figures so obtained are reliable to within a factor of 2.

1.4 DATA FORMAT AND INITIAL SORTING.

Through the kindness of Dr. I.B. McDiarmid of the Canadian Research Council, 4800 ft. of magnetic tape containing the primary data of the particle detector experiments aboard Alouette I were made available to the writer and his colleagues. Records on these two reels of magnetic tape were filed by station and were written in 9-track EBCDIC code which the computer in operation at Rhodes University was not capable of decoding. The one tape containing records received at the South Atlantic station was very kindly converted to 7-track BCD format by Messrs. I.C.L. Limited. As well as decoding the tape, a small

sorting procedure was also carried out which created records on the new tape slightly different in structure to the original.

This master data tape named ALOUETTE 556 contained 14,628 records which had been received at the station South Atlantic. Each record contained data collected by the satellite in the 10 second period immediately prior to the transmission, as well as co-ordinate, time, date and identification information which had been merged with the particle data back on earth.

The following fields within each record were important:-

1). Station Identifier (South Atlantic = 0)

2). Pass number

3). Kp for 3 hour period in which pass starts

4). Date and universal time

5). Geographic latitude and longitude

6). Magnetometer reading (Bmag)

7). Computed geomagnetic field value (B)

8). Altitude of satellite

9). Pitch angle (α)

10). Invariant radius (R)

11). L Parameter

12). Invariant latitude ($\lambda = \cos^{-1}\sqrt{\frac{R}{L}}$)

13). Log_{10} 223 counting rate

14). Log_{10} 302 counting rate

What remains to be done is a conversion from Log_{10} 223 counting rate to a directional flux density of electrons with energies greater than 40 keV. After this, the investigation of the distribution of the flux with various parameters may be carried out.

1.5 CONCLUSION

From this point on the data loses the "personality" of the satellite and, except for one short section where we will discuss the reduction of particle

pitch angles from satellite pitch angles, we shall be in a position to ignore the existence of Alouette I. For our purposes it has done its job, but the writer notes with a sense of ownership that the 1971 Data Catalog of Satellite Experiments lists Alouette I as still operational. The useful particle data was obtained only until it lost spin stability and assumed a gravitational gradient stability. From a satellite very near the top of the lists of the ancients, we hope to achieve some worthwhile results.

--- 0 ---

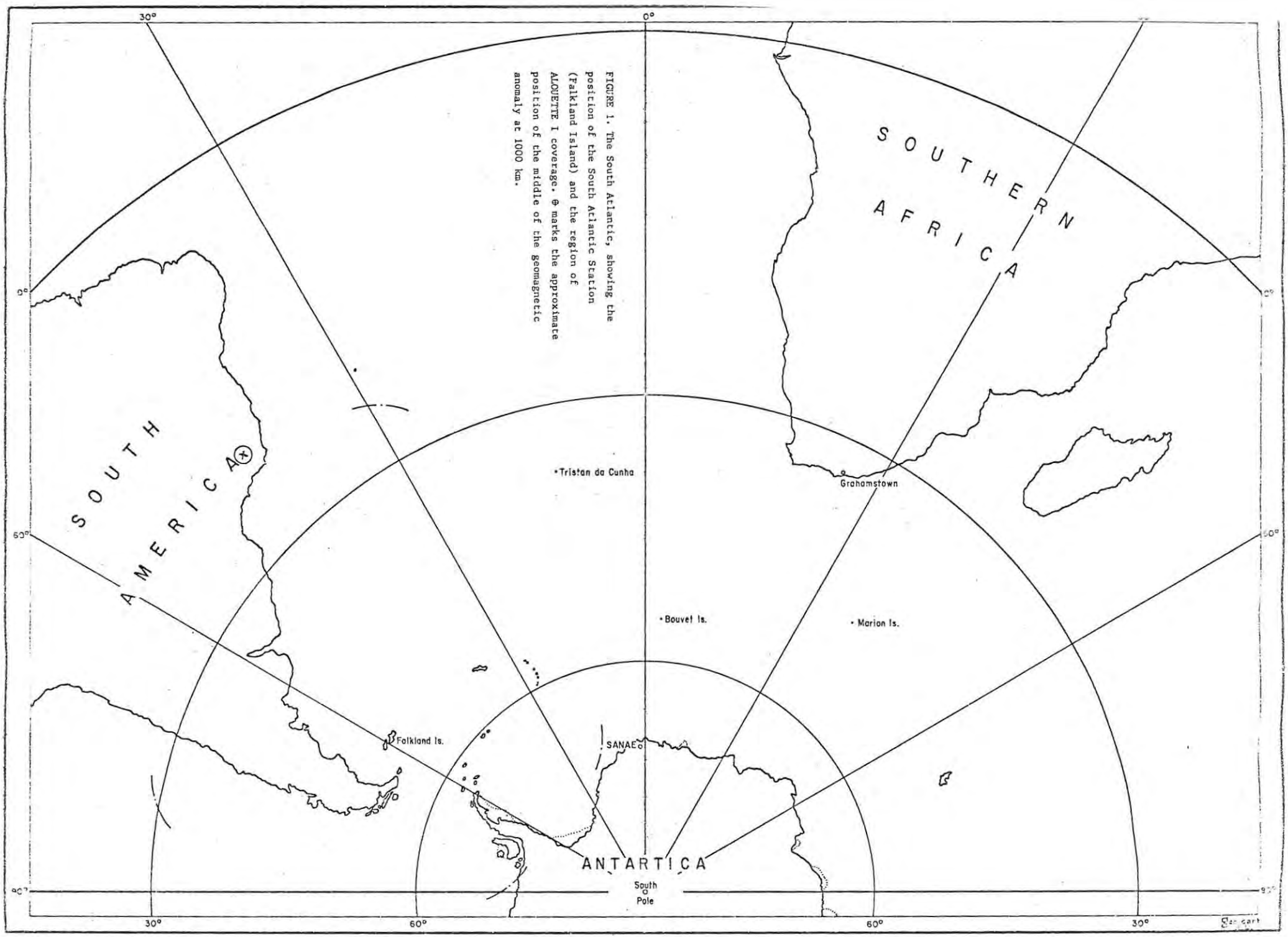

FIGURE 1. The South Atlantic, showing the position of the South Atlantic Station (Falkland Island) and the region of ALOUETTE I coverage. ⊕ marks the approximate position of the middle of the geomagnetic anomaly at 1000 km.

CHAPTER 2

THE DATA ANALYSIS

2.1 INTRODUCTION

In this chapter we shall explain the steps taken in the analysis of the energetic electron data obtained from the satellite Alouette I. Appendix 2 has been complied as a write-up of the computer system that was developed to carry out the procedures required in the analyses.

Before presenting any of the initial results of the analysis we shall introduce some simple concepts from the theory of charged particle motion in the geomagnetic field. Also as an aid to interpretation of the results and their implications we have drawn two maps of the region covered by the satellite while collecting the data.

A presentation of the statistics of the analysis is given, together with a comment on a surprising feature of the data that may perhaps be used to give an indication of energy spectra of particles in the outer zone of the radiation belt.

2.2 A MAP OF THE SOUTH ATLANTIC REGION

Before any of the electron flux distributions can be presented it is essential to have a clear picture of the area concerned. In figure 1 we have a map of the entire South Atlantic area. We have indicated the positions of the South Atlantic station, SANAE and several other prominent locations. Also shown are the approximate geographic limits of the area covered by data received at South Atlantic station.

Figure 2, plotted on a different projection, covers an area 90^{o} westwards from the Greenwich meridian and between the 10th and 80th southern parallels. Again we have marked the positions of various prominent locations. We have also plotted a grid of values of λ - the invariant latitude - at an altitude of 1000 km. The two curved contours are the 1.7×10^{-5}T and 1.9×10^{-5}T

11/.....

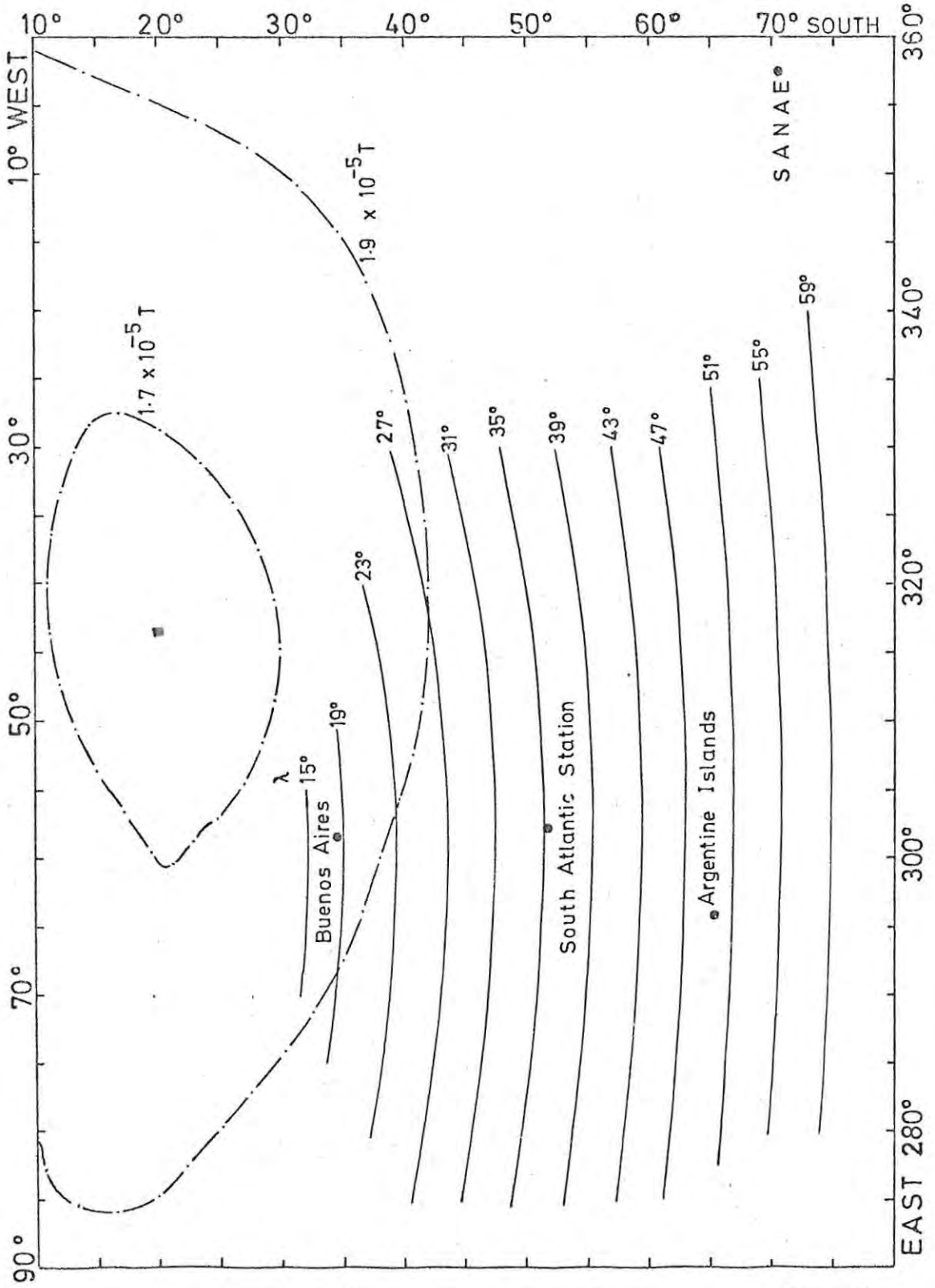

FIGURE 2. A grid of λ superimposed on the South Atlantic region. Two geomagnetic field contours are shown.

geomagnetic contours at 1000 km encircling the position of the geomagnetic minimum. These contours are obtained from Roederer et al. (1965).

The λcontours were obtained from the Alouette I records. For each selected value of λ , the data file was scanned and all records with a value of λ close enough to the selected value, were extracted. The pairs of geographic co-ordinates for each extracted record were then used in a least squares fit for a third degree polynomial. In all cases this cubic provided a sufficiently good fit for it to be used to represent the 1000 km contour for the selected value of λ

From the map in figure 2 we can see that the area covered by the satellite - roughly the region for which the grid is shown - is very favourably placed for an analysis or the effects of the anomaly. The range of longitude includes the 'eye' of the anamoly to the north. The range of invariant latitudes available very nearly includes the centre of the geomagnetic minimum. From the flux distribution of electrons at this northern end of the satellite region it should be possible to obtain information about particle dumping rates and related results.

2.3 THEORETICAL CONSIDERATIONS

Many excellent expositions on the motion of particles in the geomagnetic field have appeared, especially since the initial discovery of the radiation belt in 1958 by the University of Iowa group under J.A. Van Allen e.g. Northrop (1963), Van Allen (1968), Hess (1968) and Roederer (1970). We would like to quote one expression only, for it embodies nearly everything that we shall investigate with the data.

Alfvèns Mirror Equation:-

$$B_m = \frac{B}{\sin^2 \alpha}$$

where: Bm is the magnetic field strength at the point on the field line where the particle mirrors (here $\alpha = 90^\circ$)

B is the magnetic field strength at any other point on the guiding

12/....

field line and at this point the particle velocity vector makes an angle α with the direction of the magnetic field (the particle pitch angle).

We are to analyse data in a region of space where the geomagnetic field values at a given magnetic latitude and altitude are considerably lower than at the equivalent northern latitude. Hence charged particles mirroring at a field value Bm in the northern hemisphere at an altitude greater than 1000 km will have to spiral much closer to the earth in the anomaly region of the southern hemisphere to reach the required value of Bm. It may happen that on a particular shell the position of the value Bm may be deep inside the atmosphere. In this case we consider the particle to be 'precipitated' as it collides with atmospheric molecules and loses its energy and its place in the radiation belt.

These considerations immediately suggest that our primary analysis should be of a geographic nature and that a secondary investigation should be of particle pitch angle distributions. More brief theoretical sections are included where necessary in the text and the reader is reminded of Appendix 1 which explains and defines the concepts of directional flux, omnidirectional flux, geometric factors and other pertinent terms.

2.4 INITIAL ANALYSIS OF DATA

The data consisted of directional flux values for electrons with energies greater than 40 keV at various points in space and time. These electrons were either trapped, or precipitated into the Earth's atmosphere. The motion of all charged particles, and in particular these electrons, in the radiation belt, is magnetically controlled. The obvious method of analysis therefore was to divide the records into groups depending on the value of some magnetic co-ordinate and then to examine the mean flux in each group. In this way the presence of the centre of the geomagnetic anomaly at the northern edge of the region (see figure 2) should be detected.

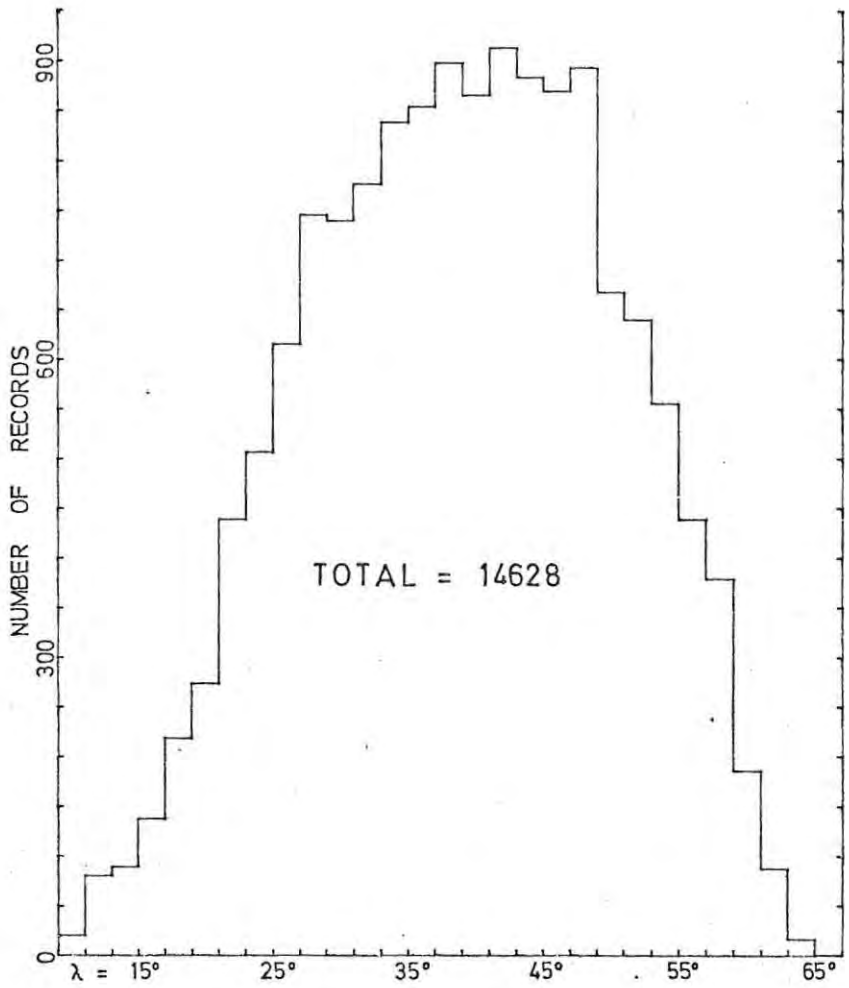

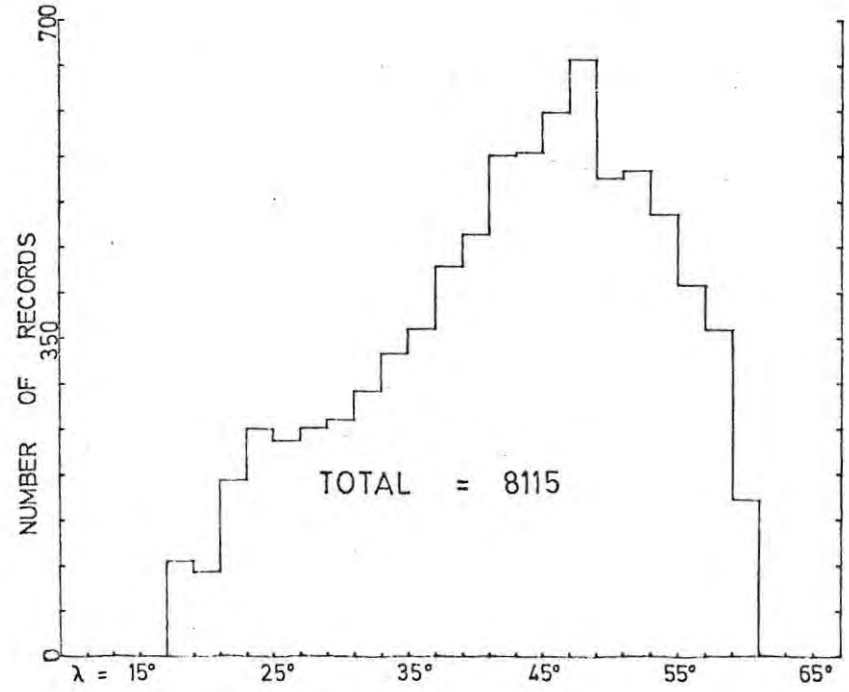

FIGURES 3(a). Distribution of ALOUETTE I records in invariant latitude (λ).

3(b). Distribution of records finally used in analysis.

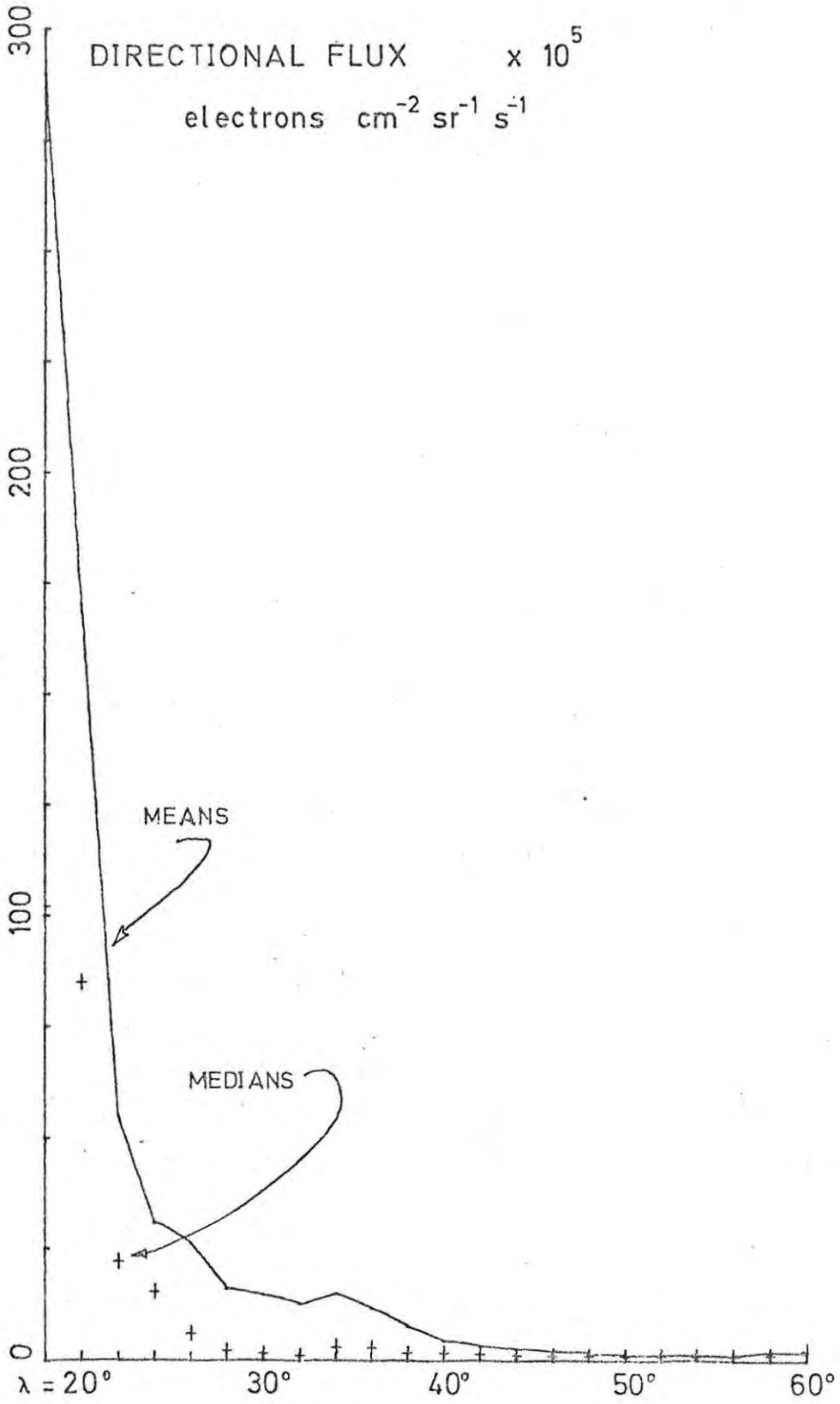

FIGURE 4. Mean and median directional flux values for each invariant latitude 'strip'.

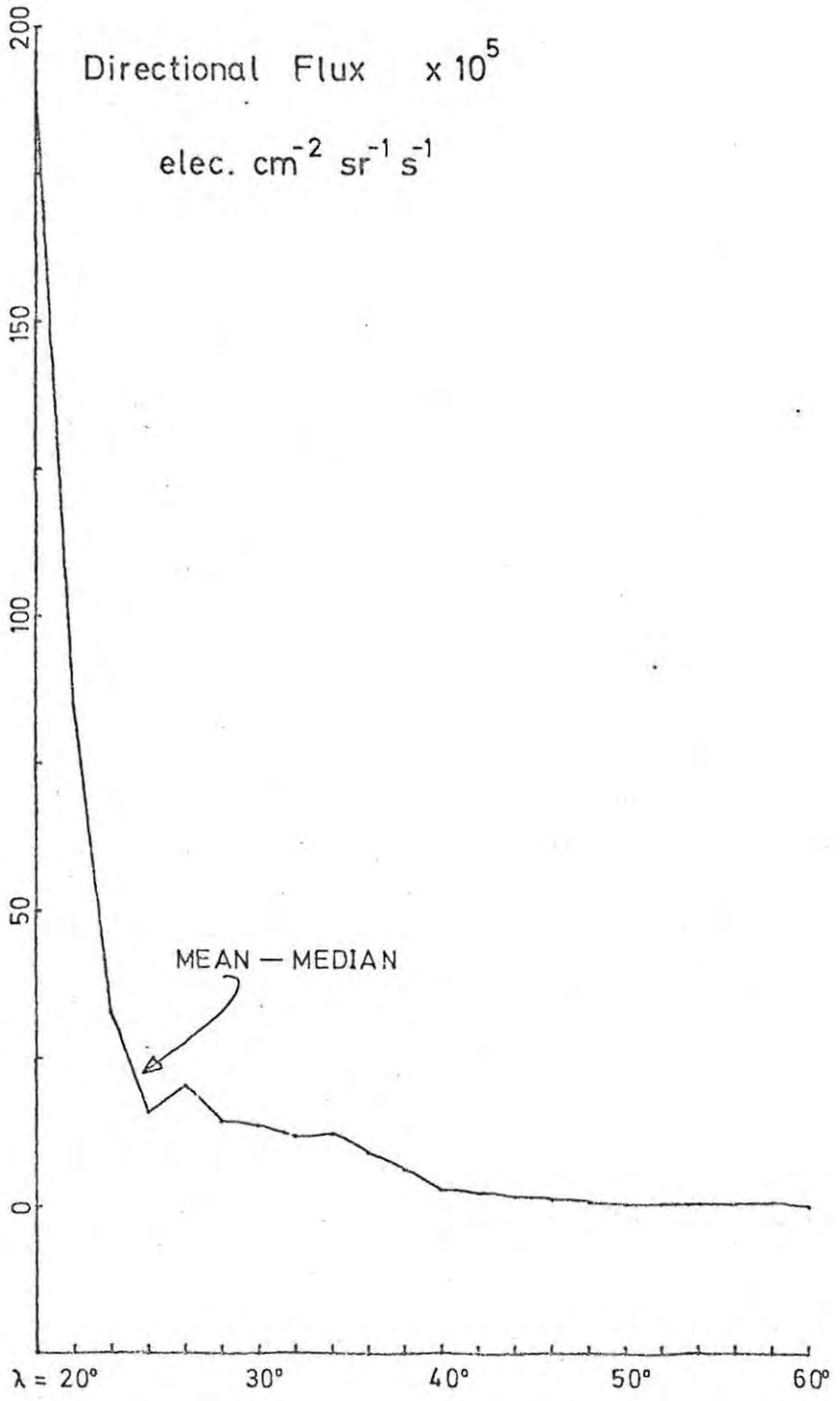

FIGURE 5. The difference, (mean-median) of directional flux values.

By referring to figure 2 again, we see that an analysis of flux variation with geographic longitude also will be of interest. Any effects that the low values of the magnetic field may have on the electron population of the radiation belt as they drift eastwards across the anomaly may be shown in a longitudinal scan.

Before we continue to these two analyses we would like to make an introductory comment on the fact that nearly 42% of the records yielded negative values for the background corrected 223-type count rate. Although Rose (1966), writing about Alouette I results obtained in the northern hemisphere, states that correction of any counter for background never proved worthwhile, we, however, have found that a very high proportion of the results have been rendered 'useless' by the correction procedure. We have investigated this phenomenon. The factor (0.333) controlling the proportion of the 302-type count rate that represents background counts in the 223-type counter, is purely geometric and unlikely to be the source of the error. Some results that will come out of the forthcoming analysis have helped to shed light on the problem and we shall discuss it again later.

2.4.1 DISTRIBUTION IN INVARIANT LATITUDE

The 14,628 records were sorted into 2^{o} wide intervals of invariant latitude. The histogram in figure 3 (a) shows the outcome of this sorting procedure. It should be remembered that the value of λ - the invariant latitude - used here is the value at an altitude of 1000 km and not the value at the same geographic co-ordinates on the Earth's surface. This distribution in figure 3 (a) approaches a normal distribution centered above the station of South Atlantic.

At this stage a decision was made to discard all those intervals containing less than 1% of the total number of records. It was decided that there were too few records in these intervals for any statistic from them to be

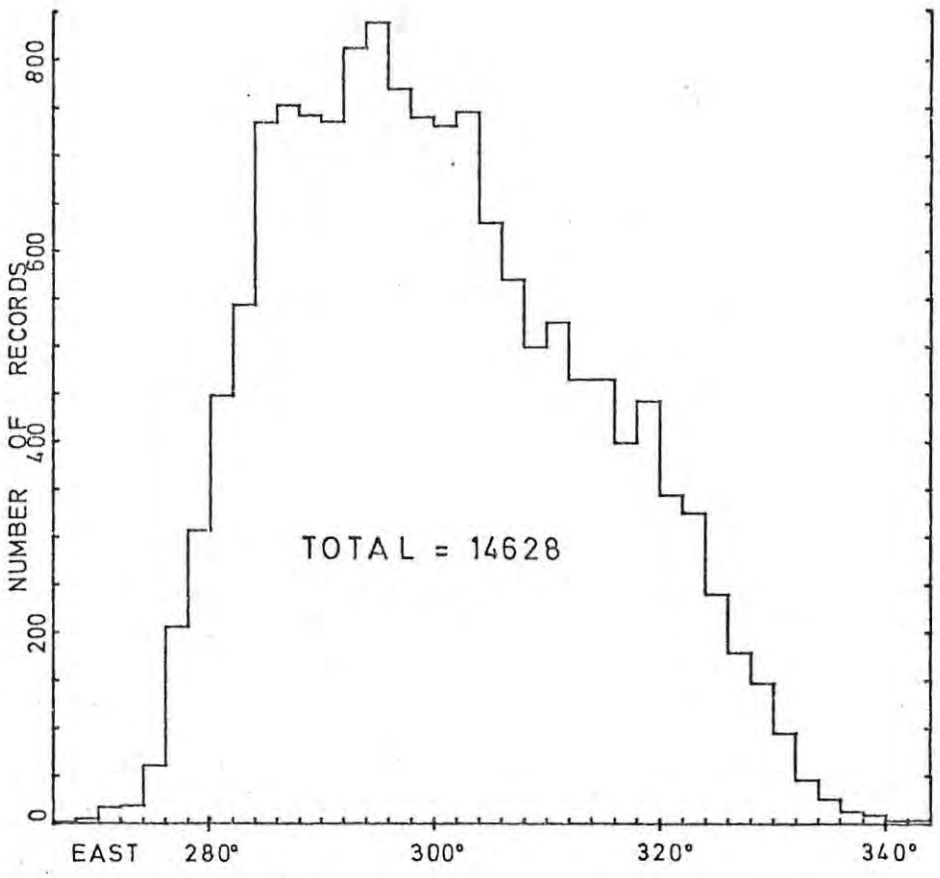

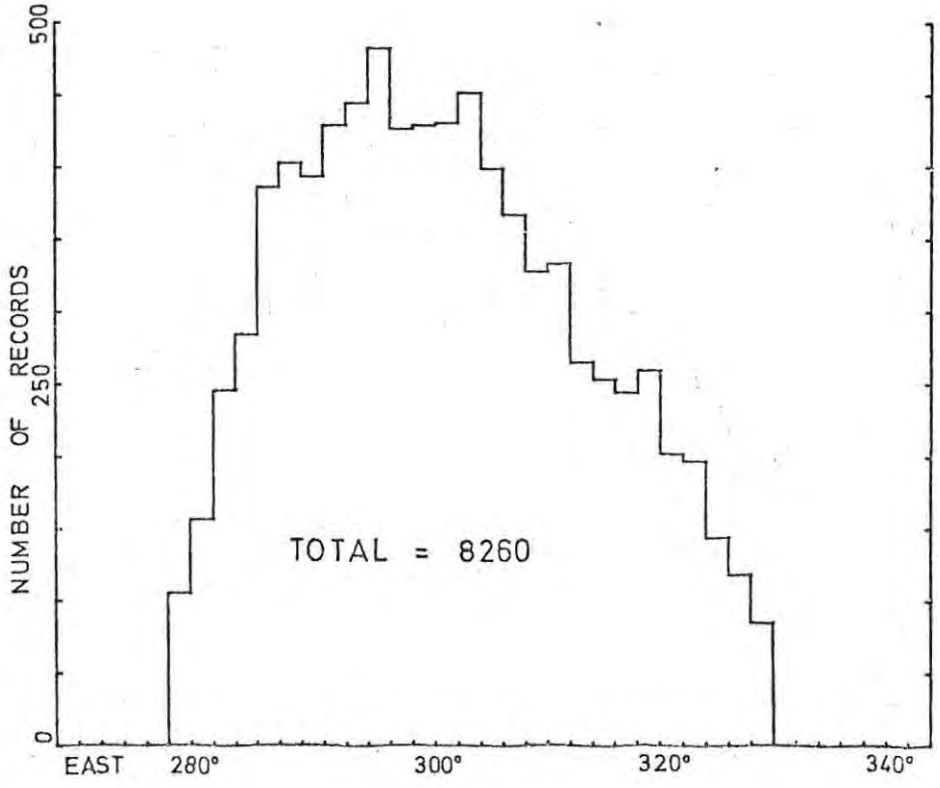

FIGURES 6(a). Distribution of ALOUETTE I records in longitude.

6(b). Distribution of records finally used in analysis.

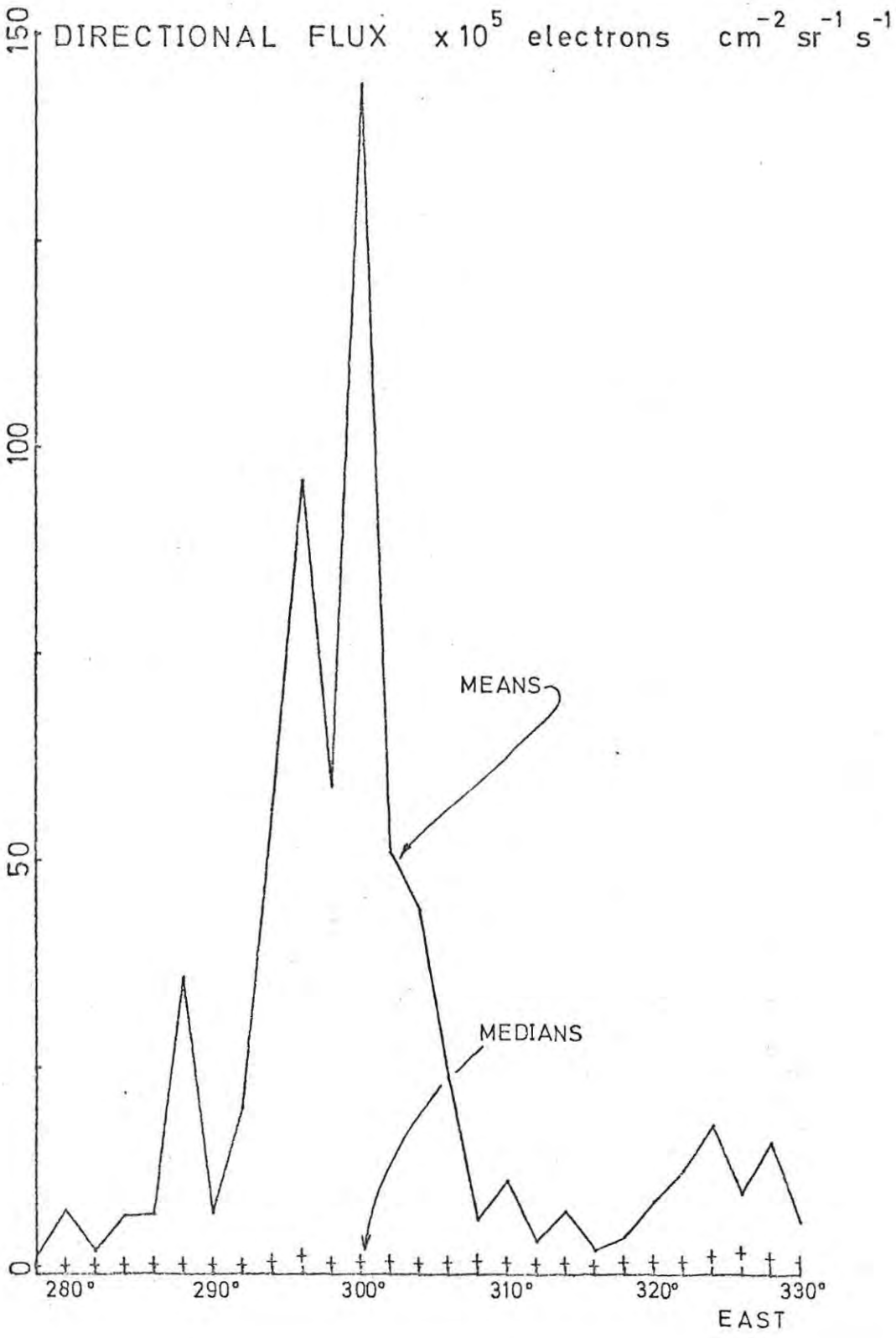

FIGURE 7. Mean and median directional flux values for each geographic longitude 'strip'.

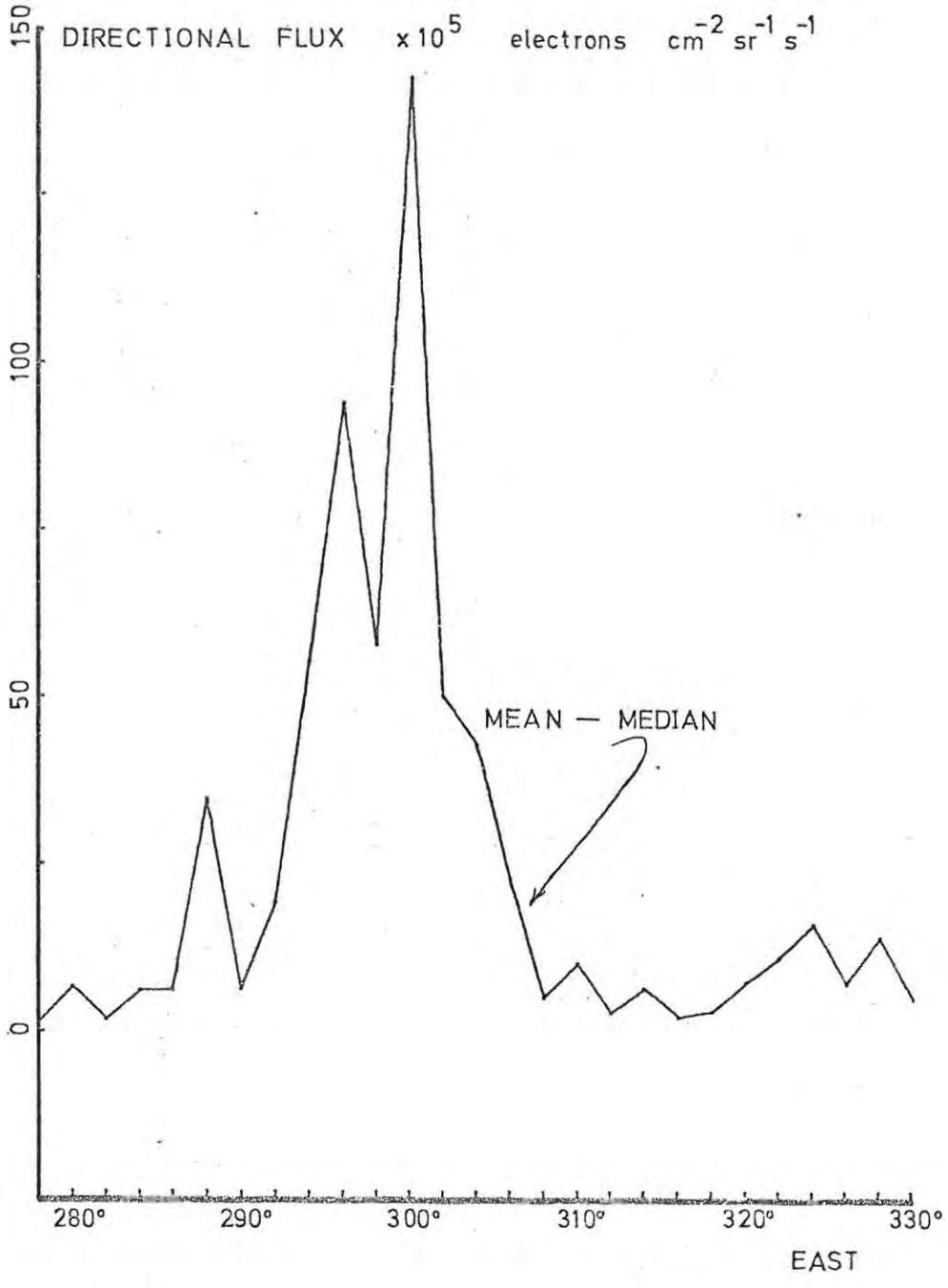

FIGURE 8. The difference, (mean-median) of directional flux values.

reliable or representative. All those records within each interval that had been 'overcorrected' and so could not have any value for the electron flux, were also discarded. In figure 3 (b) we show the number distribution of the 8,115 remaining records.

The mean flux and the median flux value in each of the 22 intervals have been plotted in figure 4. In all intervals except the one centred on $\lambda = 60^{\circ}$ the mean exceeds the median value. Both curves, however, display the marked effect of the geomagnetic anomaly on the electron flux.

The absolute difference between mean and median values of the flux in each interval is plotted in figure 5. It is suggested that this difference may be used as a rough criterion for judging whether or not the set of data contains exceptionally high values. Some idea of the spread of the data can then be obtained. From figure 5 it is obvious that equatorward of $\lambda = 28^{\circ}$, the data contains some very high fluxes. In Appendix 3 we have presented 22 histograms showing the number distribution of the fluxes in each of the intervals of invariant latitude. The conclusion derived from these histograms merely confirms what we have said above and no further mention will be made of them.

2.4.2 DISTRIBUTION IN LONGITUDE

Intervals of longitude 2° wide were found to be suitable for giving a reasonable number of records per interval. The preparation of the final number distribution shown in figure 6 (b) from the original number distribution of figure 6 (a) was similar to the case for the invariant latitude distributions. In figure 7 we have plotted the mean and median fluxes for each interval.

The difference in the shape of the two curves is very marked and we suggest that the median value is the most representative of the fluxes in each longitude interval. The large differences in the two values of each interval plotted in figure 8 does, however, indicate that the very high fluxes which are known to exist at the northern end of the region are distributed in a fairly narrow band of longitude 294° - 304° East. It is over this region that the

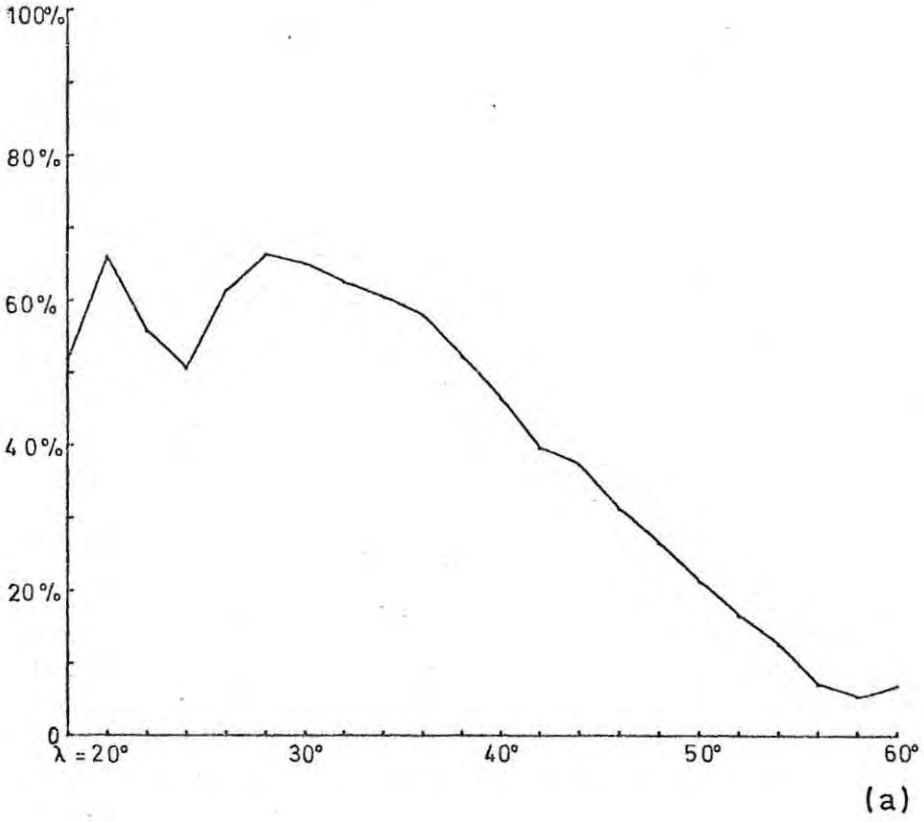

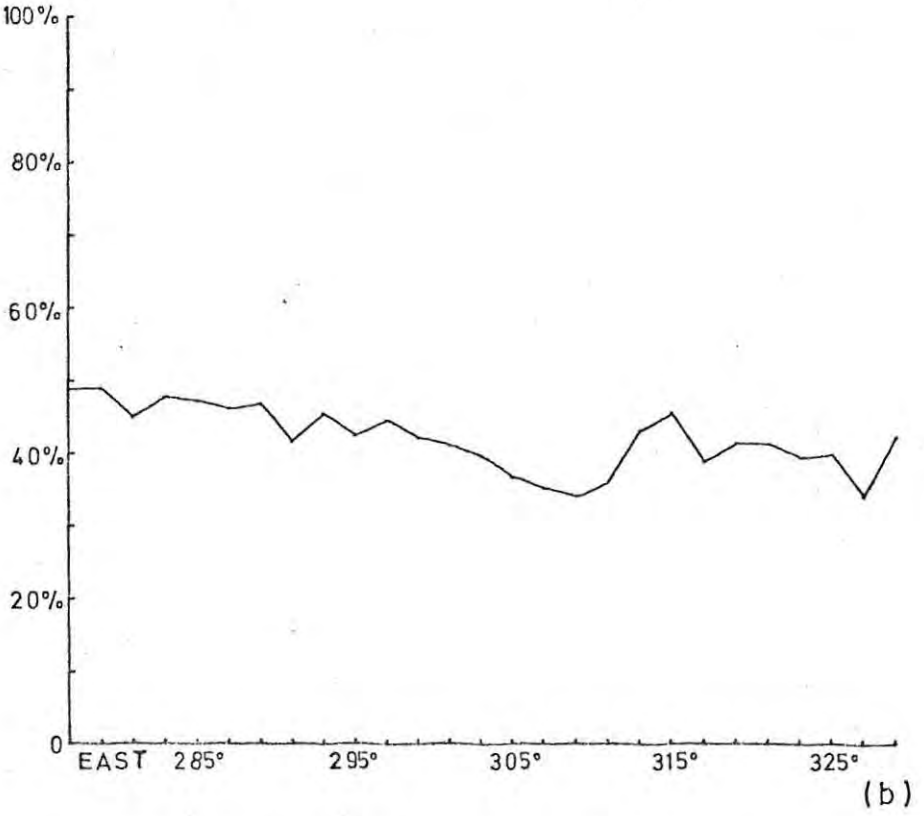

FIGURE 9. The percentage of records that were 'overcorrected' within each invariant latitude (a) and longitude (b) interval.

relatively few high fluxes have had the most influence on the means of the longitude intervals. This conjecture is confirmed by the histograms in Appendix 3 where the flux distribution for the 7 longitude intervals from 292^{o} East to 306^{o} East show a considerable number of very high flux values ($\geq 5 \times 10^{7}$ electrons cm^{-2} sr^{-1} s^{-1}) in comparison with the distribution for the other regions of longitude.

2.5 BACKGROUND OVERCORRECTION FEATURE

For every interval in both the distributions we have presented so far, we have prepared a plot of the number of records that suffered 'over-correction,' expressed as a percentage of all the records in that interval. The shape of this curve in the case of the invariant latitude distribution (figure 9 (a)) is in startling contrast to the similar plot for longitude (figure 9 (b)). The values in this latter case are all near to 42%, which is also the average overcorrection statistic for the whole sample, while the λ curve peaks at 27^{o}, where more than $^{2}/_{3}$ of the records have negative corrected 223-type count rates. This peak drops very steadily to below 6% at 57^{o} invariant latitude.

We have rejected any idea that this result may be connected with the high fluxes measured at the low λ values. The two curves peak at different points and fall off at different rates. We have considered the nature of the counts of particles from the two detectors:-

directionally the 223-type detects electrons $>$ 40 keV

Omnidirectionally the 223-type detects electrons $>$ 3 MeV

" " 302-type " " $>$ 3 MeV

By subtracting a geometrically specified fraction of the 302 count we hope to remove from the 223 count all electrons, $E > 3$ MeV, and protons, $E > 33$ MeV which have been detected omnidirectionally by the 223 counter. If, however, the energy spectrum of the particles is very hard, in particular there are very many electrons with $E > 3$ MeV and protons with $E > 33$ MeV in comparison with the number of electrons with energies in the range of 40keV to 3MeV, then the

count in the 223-type is going to be predominantly due to its omnidirectional properties. This is especially true if the particles are anisotropically distributed in pitch angle and for that sample the collimator of the detector is pointed away from the principal pitch angle direction. Therefore, after due geometrical correction the two counters will have nearly equal large counting rates. From such a situation it is not difficult to see how negative corrected count rates may arise.

For a soft spectrum very little of the 223-type count rate is due to its omnidirectional properties and the background correction will carry out its required and expected function. We suggest that this 'percentage overcorrected' statistic may be used to give an indication of the energy spectrum of the particle distribution. We can not, however, decide whether the high energy peak in the case of a hard spectrum is due to electrons or protons. In the next section we suggest that it may be due to electrons from the Soviet atomic bomb blasts of October/November, 1962.

2.5.1 SOVIET NUCLEAR TESTS?

Unfortunately for the users of Alouette I data, the USSR exploded 3 high altitude nuclear devices about one month after Alouette I was launched. West (1966) discusses the distribution and energy spectra of one of these explosions in detail and Hess (1968) lists the known information about the size of the bombs and their approximate positions in magnetic shell space. All three bombs were probably exploded above the atmosphere in L values between 1.8 and 2.0. ($\lambda = 34^{\circ} - 37^{\circ}$ at 1000 km). West shows results (his figure 18) from Explorer XV that confirm our suggestion that the curve of figure 9 (a) illustrates the existence of a hard spectrum at $\lambda = 35^{\circ}$ that softens towards the north. The principal particle product of a fission reaction is the electron and we can again confirm our suggestion that the hard spectrum refers mainly to the electron component.

It is of interest to note that the background correction process has removed the particles introduced by the bombs. Hence we can continue to use the flux

distribution curves of figures 4 and 7 with every confidence that they represent the natural radiation levels for the outer zone of the radiation belt.

2.6 FURTHER ANALYSES

We have presented the distribution of directional flux values for electrons with energies greater than 40 keV. It has been possible to show a strong geographical dependance of these fluxes on distances from the centre of the southern geomagnetic anomaly. As pointed out in section 2.3 it would be of considerable interest to obtain some information concerning the distribution of those particles with their pitch angles as well. Distributions on a diurnal time scale should also be of great value. It is by now widely acknowledged that precipitated particles from the radiation belt play a significant role in the production of ionization in the ionosphere. Ionospheric parameters have well known diurnal rhythms and data on changes on a similar time scale of particle fluxes are essential to research into the effects of this "corpuscular radiation". Accordingly, for each of the 22 intervals of invariant latitude and the 27 intervals of longitude described in section 2.4, the records in each interval were sorted according to their pitch angle value and their local time value. These analyses are described and discussed in Chapters 4 and 5.

2.7CONCLUSION

We have considered the results of the rudimentary flux distribution analysis. The data obtained have been encouraging in that definite trends in the flux values can be recognized and attributed to the presence of the geomagnetic anomaly. In the following chapter this dependence is surveyed in detail.

At the end of this chapter we may take leave of another essential piece of 'hardware' in the project. We refer, of course, to the tireless and tiresome digital computer that was eventually instructed correctly to perform the laborious tasks that this project relied upon. All future chapters refer to

results which were obtained in the computer runs that produced the simple data that we have presented in this chapter. For the remainder of this thesis, therefore, we are free to concentrate on the analysis of these results.

--- 0 ---

CHAPTER 3.

SPATIAL DISTRIBUTIONS OF ELECTRON FLUXES

3.1 INTRODUCTION

A detailed and rigorous survey of the flux values obtained by Alouette I for electrons with energies greater than 40 keV is presented in this chapter. Initially we shall demonstrate a statistical verification of the flux increases detected close to the anomaly. This analysis is then extended to produce iso-flux contour maps of both the South Atlantic region and the conjugate northern hemisphere area.

Throughout this chapter we consider results which are total directional flux values obtained from a set of records covering a large period of time (Table 1). No distinction is made between the trapped and the precipitating components of the flux.

By comparison with similar data obtained in the northern hemisphere we are able to present pertinent results concerning the effect of the anomaly. Finally in this chapter, a discussion is presented of the relevance of mean and median values and of the difference between these two statistics.

3.2 THE INVARIANT LATITUDE ANALYSIS.

The title of this section could be considered misleading for we shall show here the distinct influence of the geomagnetic minimum on the fluxes as we consider successive 'strips' of longitude, each one closer than the last to the meridian passing through the 'eye' of the anomaly. The section title refers to the use of the data from the 22 invariant latitude 'strips' of section 2.4.1. as the basis for the analysis. We are aware that the many analyses described and carried out are liable to have been confusing. In an attempt to clarify the present analysis, the steps carried out shall be described in detail.

Each set of records for each of the 22 invariant latitude intervals was considered in turn. A single set at a time was subjected to a longitude

TABLE 3

DIRECTIONAL FLUX VARIATIONS IN LONGITUDE

Invariant Latitude	L O N G I T U D E (degrees East) 270-280	280-290	290-300	300-320	310-320	320-330	330-340	Row Mean
17° - 19°	-	1.00	1.10	3.00	1.00	-	-	1.53
19 - 21	-	1.30	1.00	1.10	-	-	-	1.13
21 - 23	0.44	1.30	0.94	1.14	0.93	-	-	0.95
23 - 25	0.21	0.70	1.05	1.01	0.72	-	-	0.74
25 - 27	0.43	0.74	1.17	0.74	0.82	5.60	-	1.58
27 - 29	0.69	0.89	2.13	0.78	1.12	6.40	22.2	4.89
29 - 31	0.69	0.66	0.68	1.58	1.13	5.52	20.3	4.37
31 - 33	0.48	0.36	0.77	3.53	1.65	27.40	-	5.70
33 - 35	0.47	0.28	0.60	3.15	0.59	4.40	-	1.58
35 - 37	1.44	0.40	0.70	1.62	1.16	4.26	-	1.60
37 - 39	3.92	0.65	0.72	1.42	2.05	5.68	-	2.41
39 - 41	1.23	0.38	0.52	1.39	1.20	2.94	-	1.28
41 - 43	2.29	0.49	0.67	1.03	1.85	2.35	-	1.45
43 - 45	0.95	0.58	0.83	0.68	1.81	1.60	-	1.08
45 - 47	0.35	0.80	0.75	0.72	1.63	1.00	-	0.88
47 - 49	0.46	0.72	0.75	0.65	0.66	0.28	0.94	0.64
49 - 51	0.23	0.62	0.74	0.51	0.55	0.28	0.43	0.48
51 - 53	0.23	0.94	0.59	0.44	0.56	0.32	0.52	0.51
53 - 55	0.09	0.80	0.44	0.70	0.45	0.86	0.67	0.57
55 - 57	-	0.37	0.84	0.84	0.80	0.78	1.11	0.79
57 - 59	-	-	1.90	1.20	0.96	1.03	-	1.27
59 - 61	0.83	-	0.43	0.90	1.05	0.82	-	0.81
Column mean	0.86	0.70	0.88	1.28	1.08	3.97	6.60	

sort into intervals of 10^{o}. Seven such longitude intervals were required to span the range of the data. Within each block - 10^{o} of longitude wide and 2^{o} of invariant latitude high - the records were ordered according to their flux values (corrected 223-type) and in this way a median value was computed. For some blocks near the limits of the satellite's range there were too few records for a useful or representative median to be extracted. Such blocks were considered empty. In Appendix 6 we have presented the 22 histograms of the flux distribution in longitude. Obviously these histograms were too unwieldy to provide a convenient analysis, therefore the operation described below was carried out.

The median value of the flux in each invariant latitude strip (figure 4) was used to 'normalize' each block median in that strip. Table 3 shows the final result of the mathematical juggling. It was hoped that this normalization procedure would remove the inter-row differences in the flux values and yet retain the shape of the histogram for each strip.

The east / west nature of the flux distribution could then be observed. For each column of longitude, the mean was computed and a one-way analysis of variance test was carried out to test for significance in the differences between these means. A variance or F - ratio of 4.96 was obtained which indicated that the differences between the means were significant (Huitson (1966)). In simple terms the result tells us that the elements of the table are unlikely to be random numbers, and so the observed increase in the fluxes towards larger longitudes is likely to be real. By contrast a similar computation to derive the F - ratio for the table when viewed sideways, yielded an F-ratio of 1. 3. This value falls below the F 0.1, 21, 100 confidence level, indicating that the differences between the means of the invariant latitude strips are not significant. This last result confirms the efficacy of the normalization procedure.

The mean of all the values listed in Table 3 was 1.70. It can be seen that the values often differ wildly from this mean. The standard deviation

TABLE 4.

DIRECTIONAL FLUX VARIATIONS IN INVARIANT LATITUDES

Longitude	INVARIANT LATITUDE											
	10^{o}-15^{o}	15-20	20-25	25-30	30-35	35-40	40-45	45-50	50-55	55-60	60-65	Row Mean
278^{o}	-	-	-	1.88	-	3.53	3.58	0.40	0.21	-	-	1.92
280	-	-	15.66	1.35	0.44	8.38	0.93	0.57	0.45	-	-	3.97
282	-	24.05	7.62	1.69	0.65	0.50	0.53	1.32	0.92	-	-	4.66
284	-	-	8.39	1.41	0.48	1.21	1.03	0.83	0.76	-	-	2.02
286	-	-	18.30	2.65	0.30	0.81	0.26	0.59	0.51	1.38	-	3.10
288	-	142.7	33.48	0.91	0.36	0.68	0.46	0.53	0.44	-	-	22.45
290	-	-	24.79	3.35	0.29	1.10	1.10	0.62	0.41	0.55	-	4.03
292	-	271.7	18.76	2.02	0.85	0.62	0.80	0.40	0.38	1.36	-	32.99
294	374.7	201.7	10.23	3.16	0.32	1.00	0.25	0.43	0.21	1.71	-	39.37
296	265.2	94.05	11.51	1.37	0.55	0.63	0.38	0.44	0.16	0.66	-	37.49
298	800.0	623.0	10.64	4.23	0.75	0.45	1.02	0.51	0.42	0.54	-	144.16
300	578.0	140.0	18.57	2.64	3.14	1.79	0.50	0.82	0.23	0.20	-	74.59
302	605.7	216.0	10.93	2.63	4.94	0.84	0.56	0.71	0.34	0.54	-	84.32
304	388.0	-	7.00	2.68	1.68	2.42	0.63	0.49	0.34	0.74	-	44.89
306	-	232.0	12.82	0.40	5.13	3.18	1.12	0.30	0.25	0.82	-	28.45
308	-	-	23.44	2.83	2.21	3.18	1.19	0.36	0.11	0.71	-	4.25
310	-	251.0	23.47	-	6.42	1.49	1.08	0.33	0.30	1.27	2.44	31.98
312	-	-	12.91	4.72	1.23	2.61	0.87	0.61	0.24	1.00	2.00	2.91
314	-	-	24.67	-	0.57	0.62	2.30	1.09	0.31	1.27	1.87	4.09
316	-	-	8.14	1.73	0.53	1.51	4.85	0.70	0.36	0.71	2.49	2.34
318	-	-	-	-	5.07	1.15	1.36	0.48	0.31	0.59	1.98	1.56
320	-	-	-	2.09	0.33	2.28	0.84	0.41	0.20	0.52	2.99	1.10
322	-	-	-	-	8.70	7.50	0.63	0.16	0.26	0.49	0.87	2.66
324	-	-	-	12.69	5.04	1.45	1.57	0.21	-	0.40	0.99	3.19
326	-	-	-	-	4.58	5.56	1.03	0.06	-	0.66	0.78	2.11
328	-	-	-	-	-	9.00	3.06	0.15	0.07	0.98	0.82	2.35
330	-	-	-	-	17.07	3.41	2.19	0.61	0.61	-	0.91	4.13
Column mean	501.93	219.62	15.86	2.82	2.87	2.48	1.26	0.52	0.35	0.81	1.57	

of the values was 3.58. Thus the operation may be suspect from a rigorous (or even not so rigorous) statistical viewpoint. We do, however, feel that we have shown a feature not seen in figure 7 i.e. the electron directional flux increase towards the meridian passing through the centre of the anomaly.

3.3 THE LONGITUDINAL ANALYSIS.

The same opening remarks made in section 3.2 apply here. The 27 intervals or 'strips' of longitude shown in Figure 6 were split into blocks using a grid of invariant latitude with 5^{o} spacing. Appendix 6 also contains the histograms of this analysis. Each block median was normalized by dividing by the median value of the longitude strip (figure 7) in which it lay. Table 4 contains the result of these computations.

In this case the normalization was intended to remove the longitudinal character of the flux medians so the north/south variations could be studied. Once again a one-way analysis of variance was used to test the significance of the difference between the column means. An F-ratio of 89.78 indicates a very high significance, while the test carried out again for the rows gave an F-ratio of 1.03, a reassuring confirmation of the effectiveness of the normalization process. The mean of the 218 table entries was 26.58 with a standard deviation of just over 100.

The results of this analysis have confirmed the results of Figure 5 where the invariant latitude 'strip' calculations also showed large fluxes north of $\lambda = 24^{o}$. The coarser scale of Table 4 only allows for $\lambda = 20^{o}$ to be set as the boundary of dramatic flux increases.

3.4 ISOFLUX CONTOUR MAPS

In order to obtain a more physical picture of the nature and 'shape' of the effect that the geomagnetic anomaly has on the fluxes of electrons, the map shown in figure 10 was prepared. On a geographic co-ordinate grid of latitude and longitude the position of three magnetic latitude grid lines ($\lambda = 20^{o}$, 35^{o} and 55^{o}) are marked together with the contours of constant B

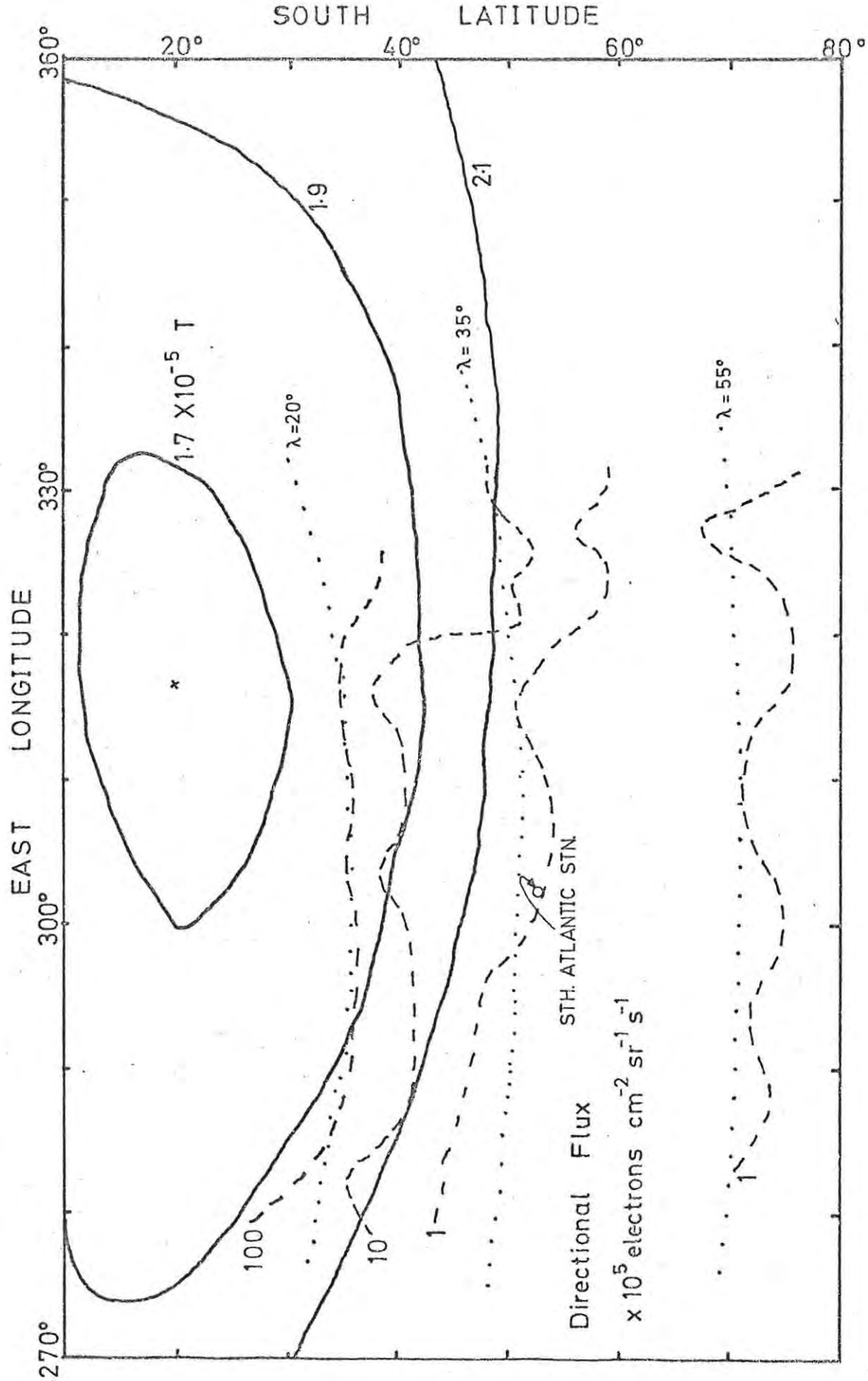

FIGURE 10. The South Atlantic region, isoflux contours using median flux values.

for three geomagnetic field strengths (1.7, 1.9 and 2.1 x 10^{-5}T). From the grid of median flux values obtained in the preparation of table 4 it was a simple matter to draw in the positions of the isoflux contours. In view of the very large flux values detected at the equatorward edge of the region, the isoflux contours for three values an order of magnitude apart were chosen (10^5, 10^6 and 10^7 electrons cm^{-2} sr^{-1} s^{-1}).

Two very interesting observations that can be made from this map prompted several more maps to be prepared. These observations were, the sudden departures made by the isoflux contours from paths parallel to the magnetic co-ordinates at about 320°E, and the emergence of a low flux trough near $\lambda = 50^{\circ}$ at the poleward edge of the region.

Any characteristics found in the electron flux distributions which are not a result of the presence of the anomaly, should also be detected at the 'other end' of the geomagnetic field line passing through the characteristic. We have used this principle to investigate the valley found in figure 10. Also it is necessary to have a knowledge of fluxes at 1000 km in the conjugate region to be able to show which are the flux increases due to the anomaly in the south. The sudden deviations of the isoflux contours mentioned above are likely to be due to the anomaly and this can be verified in a similar manner.

Using data received from Alouette I by the two northern hemisphere stations of Ottawa and St. Johns, a flux map covering both north and south was prepared. A more convenient co-ordinate system was used in the preparation of this and following maps, where geographic longitude and geomagnetic (invariant) latitude, were the chief co-ordinates. The northern hemisphere survey covered a longitude range from 270°E to 350°E and an invariant latitude range from 35° to 75° i.e. further east and further polewards than the South Atlantic data. This unfortunately did not allow for complete conjugate area coverage but the loss of overlap is not important. In figure 11 where the isoflux contours using median fluxes are presented, we have drawn two lines to show the approximate direction of the geomagnetic field lines projected onto the

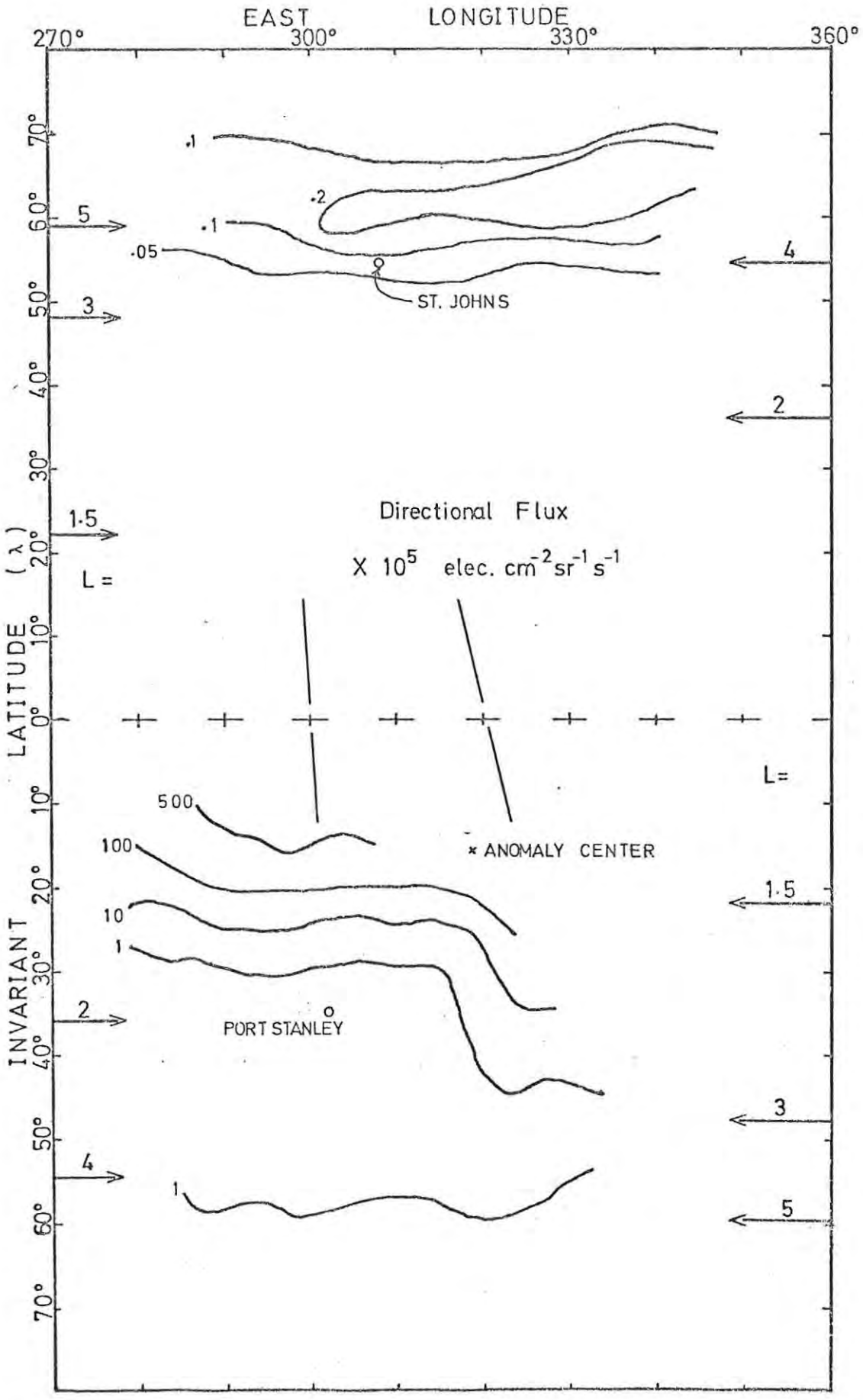

FIGURE 11. Isoflux contours using median flux values. The two diagonal lines indicate approximate local geomagnetic field directions.

surface of a 1000 km altitude sphere. These two lines are in fact portions of the lines joining the locations of Port Stanley in the Falkland Islands and St. Johns, Newfoundland with their respective conjugate points. The extent of the non-overlapping of the two regions can now be seen. Also in this and subsequent maps we have drawn the positions of the L value grid lines for selected values of L.

This presentation of the data helps to clarify the situation. The absence of any isoflux contours in the northern hemisphere from the equatorward limit of the data ($\lambda = 35^{o}$) until $\lambda = 52^{o}$ indicates a large region where the electron fluxes are very stable. Polewards of $\lambda = 52^{o}$ a pre-trapping boundary enhancement is found which peaks at around $\lambda = 65^{o}$ (O'Brien (1962,a) Rose (1966)). The exact position of this northern trapping boundary is obviously impossible to determine since the variation of about 8^{o} in its position (e.g. Frank and Ackerson (1972)) due to local time and magnetic disturbance has been averaged out (McDiarmid and Burrows (1968)). However, it is now possible to identify the poleward 10^{5} electron cm^{-2} sr^{-1} s^{-1} contour of the southern hemisphere analysis as the start of this trapping boundary enhancement. Unfortunately data coverage does not allow for verification of the position of the peak of this southern enhancement. The valley found in figure 10 now appears to be a small region of the even flux plain that has been hemmed in on the equatorward side by high fluxes associated with the anomaly.

We can now make a comparison of flux values in the north and south conjugate regions. Consider the following table 5.

TABLE 5

OBSERVED NORTH/SOUTH DIRECTIONAL FLUX

DIFFERENCES FROM FIGURE 11

L	DIRECTIONAL FLUX (j)			RATIO
	j (South)		j (North)	j (South) / j (North)
	$<320^{o}E$	$>320^{o}E$		
2	$< 10^{5}$	$\sim 10^{6}$	$< 5 \times 10^{3}$	> 20 - 200
3	$< 10^{5}$	$< 10^{5}$	$< 5 \times 10^{3}$	> 20
4	$< 10^{5}$	$\sim 10^{5}$	$\sim 10^{3}$	$\sim$ 100
5	$\sim 10^{5}$	$> 10^{5}$	$\sim 2 \times 10^{3}$	> 50

units: electrons cm^{-2} sr^{-1} s^{-1}

24/.....

In other words we observe an increase of about two orders of magnitude of southern hemisphere fluxes over northern hemisphere fluxes. Because of data limitations it is not possible to extend the table below L = 2 but we would expect even larger differences in this region, judging from the large fluxes observed in the south. These differences are astonishingly high and can not be due simply to the geomagnetic anomaly mirror point lowering, as we can show below.

We consider two points, one, a thousand kilometers above the South Atlantic station and the other 1000 km above the conjugate point of the station in the northern hemisphere. We use Alfvèn's mirror equation to compute the pitch angle of an electron 1000 km above South Atlantic station assuming the particle mirrored at 1000 km altitude above the conjugate point.

$$\text{(North)} \quad \frac{\sin^2 90^\circ}{2.9 \times 10^{-5}} = \text{(South)} \quad \frac{\sin^2 \alpha}{2.2 \times 10^{-5}}$$

$$\therefore \quad \sin \alpha = \sqrt{\frac{2.2}{2.9}} \sim .87$$

$$\therefore \alpha \sim 60^\circ$$

(geomagnetic field values from Roederer et al. (1965)).

If we assume an isotropic distribution of flux with pitch angle (highly unlikely) at the southern hemisphere point, the implication of the above result is that the flux indicated by the shaded portion in the diagram consists of particles which mirrored at, or below the northern hemisphere point. The non-shaded region, which in this case is as large as 50% of the shaded region, represents the extra flux seen in the south due to reduced geomagnetic field strengths. The flux increase is then of the order of double or less. Even a realistic pitch angle distribution peaked at 90° and falling to zero for very small pitch angles can not produce theoretical flux increases of the size shown in table 5.

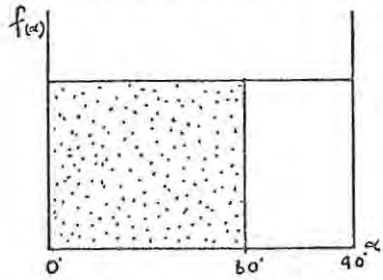

The results of Rose (1966) point to a complication in the above analysis.

25/.....

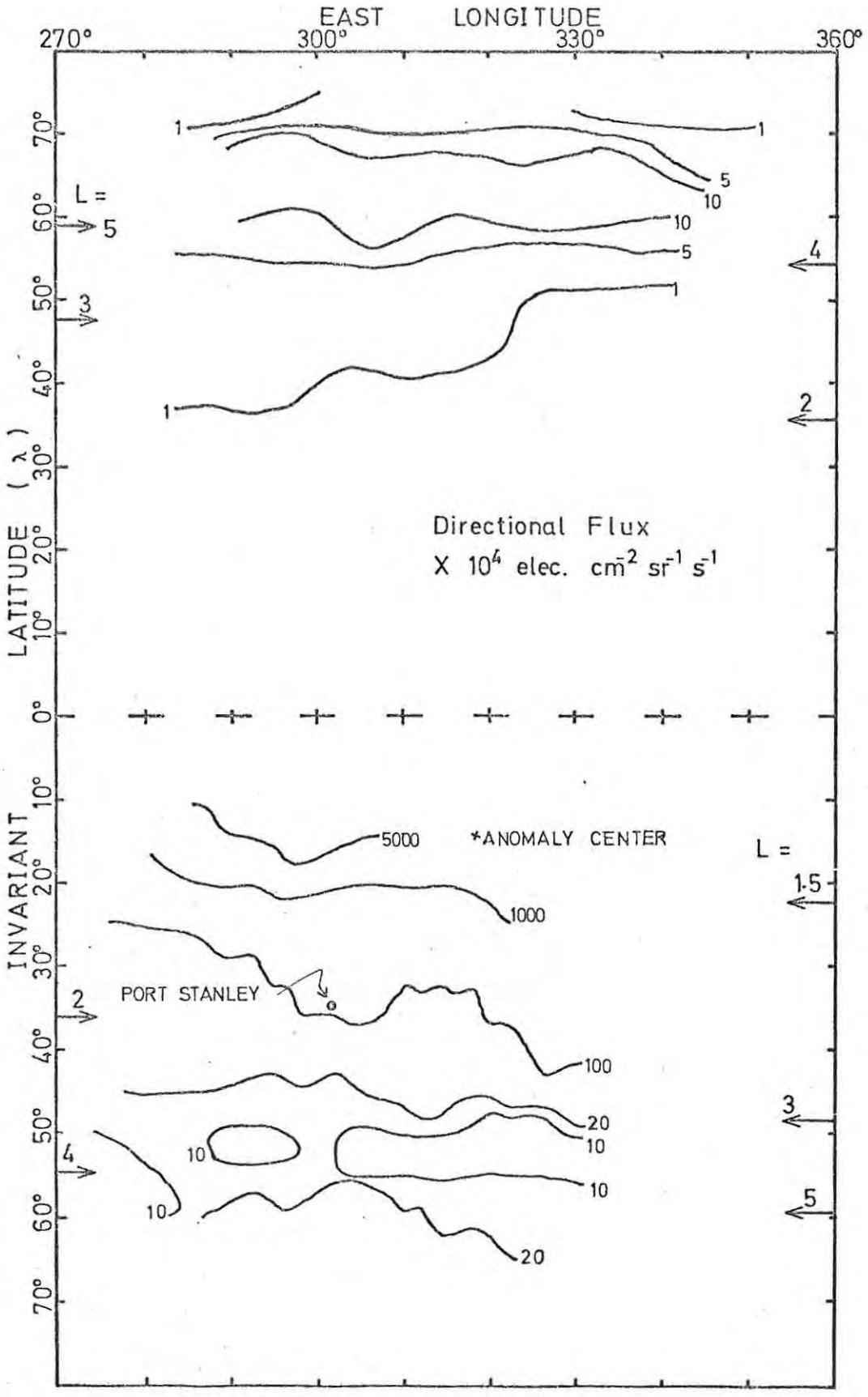

FIGURE 12. Isoflux contours using mean flux values.

Presenting the Alouette I results in the Northern hemisphere, he shows the trapping boundary enhancement to peak at L $\sim$ 5.5 with average directional flux of $\sim 2 \times 10^5$ electrons cm^{-2} sr^{-1} s^{-1}. This value is an order of magnitude larger than the result obtained in figure 11. Accordingly figure 12 was prepared using a grid of mean directional flux values. The isoflux contours derived from this analysis differ in several respects from the contours in figure 11.

Firstly the peak intensity in the northern hemisphere 'ridge' has increased about five times, although the structure of the ridge has remained virtually unchanged. The peak value of $\sim 10^5$ electrons cm^{-2} $sr^{-1}s^{-1}$ confirms the results reported by Rose. Small differences may be due to the fact that the present analysis ignored the magnetic disturbance criterion, considered all pitch angles, and also included background count correction. The appearance of the southern hemisphere isoflux map in the new average flux plot is not radically different from the median case either. The 10^6 electron cm^{-2} sr^{-1} s^{-1} contour line follows a more general poleward trend over the whole longitude range rather than the sudden divergence seen in figure 11. The structure of the 'valley' has become more defined, while flux values have remained almost unchanged.

We have already discussed the implication of large differences between the median and mean values of a set of fluxes. In cases where the mean is five to ten times larger than the median we can regard the difference as an indication that the fluxes are very variable. Ideally the mean and median will only co-incide in the case where the fluxes are distributed normally. (diagram (a)).

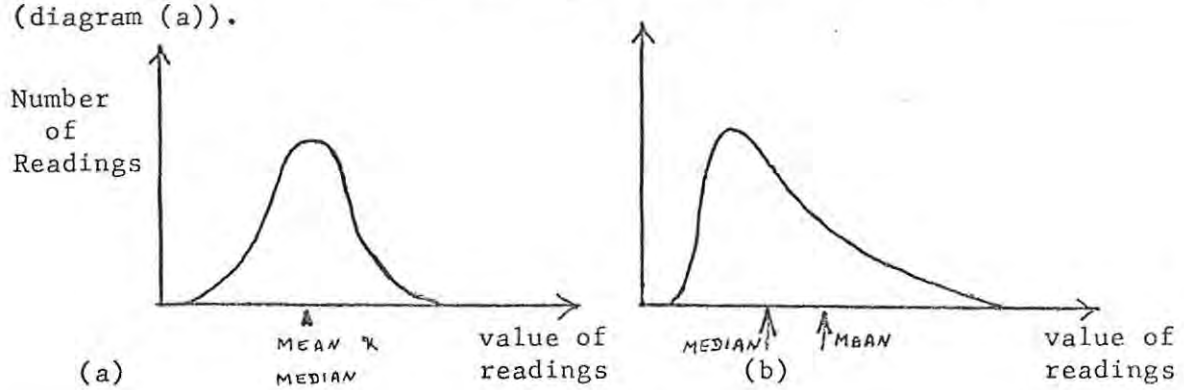

26/.....

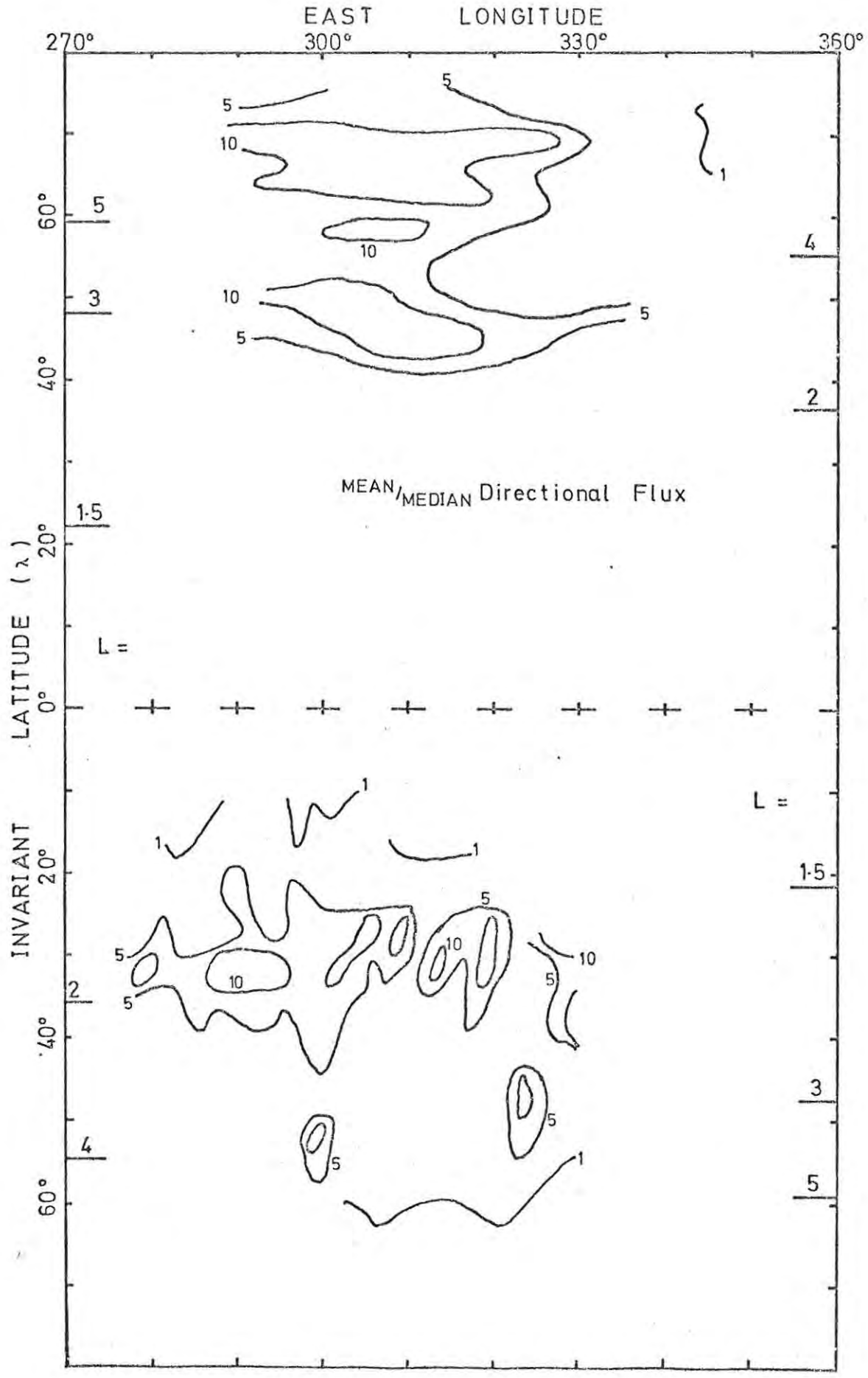

FIGURE 13. The ratio of $\frac{\text{mean}}{\text{median}}$ flux values displayed as a contour map.

A skewed distribution diagrammed in (b) above will produce the mean larger than median situation. The opposite situation does not occur often in the data and when it does the differences can safely be ignored.

In figure 13 we have attempted to utilise this distribution information by plotting the ratio of mean to median in a map similar to the previous two. On this map high values correspond to large mean/median differences. It can be seen that the northern hemisphere area contains the largest relative area of a high mean/median ratio. The scattered regions of high ratios (>10) in the south, mainly occur at L values just less than 2, explaining the change in the position of the 10^6 electrons cm^{-2} sr^{-1} s^{-1} isoflux contour between mean plot and median plot.

A possible implication of the results of figure 13 is that the variations in the electron flux due to magnetic variations and storms, are larger in the northern hemisphere than in the south. Further analysis to correlate magnetic disturbance and fluxes in both northern and southern hemispheres is obviously required to substantiate this idea.

Returning to figure 12, the mean flux contour map, we can now compile a new table of flux differences between northern and southern regions.

TABLE 6.

OBSERVED NORTH/SOUTH DIRECTIONAL FLUX

DIFFERENCES FROM FIGURE 12

L	DIRECTIONAL FLUX (j)		RATIO
	j (South)	j (North)	$\frac{j\ (South)}{j\ (North)}$
2	$\sim 10^6$	$< 10^4$	$> 10^2$
3	$\sim 2 \times 10^5$	$\sim 10^4$	> 20
4	$< 10^5$	$\sim 5 \times 10^4$	≤ 2
5	$\sim 2 \times 10^5$	$\sim 10^5$	~ 2

Comparing the South/North flux ratios obtained in this table with those of table 5, we see that the values above are of a more realistic order. The flux differences for the lower L values are largest in the south while the

27/....

northern hemisphere fluxes are only slightly smaller than those in the conjugate southern area in the area far from the anomaly. We shall discuss these results and their implications further in the following section.

3.5 A SIMPLE MODEL

In this section we extend a line of enquiry begun in the previous section and present some calculations that may help to account quantitatively for the north/south flux differences that we have reported. For this model we employ the Alfvèn mirror equation. We consider a particle that mirrors at an altitude just greater than 1000 km in the southern hemisphere, and compute the pitch angle of that particle when it is at the magnetic equator. We call this angle, α_s. By choosing points in the southern hemisphere that lie on identifiable geomagnetic field shells it is a simple matter to find the conjugate point in the northern hemisphere. The second calculation derives the equatorial pitch angle (α_n) of a particle that mirrors just above 1000 km at this northern hemisphere position.

TABLE 7

THE MODEL

L	λ	B 1000 South	B 1000 North	BE (L)	α_s	α_n	$\alpha_s - \alpha_n$
1.25	7°	1.70×10^{-5}	2.00×10^{-5}	$.96 \times 10^{-5}$	48.7°	43.8°	4.9°
1.50	22°	1.87	2.52	.56	33.2°	28.1°	5.1°
1.75	30°	2.18	2.88	.36	24.0°	20.7°	3.3°
2.00	36°	2.30	3.12	.24	18.8°	16.1°	2.7°
2.50	43°	2.65	3.31	.12	12.3°	11.0°	1.3°
4.00	54°	3.07	3.60	.030	5.7°	5.2°	.5°
5.00	59°	3.25	3.69	.015	3.9°	3.7°	.2°
		tesla	tesla	tesla			

28/.....

The procedure is more easily followed by reference to table 7. A line joining South Atlantic station with its conjugate point was drawn onto a map of L co-ordinate contours at 1000 km (Roederer et al. (1965)). The geomagnetic field strengths at 1000 km at the points of intersection of this line with the northern (B_n^{1000}) and southern (B_s^{1000}) contours of seven L values was also found. We have made use of the dipole field relation

$$B \propto L^{-3}$$

to compute B_E (L), the geomagnetic field strength at the geomagnetic equator for each value of L. B_E (1.1) $\sim 2.5 \times 10^{-5}$ T was used as the reference surface equatorial field.

α_s and α_n are then found from the relations

$$\sin^2 \alpha_s = \frac{Be}{B_s^{1000}}$$

and $$\sin^2 \alpha_n = \frac{Be}{B_n^{1000}}$$

Now by assuming a pitch angle distribution for particles at the equator for each L shell we can use the differences $\alpha_s - \alpha_n$ to give an indication of the expected flux differences between northern and southern hemispheres. We shall discuss the implications of this result by considering an equatorial pitch angle distribution as shown in the diagram.

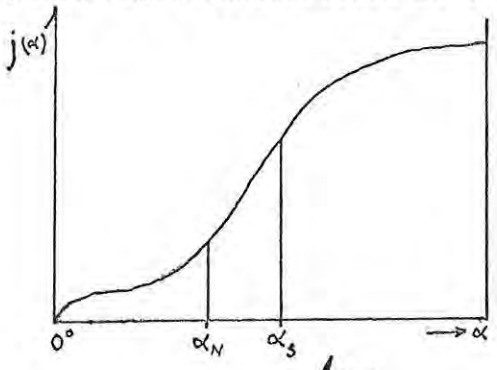

It can be seen that the ratio of southern directional flux to northern flux can be expressed as:

$$\frac{J(s)}{J(n)} = \frac{\int_0^{\alpha_s} j(\alpha)\, d\alpha}{\int_0^{\alpha_n} j(\alpha)\, d\alpha}$$

Whatever the analytic form of j (α) may be, this ratio will be dependent on the ~~proportional~~ ratio $j\alpha_s \alpha_n / j\alpha_n$ ~~to the difference ($\alpha_s - \alpha_n$) which we have listed in table 7 as well.~~

Referring to table 6 we can draw the following comparisons.

29/.....

L	Ratio $\frac{j\ (South)}{j\ (North)}$	
	predicted	observed
2	proportional to 2.7^{o} at 16.1^{o}	> 100
2.5	" " 1.3^{o} at 11.0^{o}	~ 50
4	" " 0.5^{o} at 5.2^{o}	~ 20
5	" " 0.2^{o} at 3.7^{o}	~ 2

We can not derive a functional expression for j (α) at the equator from this data, as a large range of L is involved. It is unlikely that the shape of j (α) is the same for all the magnetic shells we have considered.

We would like to make one further comment about the values shown in Table 7. Ignoring the differences that exist between α_s and α_n it is interesting to note that their value decreases with increasing L. At L = 1.25 on the equator all those particles with pitch angles around 45^{o} and less will be seen at the 1000 km height. In the southern hemisphere especially we have seen that this can be quite a substantial flux. ($\sim 10^{6}$ particles $cm^{-2}\ sr^{-1}\ s^{-1}$.) However, by moving out to L = 5 the 1000 km "visibility cone", angle has reduced to 4^{o}. Even so the flux in both hemispheres is still of healthy proportions ($\sim 10^{5}$ particles $cm^{-2}\ sr^{-1}\ s^{-1}$).

We shall leave the model at this point. In the following chapter on pitch angle distribution we shall make an attempt to make use of the results of this section.

3.6 CONCLUSION

At the close of this chapter it would seem that the spatial characteristics of the electron flux data collected by Alouette I have been comprehensively covered. However, only the directional flux distribution of all electrons with energies greater than 40 keV has been considered. The maps

30/.....

produced have agreed with results published by other workers, e.g. O'Brien (1962), Rose (1966), and some interesting reflections on the implications of mean and median differences have also arisen.

We shall continue to use median values in subsequent analyses of fluxes. The rest of this thesis is concerned only with the southern hemisphere data. For this region we have shown that the difference between mean and median values are generally sufficiently small not to affect the results being sought.

Next, consideration must be given to the pitch angle distribution of these electrons. Losses of particles from the belts are interesting for two reasons. Firstly, for what happened in the belt to cause the particle to leave, and secondly, for the future of the particle and its effect on regions of space closer to the earth. A survey, such as the one described in the next chapter, is a natural extension of the overall picture obtained in this chapter.

--- 0 ---

CHAPTER 4.

PITCH ANGLE ANALYSIS

4.1 INTRODUCTION.

The pitch angle of a particle moving in a region of space where there is a magnetic field is defined to be the angle between the velocity vector of the particle and the local direction of the magnetic field. This project is concerned with the particular case of electrons in the geomagnetic field. And while the same definition of pitch angle applies, the exact measurement of such a parameter, for any particular particle or 'bunch' of particles, is a difficult task.

The pitch angle (α) of the satellite defined the attitude of the craft relative to the local geomagnetic field direction. As a result of the method used to compute α (see section 1.2) the craft's pitch angle could lie only in the range 0° to 90°. There is therefore an ambiguity as to whether the pitch angle was the one computed or its supplement. This has repercussions in the interpretation of the directional counter data. The directional electron flux was detected by the 223-type geiger counter - the electrons having reached the counter after passing through a collimator which was inclined at 10° to the spacecraft spin axis. The pitch angle ambiguity therefore does not allow for a distinction to be made between electrons which were detected while spiraling 'down' the field line or 'up' the field line. Regarding 'down' as meaning towards the Earth, a downward going electron detected at 1000 km will have one of three possible futures. It may reach a mirroring field value and reverse its bounce path direction before reaching the upper layers of the atmosphere. Alternatively the mirroring field required by a particular electron detected at 1000 km is deep inside the atmosphere, where the electron will collide with the molecules of atmospheric constituents, and either lose its energy and be 'precipitated' from the radiation belt or else be scattered into a pitch angle direction that allows it to escape back up a field line into the belt. Such a particle is said to have been backscattered. Hence upgoing radiation will consist of backscattered and mirrored components.

32/.....

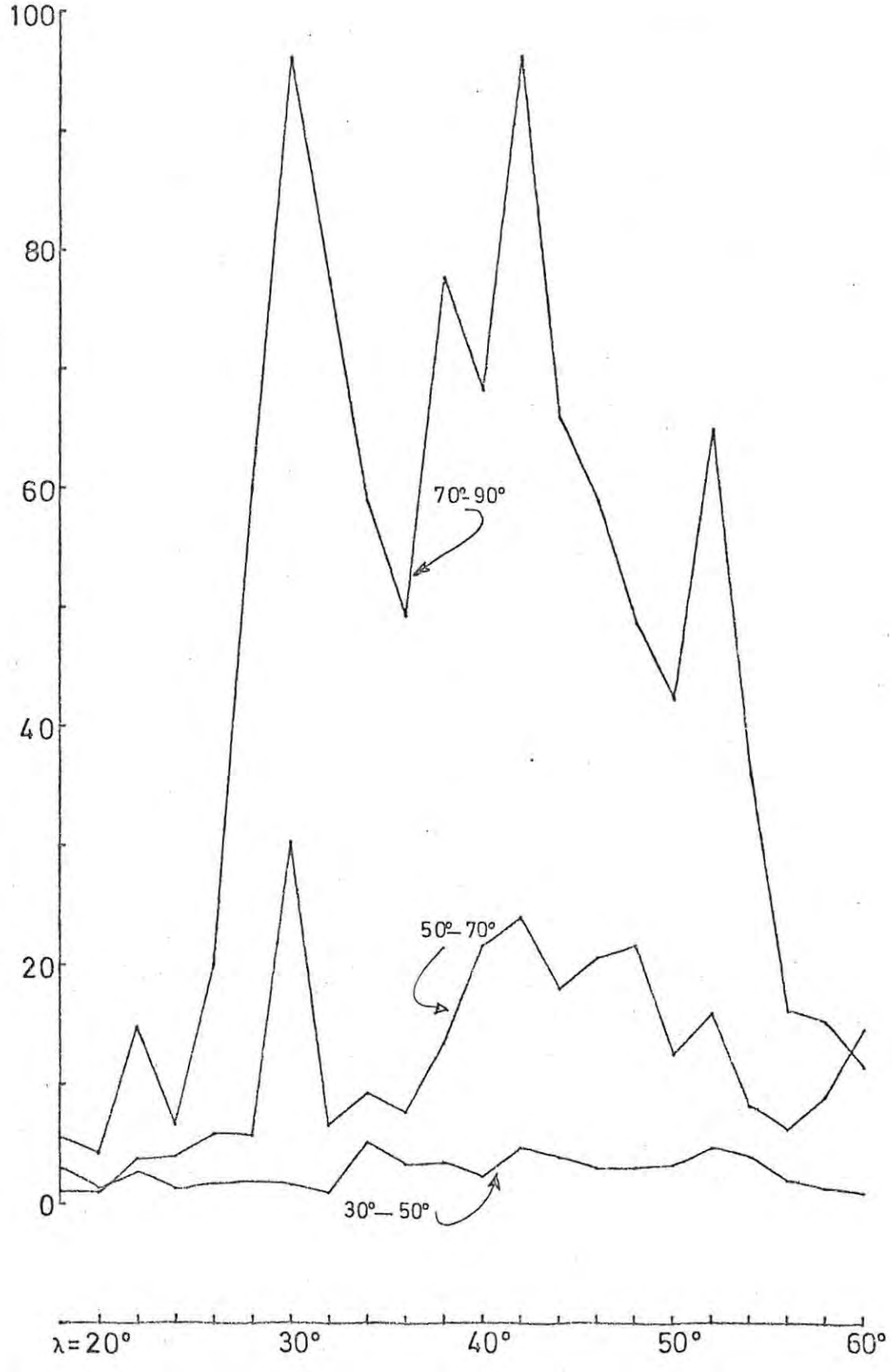

FIGURE 14. Median directional flux distributions for 3 pitch angle ranges, normalised by the median flux value for the 10°--30° range, versus invariant latitude.

A second complicating factor in this analysis of particle pitch angles arises from the fact that the satellite was spinning and therefore the collimator was swept through a 20° range in pitch angles, centred on the satellite pitch angle, in each spin period. For this reason the pitch angle analysis was confined to intervals of 20° and these were chosen centred on 80°, 60°, 40° and 20°. The interval 0° - 10° contained no records and so was ignored. For some periods during the flight of the satellite the magnetometer developed a fault and for records during these periods both magnetometer and pitch angle values have been listed as zero. For this reason the number of records available for the pitch angle analysis is less than the total number of records.

We have again relegated the raw results of the survey to an appendix. The 22 histograms of median directional flux versus pitch angle interval; one for each set of records obtained from a 'strip' of invariant latitude, can be found together with the 27 equivalent longitude strip results in Appendix 4.

4.2 PITCH ANGLE DISTRIBUTION CHANGES WITH λ

Each of the 22 histograms of pitch angle versus directional flux bears out the earlier suggestion that the flux distribution was not isotropic, but peaked at the large pitch angle end. Further it can be seen that the lowest of the four medians in each distribution is nearly always the one from the 10° - 30° range. This median value was therefore selected in each distribution as a normalizing factor for the three other values, the normalized values being used to draw a concise and simple set of curves which represented the pitch angle distribution at each invariant latitude (figure 14).

An example of the procedure for the values from the histograms for $\lambda = 30^{\circ}$ is given below:-

PITCH ANGLE	MEDIAN FLUX	NORMALIZED VALUE
10° - 30°	$.288 \times 10^{5}$ electrons $cm^{-2}\ sr^{-1}\ s^{-1}$	1
30° - 50°	$.464 \times 10^{5}$ "	1.61
50° - 70°	8.71×10^{5} "	30.25
70° - 90°	27.7×10^{5} "	96.11

33/....

The curves of figure 14 therefore contain a summary of the results of the 22 histograms found in Appendix 4. We can see that the largest fluxes always occur in the 70° - 90° pitch angle range with the distribution at $\lambda = 60^{\circ}$ being the single exception. In general, flux increasing with pitch angle is observed. There are a few strips where the 10° - 30° range does not have the lowest median flux. From our own reasoning and from the results of O'Brien (1962a,b) it is reasonable to assume that a very large proportion of the electrons detected with pitch angles in this range must be travelling down the field line towards the atmosphere, where they are almost certain to be lost. It is likely that only a small number of these electrons are in fact backscattered. It has, however, been reported that the reflection co-efficient for the backscatter phenomena is dependant on the intensity of the incident precipitating flux (Cumming et al. (1966)) and this co-efficient can get as large as 1. Nevertheless we shall assume that all electrons detected with pitch angles within the loss cone are precipitated.

The loss cone angle at 1000 km can be computed by assuming that electrons which mirror at or below 100 km are precipitated. Also we make use of the dipole field property that $B \propto \frac{1}{R^3}$. Alfvèn's mirror equation is now.

$$\sin^2 \alpha_{1000} \times (Re + 1000)^3 = \sin^2 90^{\circ} \times (Re + 100)^3$$

(Re = Earth radius)

$$\therefore \sin \alpha_{1000} = \left(\frac{(6400)}{(7300)}\right)^{3/2} \doteq .82$$

whence $\alpha_{1000} \sim 55^{\circ}$

It is now pertinent to examine the flux values themselves and examine the changes with invariant latitude. Because the difference between fluxes nearest the anomaly and fluxes in the 'valley' is about 4 orders of magnitude it was convenient to use the $\log_{10}$ of the median flux value for plotting. Hence the four graphs comprising figure 15 each has $\log_{10} j$ as their ordinate and invariant latitude as their abscissa. Each graph represents

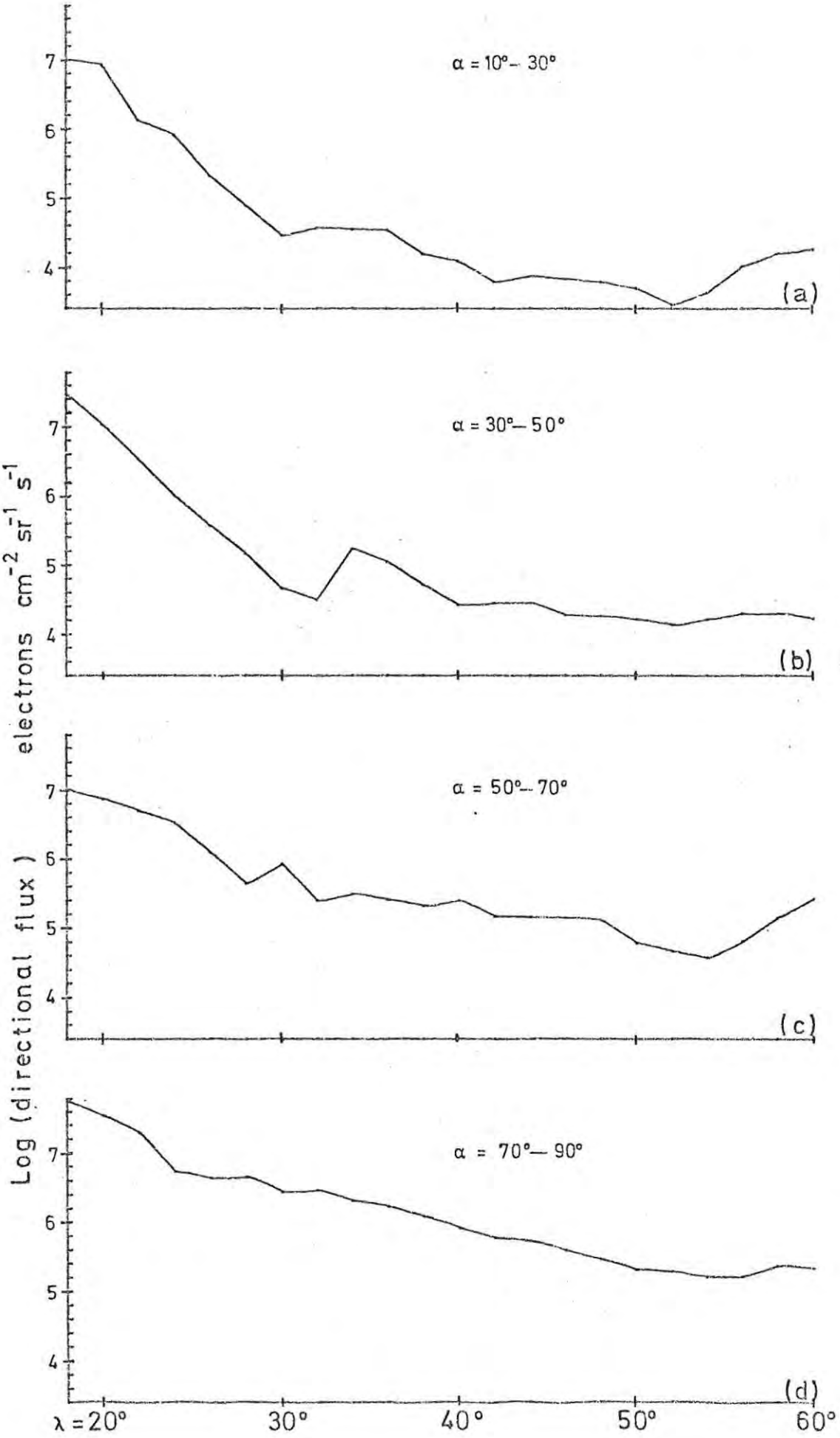

FIGURE 15. Median directional flux values for four pitch angle ranges, versus invariant latitude.

the median flux of electrons in a particular pitch angle range.

The loss cone angle of 55° unfortunately falls within one of these pitch angle intervals, but for the following discussion we shall make the convenient and not wildly inaccurate assumption that 50° represents the precipitation 'cut off' pitch angle. In this case the curves of figure 15 (a) and (b) will now represent the directional fluxes of the precipitating electrons, while curves (c) and (d) must represent the trapped portion of the flux.

A very distinctive feature of the two precipitated flux distributions is the nearly linear portion that exists from the equatorward limit of $\lambda = 18^{\circ}$ to $\lambda = 32^{\circ}$. The trapped particle distributions do not display this feature. A linear regression analysis performed on the co-ordinates of the points in these two linear regions yields slopes of - .20 and - .22 for graphs (a) and (b) respectively.

We get

$$\log_{10} j_p = m\lambda + c$$

whence

$$j_p = a\, 10^{m\lambda}$$

where: a is a constant

letting $m \sim -.21$ we obtain

$$j_p \sim a\, e^{-\lambda/2} \quad \text{electrons cm}^{-2}\ \text{sr}^{-1}\ \text{s}^{-1}$$

We can infer the existence of some process connected with the anomaly that has a very strong influence over the low pitch angle particles. To study the phenomenon further we have calculated the omnidirectional flux for each of the 22 'strips' of invariant latitude.

In spite of the crude scale employed in the analyses of directional fluxes (Appendix 4) it was possible to use a numerical integration procedure to approximate the calculation:-

35/.....

$$J(\lambda) = 2 \int_0^{\frac{\pi}{2}} j_\lambda(\alpha_\lambda)\ 2\pi \sin\alpha_\lambda\, d\alpha_\lambda$$

Where: J is the omnidirectional flux density

$j_\lambda(\alpha_\lambda)$ is the directional flux density of electrons with pitch angles in the range $(\alpha_\lambda, \alpha_\lambda + d\alpha_\lambda)$ at invariant latitude λ.

We have treated this expression as

$$J(\lambda) = 4\pi \left[j_\lambda(20) \int_{10^\circ}^{30^\circ} \sin\alpha\, d\alpha + j_\lambda(40) \int_{30^\circ}^{50^\circ} \sin\alpha\, d\alpha + j_\lambda(60) \int_{50^\circ}^{70^\circ} \sin\alpha\, d\alpha + j_\lambda(80) \int_{70^\circ}^{90^\circ} \sin\alpha\, d\alpha \right]$$

$$= 4\pi \left[.1188\, j_\lambda(20) + .2232\, j_\lambda(40) + .3008\, j_\lambda(60) + .3420\, j_\lambda(80) \right]$$

Where: $j_\lambda(20)$ is the median flux value in the pitch angle range 10° - 30° obtained for a particular invariant latitude from Appendix 4. etc.

We can also compute the omnidirectional flux of the precipitating component if we make a further assumption. We take the median flux value for the pitch angle range 50° - 70° as representative of the flux in the sub-interval 50° - 55°. This assumption would tend to yield too high a flux value.

The computation is clearly:

$$Jp(\lambda) = 2 \int_0^{55^\circ} j_\lambda(\alpha_\lambda)\, 2\pi \sin\alpha_\lambda\, d\alpha_\lambda$$

which we have treated numerically as

$$Jp(\lambda) = 4\pi \left[j_\lambda(20) \int_0^{30^\circ} \sin\alpha\, d\alpha + j_\lambda(40) \int_{30}^{50} \sin\alpha\, d\alpha + j_\lambda(60) \int_{50}^{55} \sin\alpha\, d\alpha \right]$$

$$= 4\pi \left[.1188\, j_\lambda(20) + .2233 j_\lambda(40) + .0692\, j_\lambda(60) \right]$$

Where: $Jp(\lambda)$ is the omnidirectional flux of electrons with pitch angles within the 55° loss cone at invariant latitude λ.

Units of omnidirectional flux are particles $cm^{-2}\ s^{-1}$.

The omnidirectional flux values so obtained also displayed a large variation over the range of invariant latitude. Therefore we have used the logarithm of the flux to plot the graphs shown in figure 16. This method of presentation of the pitch angle data for the electron fluxes is more convenient than the four curves of figure 15. One further aid to our discussion of the pitch angle distributions is shown in figure 16 (b) where the ratio

36/.....

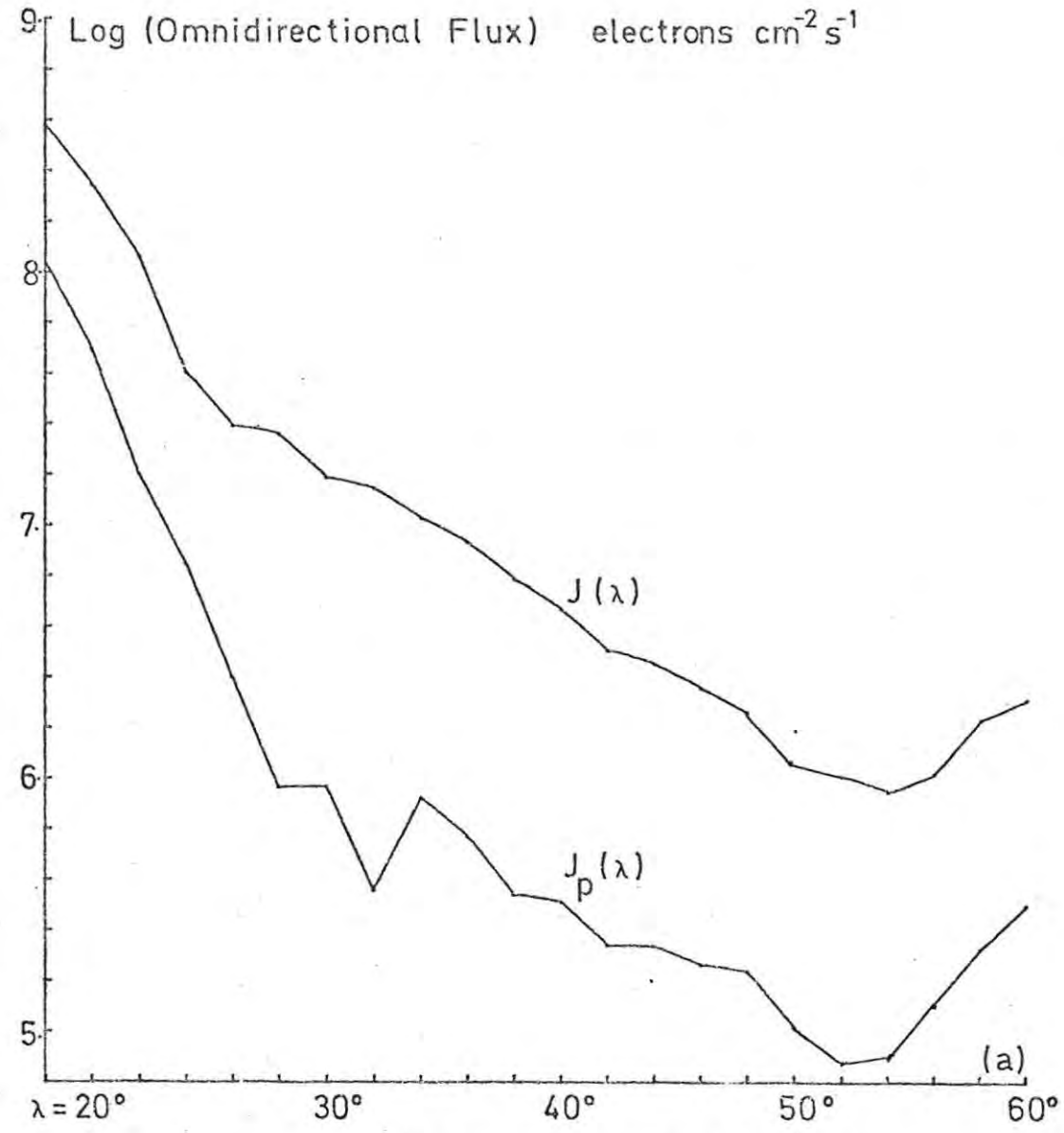

FIGURES 16(a). Total omnidirectional flux (J(λ)) and precipitated omnidirectional flux component(J_p(λ)), versus invariant latitude.

16(b). Ratio $J_p(\lambda)/J(\lambda)$ versus invariant latitude.

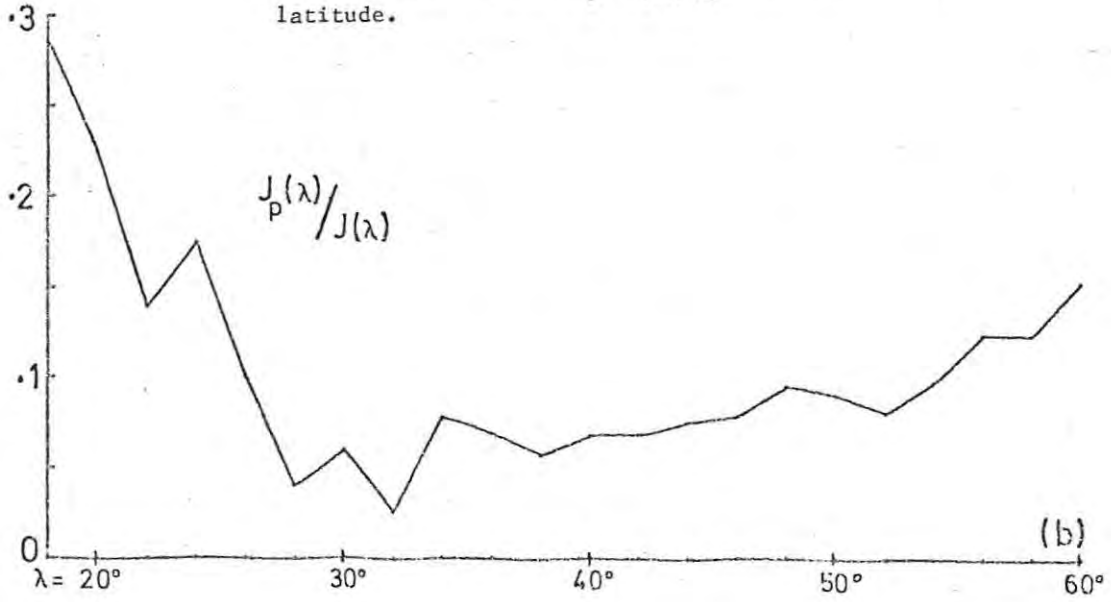

of the precipitated omnidirectional flux, $J_p(\lambda)$, to the total omnidirectional flux has been plotted. From this curve it can clearly be seen that the relative size of the precipitating component is greatly influenced by the presence of the anomaly. At $\lambda = 18^{\circ}$, the equatorward limit of the data spread, nearly one third of the observed flux is being precipitated.

Several precipitation mechanisms have been proposed. Among them we may count the leaky bucket model, successfully replaced by the splash-catcher model of O'Brien (1962, a), the interaction of electrons with whistlers proposal of Dungey (1963) and the self-excited pitch angle diffusion model of Kennel and Petschek (1966). We would like to present some calculations performed in an attempt to apply this last model to the Alouette I data.

Briefly the Kennel and Petschek model proposes that if the pitch angle distribution of the electrons is anisotropic enough, then the system will be unstable and will generate whistler waves. These self-generated whistlers may then interact with the trapped electrons and cause precipitation. The scattering process is a resonant interaction of the particle gyrofrequency and the whistler wave frequency.

Kennel and Petschek introduce a function A which is a measure of the pitch angle anisotropy of the electrons.

$$A = \frac{\int_0^{\infty} \frac{\partial f}{\partial \alpha} \tan \alpha \; v_{\perp} \; dv_{\perp}}{2 \int_0^{\infty} f \; v_{\perp} \; dv_{\perp}}$$

where: $\alpha = \tan^{-1} \frac{v_{\perp}}{v_{\parallel}}$ is the pitch angle

f is the distribution function for the electrons.

They show that if

$$A > \frac{1}{\Omega/\omega - 1}$$

where Ω is the gyrofrequency of the electron

ω is the frequency of the whistler generated by unstable system

then the system is unstable to grow whistler waves.

37/.....

By assuming the source of electrons to be at the point where $\alpha = \pi/2$, the expression for A can be reduced to

$$A = \frac{1}{2 \ln \left(\frac{1}{\alpha_o} + 1 \right)}$$

where: α_o is the loss cone angle at the equator.

We can convert the 55^o loss cone angle calculated for 1000 km altitude to the corresponding angle at the equator. Once again we use the mirror equation and also the values for Be and B^{1000}_{South} listed in table 7

L	=	1.25	1.50	1.75	2.00	2.50	4.00	5.00
α_o	=	38^o	77^o	19^o	15^o	10^o	5^o	3^o

We take $\alpha_o \sim 30^o$ ($\sim$ .5 radians) as representative of the loss cone angle at the lower L values considered in this analysis. We obtain for A, the anisotropy measure,

$$A = \frac{1}{2 \ln \left(\frac{1}{.5} + 1 \right)} = \frac{1}{2.2} = .45$$

The system will not support or initiate whistler waves if

$$\frac{\Omega}{\omega} - 1 > \frac{1}{A} \sim 2.2$$

or $$\frac{\Omega}{\omega} > 3.2$$

This lower limit for the value of the ratio of the electron gyrofrequency to whistler wave frequency can be used in the following expression. We have written the Kennel and Petschek expression for the energy associated with the resonant velocity of the electrons in the interaction.

$$E_r = \frac{1}{2} m v_R^2 = E_c \frac{\Omega}{\omega} \left(1 - \frac{\omega}{\Omega}\right)^3$$

where: E_c is the magnetic energy per particle ($= \frac{B^2}{8\pi n}$)

n is the particle number density.

We have:

$$E_r > 3.2 \left(1 - \frac{1}{3.2} \right)^3 Ec$$

$$> 1.04 E_c$$

38/.....

Now $E_c\ [\text{erg}] = \frac{B^2}{8\pi n} = C$, say, if we

express B in gauss

and n in cm^{-3}

so $E_c\ [\text{joules}] = C \times 10^{-7}$

and $E_c\ [\text{eV}] = \frac{C \times 10^{-7}}{1.6 \times 10^{-19}}$

$$= \frac{C}{1.6} \times 10^{12}$$

And so $E_c\ [\text{keV}] = \frac{C}{1.6} \times 10^{9}$

Returning to table 7 we obtain a value of $.6 \times 10^{-5}$ tesla as representative of the equatorial field BE in the L range we are considering ($L \sim 1.5$)

So $B \sim .06$ gauss

and $\frac{B^2}{8\pi} \sim 1.4 \times 10^{-4}$

We then obtain for E_c

$$E_c > \frac{1.4}{1.6} \times \frac{10^5}{n} \quad \text{keV}$$

$$> \frac{9 \times 10^6}{n} \quad \text{keV}$$

And so $E_R > 10^7$ keV

Remembering that n is the particle number density expressed in units of cm^{-3} we can see that even for a very high particle density of $10^3\ cm^{-3}$, the energy of the electrons needs to be of the order of MeV for self-excited whistler waves. Since we have concluded that there are very few natural electrons observed in this region with these energies, we may rule out the self-excited pitch angle diffusion precipitation mechanism as being responsible for the precipitation near the anomaly.

If, however, we take $\alpha_o = 3^\circ$ (= .05 radians) for the large L value edge of the data region we obtain:

39/.....

$$A \sim \frac{1}{3}$$

and $\frac{\Omega}{\omega} > 4$

so that

$$E_R > 1.69\ E_c$$

A result not very much different from the previous one.

But we have to use a value of

$$B \sim 1.5 \times 10^{-3} \text{ gauss}$$

(table 7)

and so $\frac{B^2}{8\pi} \sim 8.95 \times 10^{-8}$

Whence we obtain for Ec

$$E_c \sim \frac{8.95 \times 10^{-8} \times 10^{9}}{1.6\ n} \quad \text{keV}$$

$$E_c \sim \frac{56}{n} \quad \text{keV}$$

and so $E_R > \frac{95}{n}$ keV

This is a far more likely value for the energy of the electrons. The detector on board the satellite responded only to electrons with energies in excess of 40 keV. Taking a value of only 100 electrons cm^{-3} for n we obtain 1 keV as the minimum energy required by an electron before self excited pitch angle diffusion may take place. We may now ascribe the steady increase of the curve of figure 16 (b) towards high values to the increasing effect of this precipitation mechanism.

4.3 A MODEL OF EQUATORIAL PITCH ANGLE DISTRIBUTIONS.

Because quantities, such as the loss cone pitch angle at 1000 km can be transformed into equivalent values at the equatorial point on each field line, it is convenient to carry out comparisons between different magnetic shells at these points. In table 8 we have collected pertinent data from the previous analyses.

TABLE 8 .

DATA FOR MODEL STUDY

L	λ	α_s	α_o	$\alpha_s - \alpha_o$
1.25	7°	49°	38°	11°
1.50	22°	33°	27°	6°
1.75	30°	24°	19°	5°
2.0	36°	19°	15°	4°
2.5	44°	12°	10°	2°
4.0	54°	5.7°	5°	0.7°
5.0	59°	3.9°	3°	0.9°

The values in table 8 are most easily interpreted by reference to the accompanying diagram.

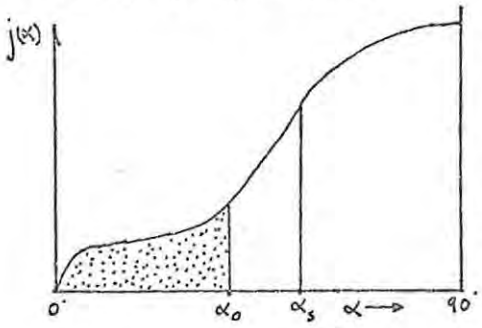

We picture a typical equatorial pitch angle distribution for electrons with energies greater than 40 keV. α_s is the maximum equatorial pitch angle possible for electrons which are to be detected at 1000 km. α_o is the loss cone angle of 55° at 1000 km projected back to the equator. Therefore the region between α_o and α_s contains those electrons which will be detected at 1000 km and which are trapped. The shaded region contains those electrons which are precipitating. We have ignored the backscattered component in this discussion.

The qualitative implications of the results of the $\frac{Jp(\lambda)}{J(\lambda)}$ graph in figure 16 (b) together with the values of α_s and α_o shown in table 9 are as discussed below. The high ($\sim \frac{1}{3}$) proportion of precipitated flux at $\lambda \sim 18°$ where α_s must be $\sim$ 40 and $\alpha_o \sim 32°$ suggests that α_o lies above the knee of the flux distribution curve. The difference $\alpha_s - \alpha_o$, would then lie along a relatively flat portion of the curve as shown in the diagram.

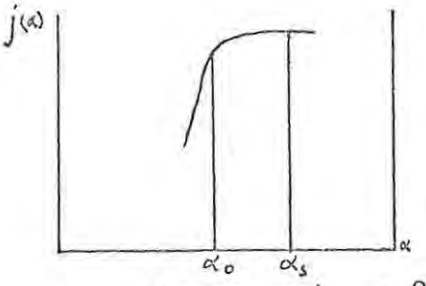

This interpretation allows for high values in both J (λ) and Jp (λ). Similarly the ratio value of $\frac{1}{3}$ is possible with such a distribution.

Moving to $\lambda \sim 33^{\circ}$, we can guess values of $\alpha_s \sim 21^{\circ}$ and $\alpha_o \sim 17^{\circ}$. Here we interpret a low $\frac{Jp\ (\lambda)}{J\ (\lambda)}$ ratio as meaning that α_o lies at the foot of the knee of the pitch angle distribution. Less flux is detected at

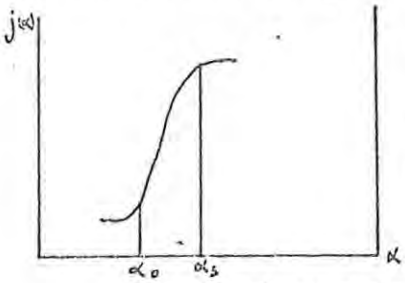

the 1000 km point and the ratio can quite easily drop to low values should the curve be very steep, implying a rather anisotropic distribution.

The final example is for L = 5 ($\lambda = 59^{\circ}$). In this case both α_o and α_s lie well below the steepest section of the pitch angle distribution curve. Once again $\alpha_s - \alpha_o$ may lie along a relatively isotropic section and the ratio $\frac{Jp\ (\lambda)}{J\ (\lambda)}$ can be expected to rise. This is observed.

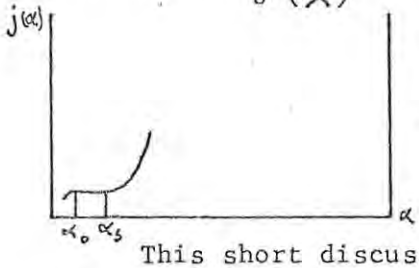

The measured fluxes should also be lower than elsewhere. Again this is observed in figure 16 (a)

This short discussion is of course very ad hoc and suffers from many shortcomings. Principal among these is the assumption of the existence of a similar pitch angle distribution curve over the full range of L. There is no reason why the pitch angle distribution should be consistent over L. The different precipitation mechanisms operating in different zones will each impose a characteristic shape on the distribution. Further we have ignored small pitch angle electrons which may have been backscattered. The consequence of this being that Jp (λ) will be slightly larger than it actually should be.

We have, however, attempted to develop a method of comparing the individual pitch angle distributions obtained for the 22 ranges of λ at 1000 km. The Liouville theorem, well known to plasma physicsts, allows us to consider

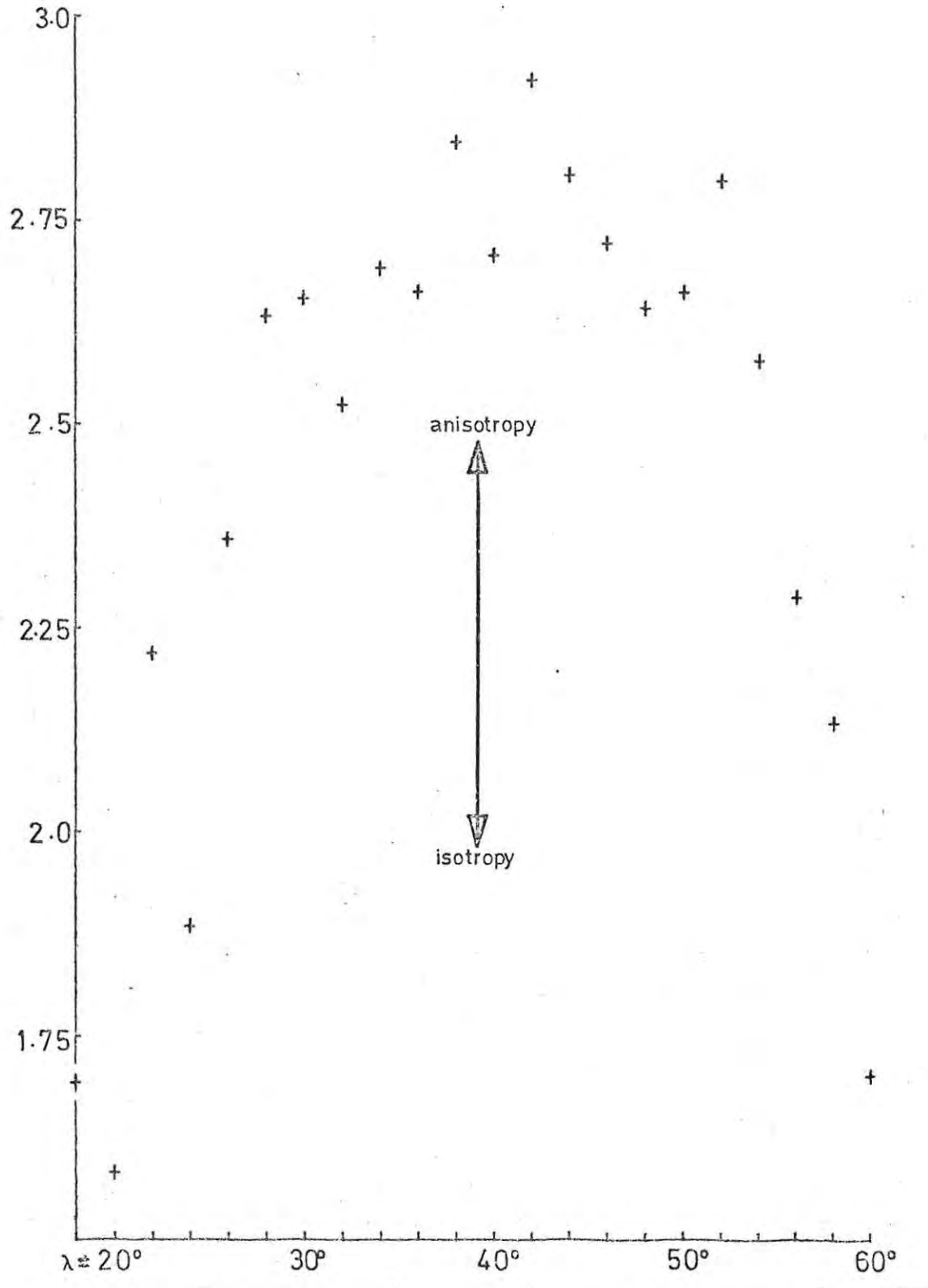

FIGURE 17. Anisotropy measure function (c) versus invariant latitude.

the observed distribution at 1000 km to be similar to the particle distribution elsewhere on the guiding field line. In this case we infer the equatorial pitch angle distribution from the 1000 km results.

Consider the diagram where we have drawn a typical pitch angle distribution curve from Appendix 4.

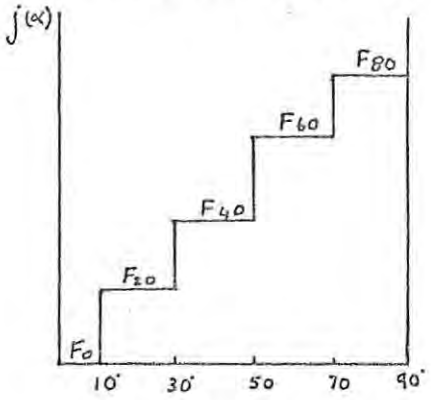

By assuming that

$$f(\alpha) \propto e^{c\alpha}$$

we may write

$$\frac{df}{d\lambda} = c\, e^{c\alpha}$$

so $$\frac{df}{f} = c\, d\lambda$$

Or $$\frac{\Delta f}{f} = c\, \Delta\lambda$$

so that $$\frac{\Delta f}{f} \propto c$$

i.e. by assuming that the distribution curve is made up of 4 portions of different exponentially increasing curves, a number, c, representing the 'steepness' of the histogram can be evaluated. The actual function used was

$$c = \frac{F80 - F60}{F80 + F60} + \frac{F60 - F40}{F60 + F40} + \frac{F40 - F20}{F40 + F20} + \frac{F20 - F0}{F20 + F0}$$

Because $F_0 = 0$, the last term is equal to 1. Large values of c will represent a 'steep' or very anisotropic distribution. Smaller values of c will result from histograms where the steps between each value are not very large. We have evaluated c using the median values displayed in the 22 histograms of Appendix 4. The result is graphed in figure 17.

The trends shown in this curve lend weight to our earlier interpretations of the data. The pitch angle distributions are more anisotropic for the middle λ values of the analysis. The two extreme edges have distributions which, while not isotropic, certainly are less steep. Because of the nature

43/.....

of the function c, a distribution containing a single large step at a middle value of α (see diagram) will yield a small value for c, reflecting the existence of two 'isotropic regions'. It is a distribution of this kind that we have already proposed to exist at the two edges of the region under consideration.

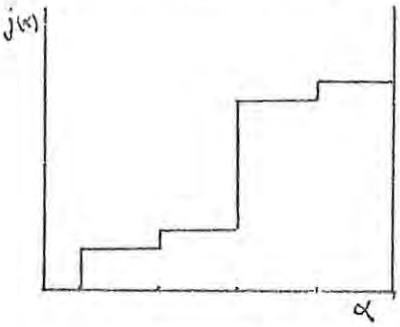

Acknowledgement is again made of the ad hoc nature of these suggestions and presentations. However, we contend that these hand-waving arguments and explanations do account qualitatively for the observations. A far more detailed and exact analysis where magnetic conditions and similar flux influencing phenomena are considered is necessary before it would be possible to nail down the behaviour of the pitch angle distribution. Also a distinction between upgoing and downgoing particles needs to be made. This has been achieved in satellites such as Injun V, carrying sophisticated particle detectors called LEPEDA (Frank and Ackerson (1971)). Nevertheless in spite of the relatively primitive devices and experiments aboard Alouette I, the results obtained are similar to those achieved elsewhere (e.g. Frank (1965), Frank et al. (1964), Paulikas and Freden (1964), O'Brien (1962, a), (1962, b), 1964). In addition we have presented some aspects of electron pitch angle distribution that we have not seen reported before.

4.4 THE SOVIET BOMBS AGAIN

We would now like to return to the statistic we introduced in section 2.5, the percentage of records in a particular set of records that have suffered 'overcorrection'. In that section we showed how this statistic allowed a rough estimate of the energy spectrum of the particles detected, to be made. We further suggested that the high percentages, which indicated hard spectra were due to the Soviet nuclear bomb tests. In this section we have prepared four graphs where we have plotted this percentage overcorrected statistic against invariant latitude. Each curve in figure

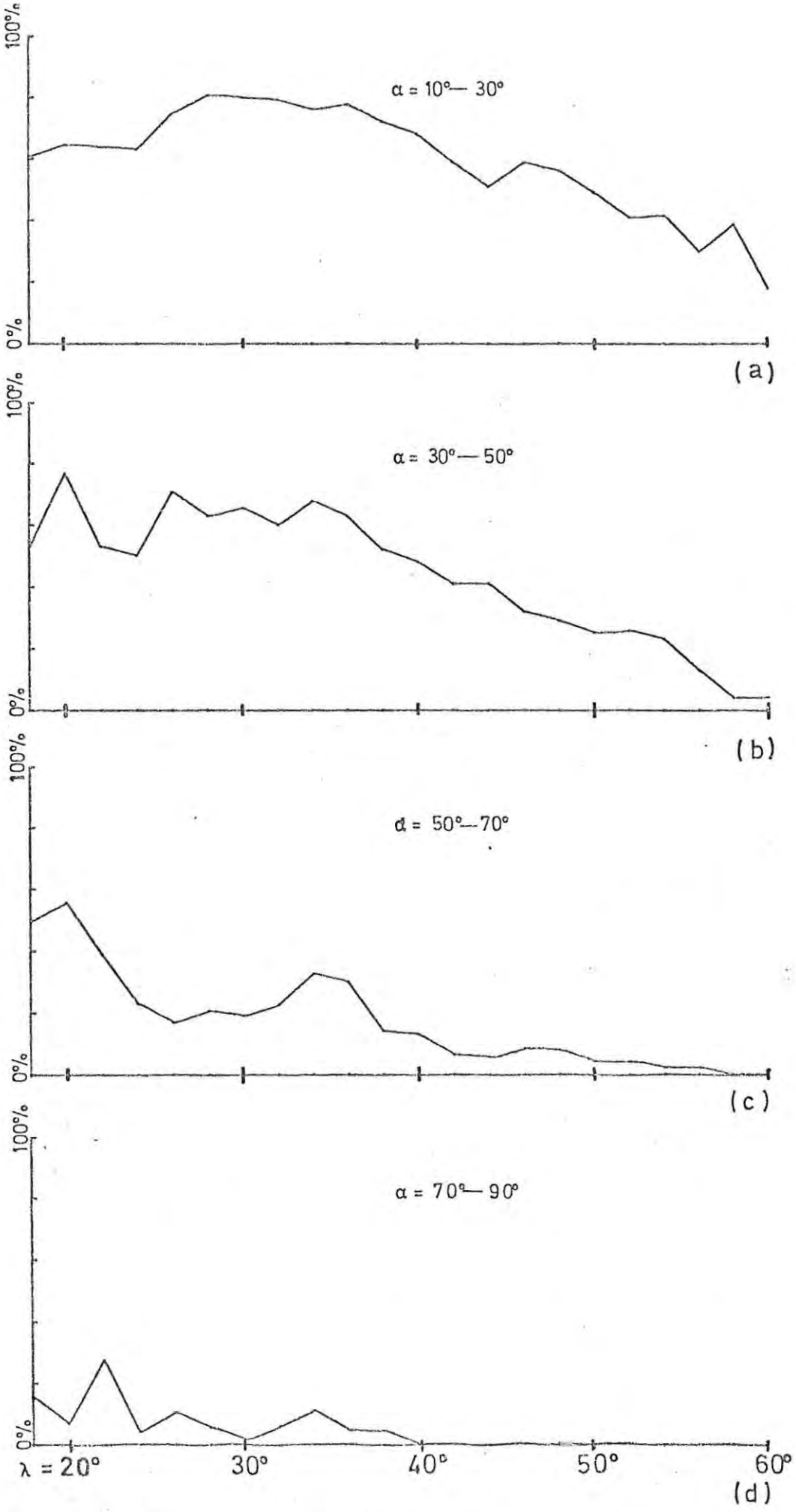

FIGURE 18. Percentage of records that were 'overcorrected' in each of the four pitch angle ranges, versus invariant latitude.

18 is for one of the pitch angle ranges described above.

The bombs were detonated at a longitude of about 60° East, and it is reasonable to assume that the high energy fission products were expelled isotropically. The electrons released must have completed at least 3/4 of a drift path around the earth before being detected by Alouette I in this region. Protons and other positively charged particles must have travelled about 1/4 of their drift path before reaching the present detection region.

The observed products of the explosion are certainly not distributed isotropically in pitch angle. Very high energy particles with small pitch angles dominate the scene. Another observation that can be made concerns the dependence of the spectra on the invariant latitude. The different pitch angle ranges react in different ways to the presence of the geomagnetic anomaly. Particles mirroring at or near to the satellite appear to be principally natural electrons. This is indicated by the softness of the spectrum implied by the low values of figure 18 (d). The hard spectra of the precipitating component of the bomb products (figure 18 (a), (b),) have a distribution in invariant latitude similar to the curve for the total spectrum (figure 9 (b)). Only the two curves representing the trapped portion of the fluxes appear to have been markedly influenced by the geomagnetic anomaly.

The lack of any bomb particles mirroring at 1000 km in this southern hemisphere region indicates that the probable heights of the detonations was below 1000 km. We have in fact observed a forward wing butterfly type of distribution described by Van Allen (1968).

4.5 ELECTRON PITCH ANGLE DISTRIBUTIONS IN LONGITUDE.

Exactly similar analyses to those described in previous sections were carried out on the results obtained from the 27 directional flux

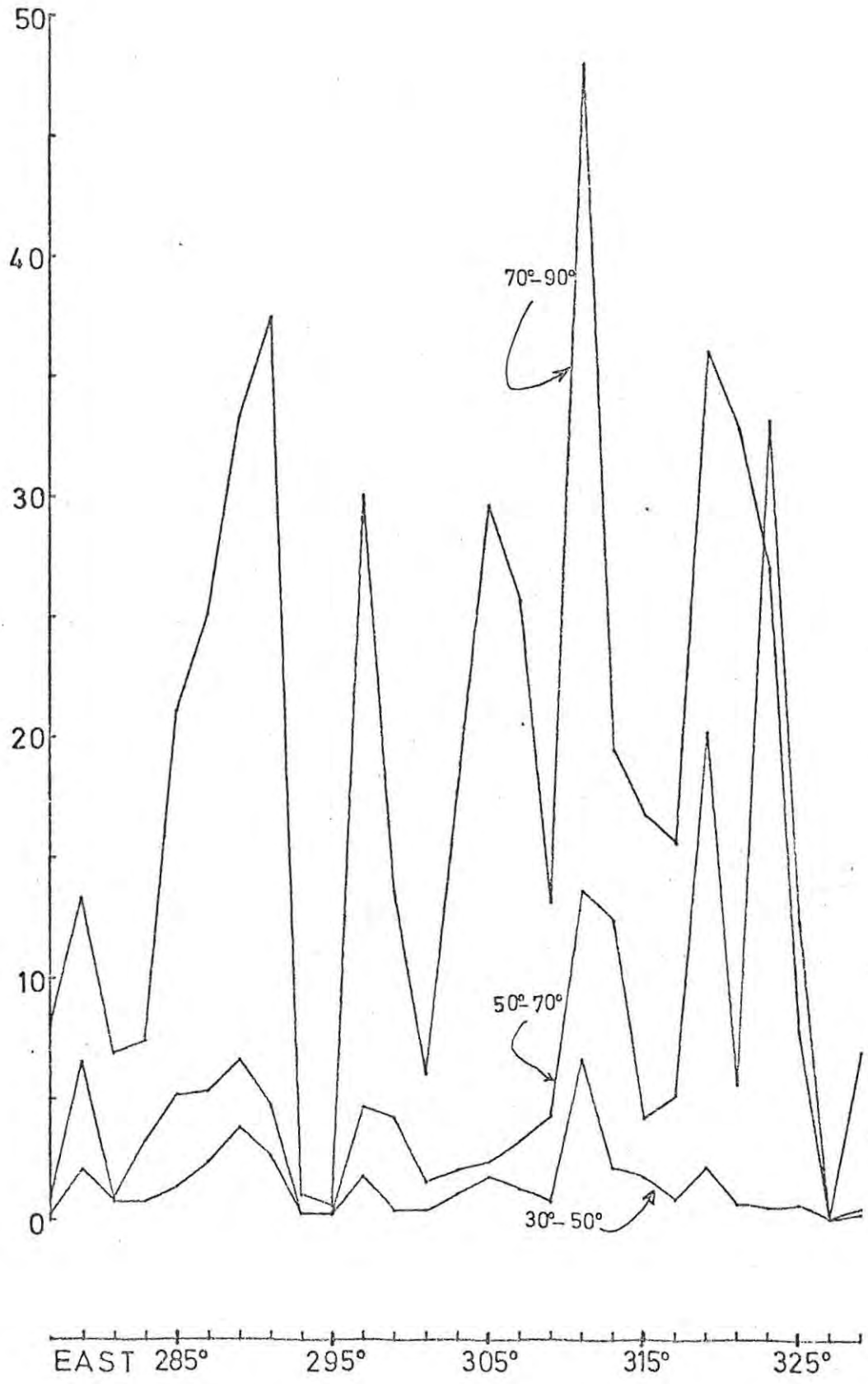

FIGURE 19. Median directional flux distributions for 3 pitch angle ranges, normalised by the median flux value for the 10°--30° range, versus longitude.

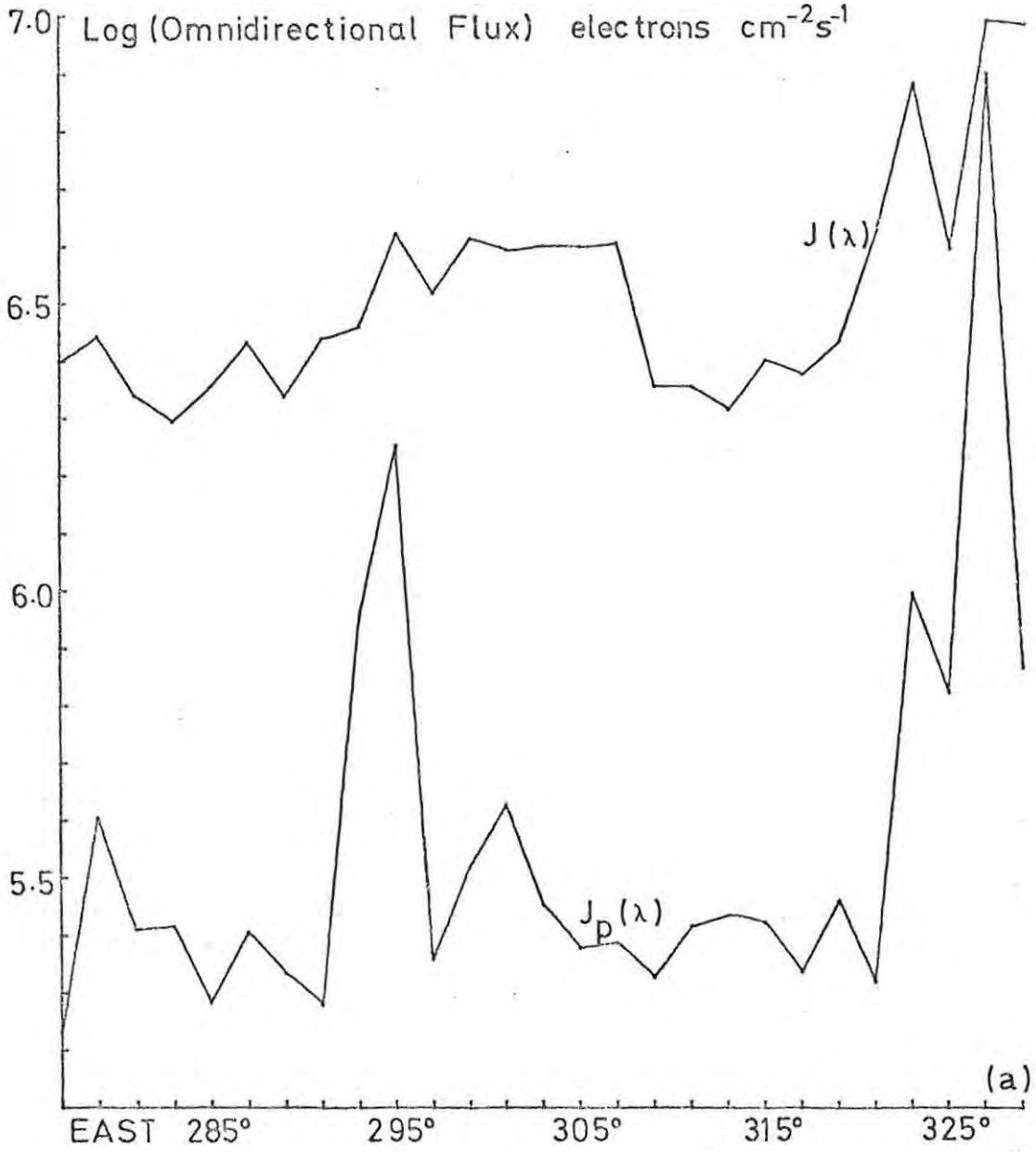

FIGURES 20(a). Total omnidirectional flux J(long.) and precipitated omnidirectional flux component J_p(long.) versus longitude.

20(b). Ratio $J_p(\text{long})/J(\text{long})$ versus longitude.

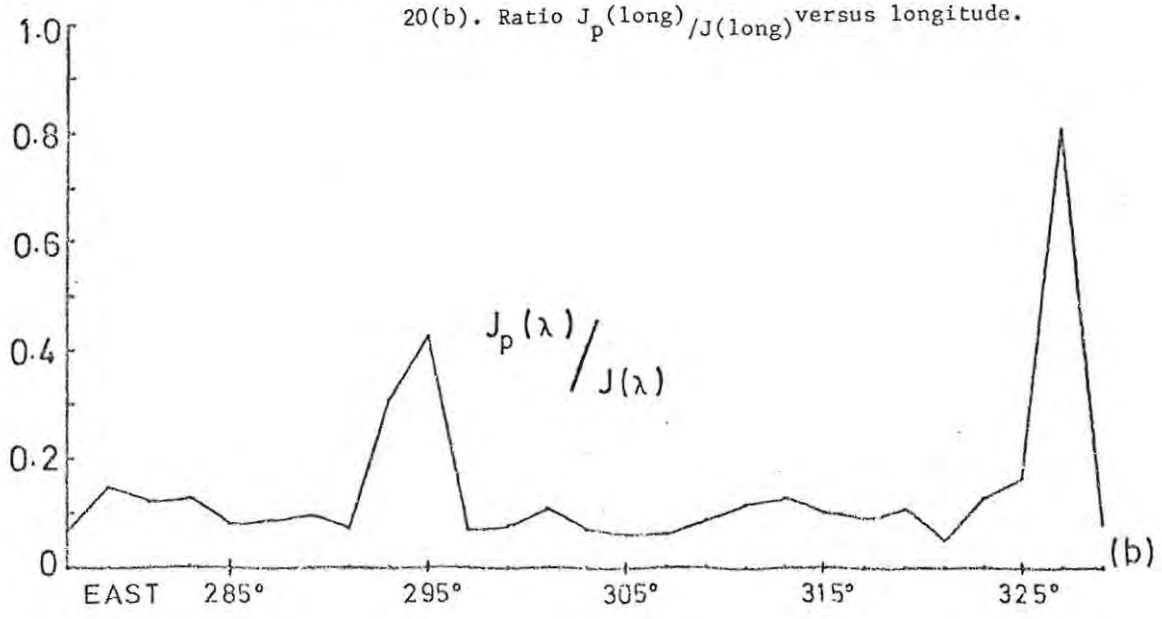

median versus pitch angle histograms, which may be found in Appendix 4. Figure 19 is the graph of the median flux values for the three pitch angle ranges above 30°, normalized by the median flux of the 10°- 30° range. It is obvious that the flux distributions are very different from those shown in figure 14 for the invariant latitude analysis. The largest median flux value for some particular longitude strip is not always the one for pitch angles in the range 90° - 70° (e.g. at 293°, 295°, 327° East). We can not ascribe these anomalous occasions to the error incurred by selecting the median rather than the mean value as representative of the set of records, since figure 8 showed a relatively small spread in the data for the records centred on those three longitude values. We can suppose that the high fluxes at small pitch angle are recorded at the northern end of the longitudinal strips which is where the high fluxes have been shown to exist. To determine changes in the flux distribution in pitch angle with longitude the omnidirectional flux for each of the longitude samples was computed. Also the precipitated component and the ratio $\frac{Jp\ (long)}{J\ (long)}$ was calculated and plotted (figure 20 (a) and (b)). In figure ~~18~~ 20 (a) the dominant features of figure 19 persist. An order of magnitude increase of Jp (longitude) over a peak width of 6° centred on 295° is observed, and an even larger increase which has a western limit at 321° East dominates the picture. Figure ~~18~~ 20 (b) emphasises the sharpness of the two peaks. The eastern prominence in these figures occurs at the same longitude where we discovered sharp increases in directional flux values when moving eastward along of constant invariant latitude near the geomagnetic anomaly (figure 10). Combining this result with the results from figure 16 (a), the omnidirectional flux distribution in λ, we can determine a boundary for the region of large precipitation of electrons:-

Equatorwards of $\lambda = 28^{\circ}$

Eastwards of 323° East.

It is harder to find a reason for the presence of the precipitation

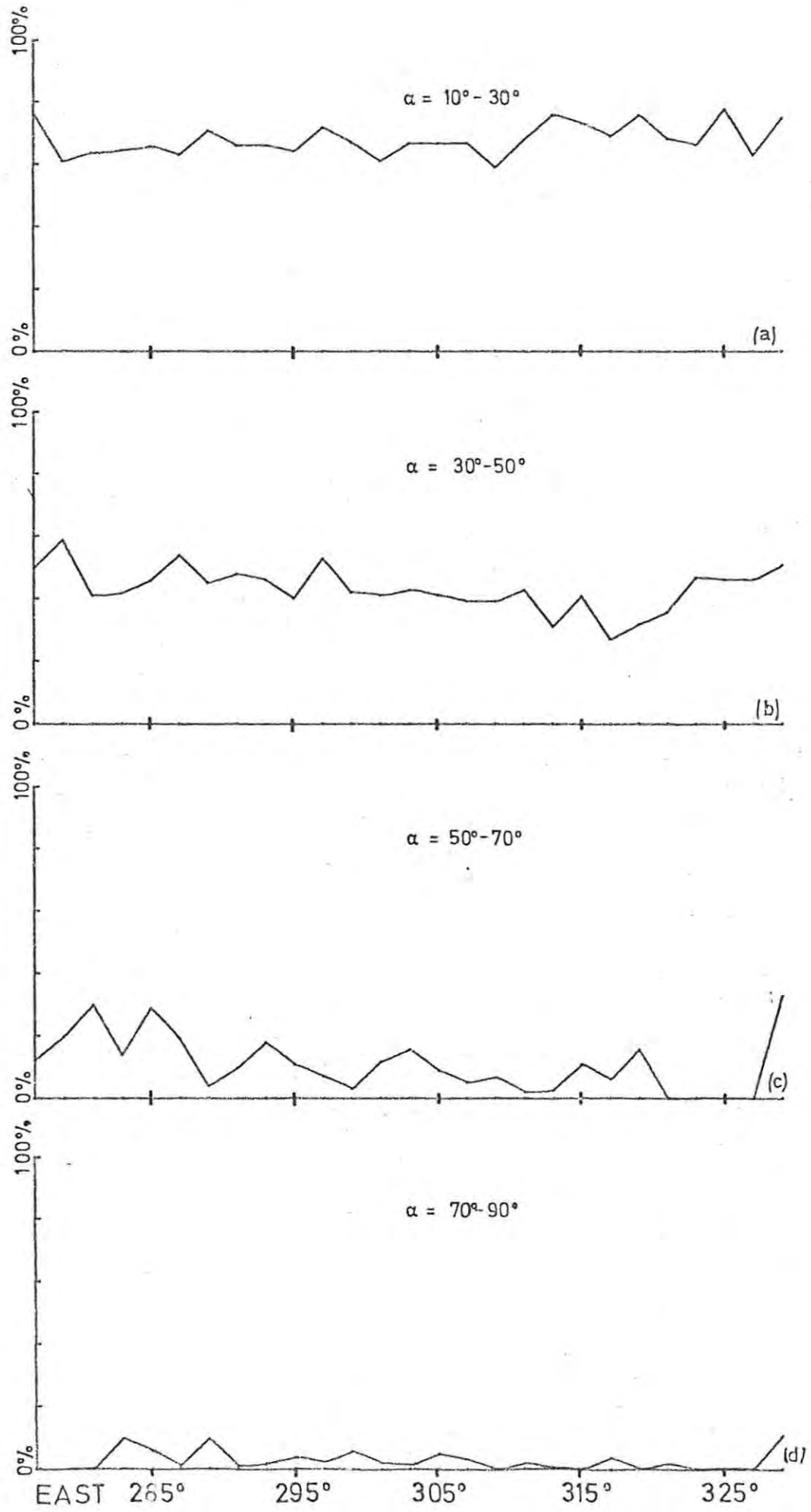

FIGURE 21. Percentage of records that were 'overcorrected' in each of the four pitch angle ranges, versus longitude.

enhancement at around 294° East. The calculation of J (long) and Jp (long) used the median flux value in each pitch angle range. The mean/median difference curve of figure 8 also exhibits a large value at this longitude. If this large difference indicates the occurence of a few large fluxes then these large values have filled the low pitch angle intervals sufficiently to influence the medians. This we can deduce from the increase of Jp (long) We suggest that we have a result of an electron precipitation event - probably along the lines of the splash catcher model.

4.5.1 THE BOMBS

In figure 21 we have plotted the percentage overcorrected figure for each of the pitch angle ranges. The results confirm the suggestion that the bombs' products have been scattered into a small pitch angle hard spectrum distribution. Each curve displays little or no longitude dependence and the average value of each drops steadily lower for increasing pitch angle. The total sample mean overcorrected figure is just over 42%.

4.6 CONCLUSION

It is not really possible to draw any conclusions from the myriad of superficial results presented in this chapter. We do not presume to be able to add any significant physics to theories which are extant. However, comments and suggestions have been made where possible about the observations and their causes. The nature of this thesis is primarily one of reporting.

--- 0 ---

CHAPTER 5.

THE LOCAL TIME VARIATION OF THE ELECTRON DIRECTIONAL FLUX

5.1 INTRODUCTION

The analysis described and discussed in this chapter was the last one carried out for this project. It is, however, pleasing to report that the old adage applied here as well, for the results are certainly not the least interesting obtained. Hess (1968) complains that the diurnal variations of trapped particle fluxes for regions where λ is less than 60° are virtually unknown. In addition the explanations for the observed patterns at higher latitudes are also not very well developed. (O'Brien (1963)).

We have carried out a local time variation investigation over the full range of λ available (18° - 62°). The survey covers the directional fluxes of electrons with energies greater than 40 keV. An analysis of the local time variations of the fluxes for different longitude regions was also performed. The results of this analysis have revealed a hitherto unreported structure in the distribution.

5.2 DATA PREPARATION.

A local time value was computed for each record. The tabulated universal time and sub-satellite longitude were used for the computation. After the initial sorting of the records into the intervals of invariant latitude and geographic longitude described before, the records within a 'strip' were sorted into 12 intervals of local time. Each of these intervals is 2 hours wide. The median value of the corrected 223-type directional electron fluxes within the interval was computed and was used to represent the flux for that time interval. In Appendix 5 we have presented the 22 + 27 median flux / local time histograms.

48 /....

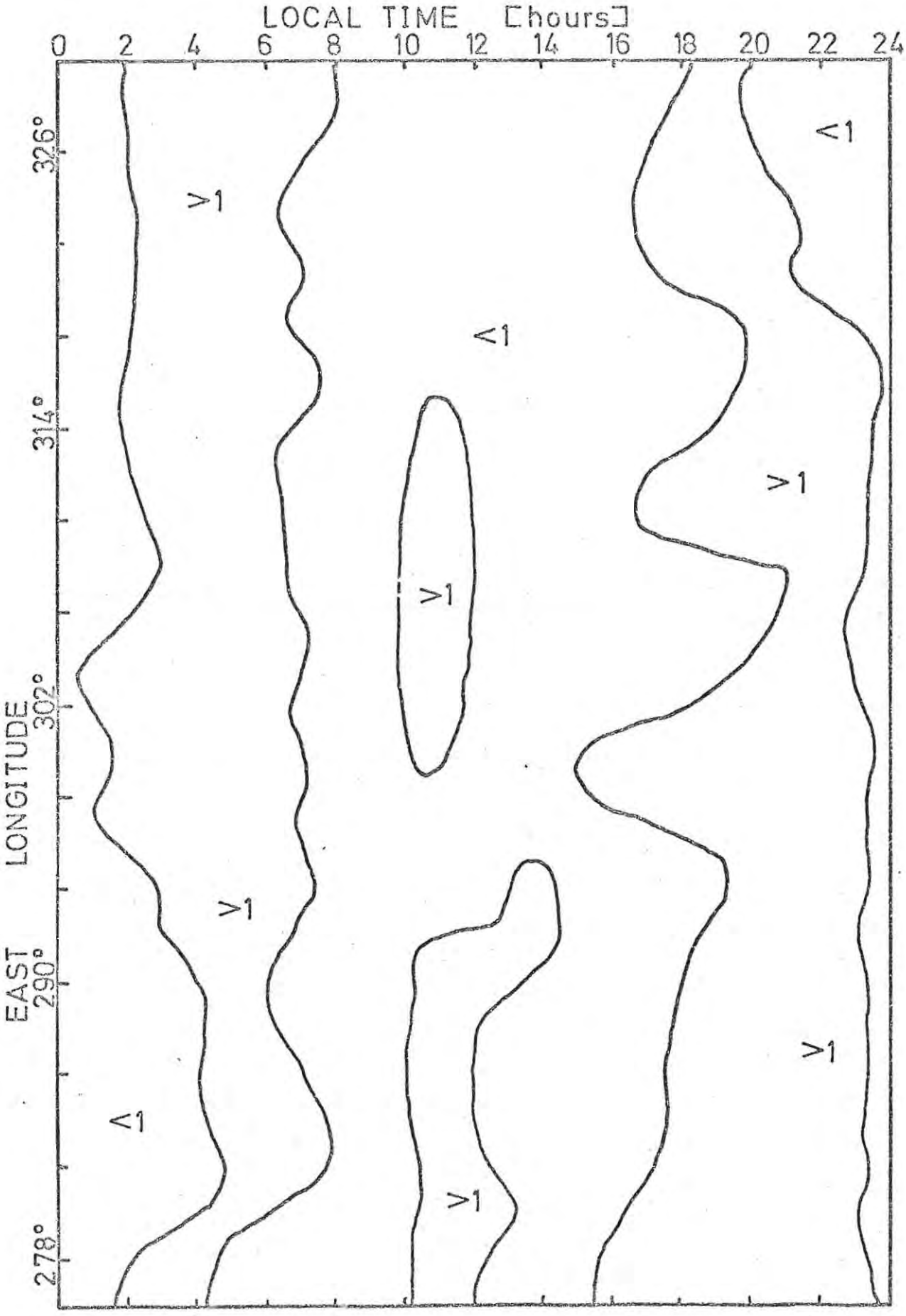

FIGURE 22. Directional flux enhancements in local time versus longitude.

With a method identical to the one used to produce the tables 3 and 4 we have produced the two 'maps' used in this chapter - figures 22 and 23. The median flux value for each time interval in each λ or longitude 'strip' was normalized by dividing by the 'strip' median. In this way it was intended to remove the flux intensity dependence on either the invariant latitude or the longitude. However, the distribution pattern of the local time variation was retained. Hence two grids, the first being 22 invariant latitude rows by twelve 2-hourly rows, and the second having 27 longitude rows, were prepared and completed. The contour maps discussed in this chapter were drawn from these grids. Only one contour line was drawn. The value of 1 was chosen for this contour line because regions greater than 1 represented times and positions where the directional fluxes were higher than normal.

We again acknowledge the statistical shortcomings of this procedure. However, the stability of position of the features of the distribution does in some measure justify the use of this method. The enormous amounts of data available necessitated some sacrifices of accuracy to be made for compatibility with page size.

5.3 DIURNAL FLUX DISTRIBUTION IN LONGITUDE

It is convenient to present and discuss the longitude map first (figure 22). The prominent feature of the diagram is the night time enhancement of flux intensity that is clearly split by a very narrow post-midnight trough. The two portions of an enhancement near local noon are numerically much smaller than the values within the principal feature, and so are probably insignificant by comparison.

Several factors need be considered in the discussion of this night-time enhancement. Obviously the term night-time can not be applied meaningfully. Most of the records were obtained during a southern hemisphere summer. At 1000 km therefore, in some of the latitudes we are considering, the hours of darkness are very limited. The enhancement commences at

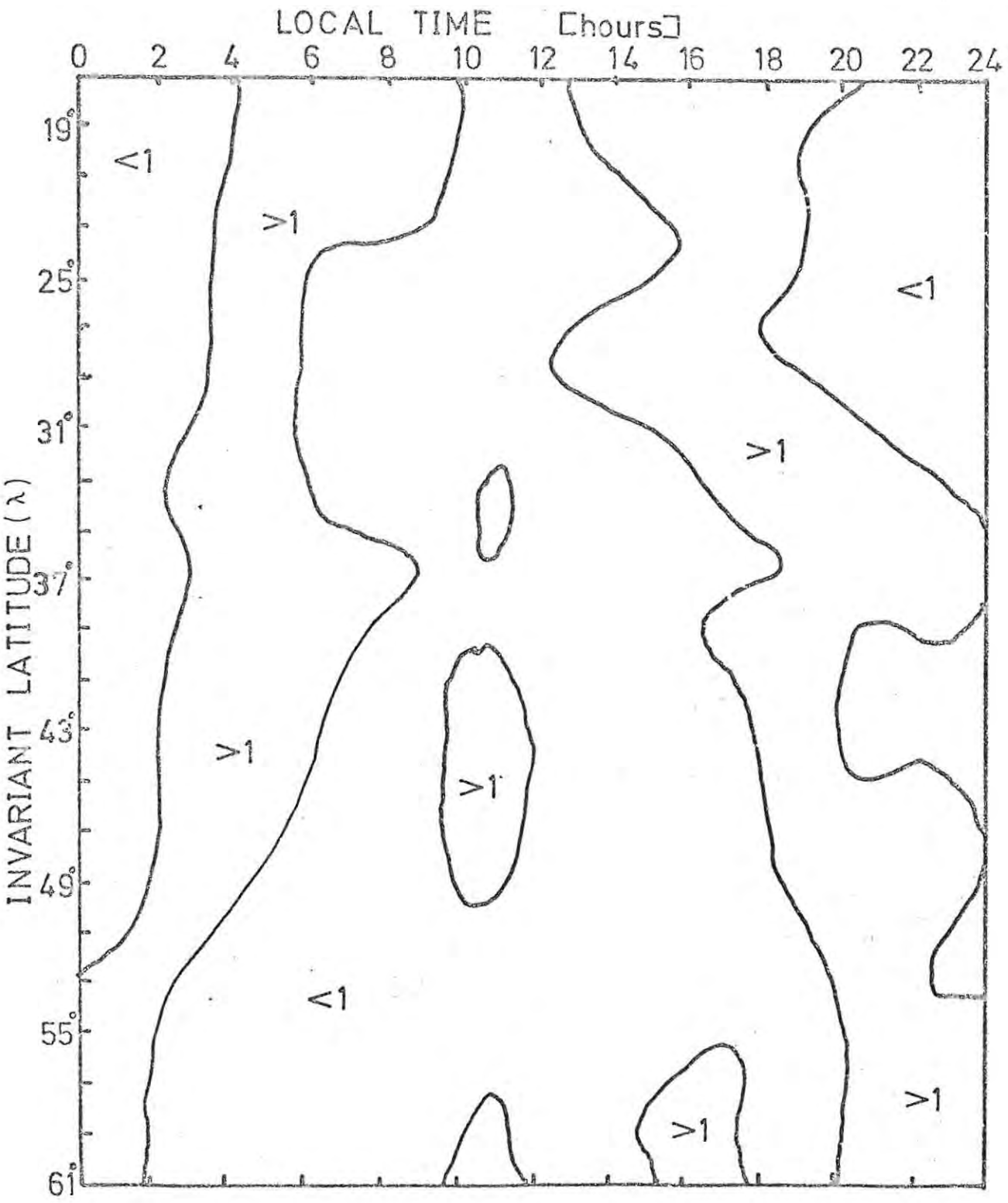

FIGURE 23. Directional flux enhancements in local time versus invariant latitude.

about 1800 hrs $\pm$ 2 hours and terminates very markedly at 0700 hours $\pm$ 1 hour. The feature observed is no doubt a function of the configuration of the geomagnetic field lines at different positions throughout the magnetosphere. The presence of sunlight clearly must have no effect on electron fluxes of this energy range in the radiation belt.

The midnight slot is seen to be between two and three hours wide and commences very soon after midnight. Because the units of time are 2 hours wide it is not possible to detect whether the slot may in fact start just before midnight. There is no great variation of the pattern with longitude. What variations that do exist are likely to be due to data irregularities rather than real effects.

5.3 DIURNAL FLUX DISTRIBUTION IN INVARIANT LATITUDE

The contour map obtained from the invariant latitude analysis is shown in figure 23. Again the contour line separates areas where the flux was larger than the ambient conditions for that latitude. There is certainly a co-ordinate dependence of the distribution of the fluxes in this map.

The night-time enhancement is present at $\lambda \sim 18^{\circ}$ but appears as two very distinct features. The first is centered at 0700 hours and the second at 1700 hours. With increasing invariant latitude the two enhancement features approach each other, 'squeezing' the midnight slot. At $\lambda \sim 53^{\circ}$ the enhancement becomes a single feature. This peak retains its width (about 4 hours) and position for the remainder of the invariant latitude scan. The two small regions of high flux equatorward of $\lambda = 50^{\circ}$ at local noon are relatively insignificant. The appearance of two enhancement periods at the higher latitudes are numerically not very large either. Data coverage does not allow for verification of the emergence of a noon peak as observed by Frank et al. (1964).

50 /.....

5.4 A DISCUSSION.

Increases in counting rates, simply imply that more electrons are being detected per unit time than were previously being detected. Because the detector (223-type geiger counter) that we have used for our analysis only detected electrons with energies greater than 40 keV, counting rate increases can also signify the occurrence of acceleration processes raising more electrons to energies above this 40 keV threshold.

The flux enhancements noted in the local time analyses that we have performed in this chapter are likely to be due mainly to the action of an acceleration process. This process must be a result of the geomagnetic field line distortions that occur during the passage of a field line in each revolution of the Earth.

An attempt was made to construct a model of the magnetosphere following the ideas of Mead and Beard (1964) and Mead (1964). For our model we proposed to use the eccentric dipole internal geomagnetic field source. Further, the model was to cater for a range of the Earth spin axis angles (seasons). Computations were abandoned because of numerical problems in the mathematical model on the computer before the first complete magnetospheric surface (Mead and Beard) was obtained.

We suggest that a knowledge of the behaviour of the field lines passing through the region being considered would be of great value in assessing the possible acceleration processes. It is possible that some of the field lines we are considering are distorted right out to the earthward edge of the plasma sheet at local midnight (Frank (1971)).

Frank and Ackerson (1972) have investigated the diurnal dependence of the precipitated portion of the electron flux. They observe enhancements in the late evening, early morning and at midnight. In their work they suggest that the plasma sheet may be a source of the electrons which are energised once they enter the belt. However, the processes of energization and entry are still not clear.

51/.....

5.5 CONCLUSION.

The two maps which have resulted from the analyses described in this chapter will have to stand for themselves. It appears that even in the current literature there is much doubt as to the source of the trapped particles in the radiation belts and the energization processes. We hope that this presentation of the previously unnoticed features will add to the evidence needed for the formulation of a successful model.

--- 0 ---

CONCLUSION

The nature of this thesis has been simply to present, in the best possible way, the results of certain analyses. The analyses concerned the distribution of Van Allen radiation belt electrons of a certain energy range. It was certainly not within the writer's capability to do more than comment on the results obtained and discuss their implications through comparisons with the literature. The overall characteristics of the radiation belts are becoming more and more well defined and we hope that the small contribution made by this thesis will complement past studies and direct future ones.

The energetic particle data from Alouette I is indeed limited in its coverage and in its particle energy information. However, as was inevitable, several possibly useful and interesting lines of further research emerged during the compilation and write-up of this present survey. First of these lines would be to take the magnetic conditions into account when considering electron fluxes. A rudimentary analysis identical to the one described in this thesis, but performed only on records where K_p was 4 or less was carried out. The results showed no significant distribution changes, but flux levels dropped by about a third. Following the ideas of other workers it appears that it would be necessary to compare this analysis not with the total records analysis as we have done, but rather the comparison should be made with an analysis performed on records where K_p was greater than 4.

A second follow-up topic of research would be to attempt to find particle pitch angles in the range 0^o - 180^o. Some figures and graphs sent to the research group by McDiarmid make it possible to obtain the actual direction of the satellite spin axis in space. In this way the pitch angle data could be sorted into upcoming and downgoing components. Consequently the action of the various proposed precipitation mechanisms could be investigated and tested more rigorously than was possible in this thesis.

The local time/.....

The local time distribution of electrons at low magnetic latitudes is obviously a field for much further investigation. We consider, however, that the Alouette I data is of little more use in yielding data concerning this distribution in the South Atlantic region. Data from another satellite will be required for further work in this connection. The local time distribution of trapped electron fluxes can provide a wealth of information about the loss rates and acceleration processes which are at work in the magnetosphere. This particular line of research when coupled with pitch angle analyses is therefore of the greatest interest and value.

At the time of writing this thesis the research group here at Rhodes University was eagerly awaiting data tapes from the Injun $\underline{\overline{V}}$ satellite. This data kindly promised by Dr. J.D. Craven,will no doubt complement and enhance the studies completed so far.

--- 0 ---

ABSTRACT

Directional flux distributions of electrons with energies greater than 40 keV at an altitude of 1000 km are presented. The survey covers a region south-west of the geomagnetic field strength anomaly in the South Atlantic.

The distribution of these electron fluxes measured over a range in L of 1.3 to 5.0 are contrasted with distributions observed in the conjugate area. A simple model to explain the effect of the geomagnetic anomaly on the fluxes is discussed.

An analysis of the observed pitch angle distributions is linked to a discussion of the possible particle precipitation mechanisms.

Finally the local time distribution of the electron fluxes is presented and discussed. A post-midnight 'slot' in a night-time flux enhancement feature is reported.

--- 0 ---

APPENDIX 1

DIRECTIONAL FLUX, OMNIDIRECTIONAL FLUX AND GEOMETRIC FACTORS

Consider an element of area δ A, perpendicular to the magnetic field direction $\overline{B}$. We choose a set of cartesian axes with $\hat{z}$ in the direction of $\overline{B}$.

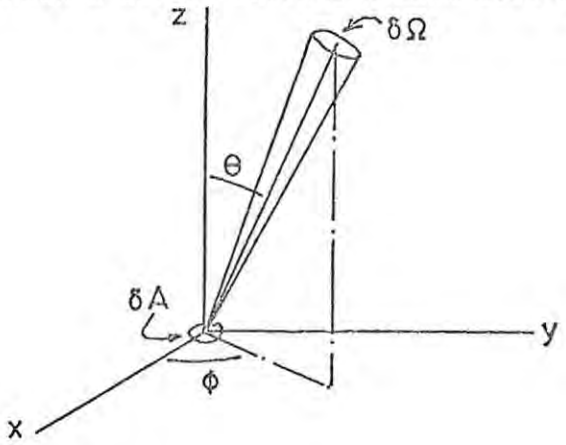

Roederer (1970) defines the directional flux density j as

$$\delta N (\Omega, E, t) = j (\Omega, E, t) \delta A \cos \Theta \quad \delta \Omega \quad \delta E \delta t$$

where: δN is the number of particles with energies in the range (E, E + δE) which crosses δA from the direction (θ, ϕ) in the solid angle $\delta \Omega$ in time δt.

In practice this definition is rather too formal and impractical for the use of the particle physicist. The most serious difficulty arises from the need to define an energy range δE for the particles to be detected. In general the only energy measure obtainable is a minimum particle detector threshold energy. Consequently the most usually measured quantity is the integral directional flux density. This is obtained by integrating the directional flux density with respect to energy from E_T to ∞, where E_T is the threshold energy. It is this quantity that we have used through this work, but we have used the notation j (α) as is conventional. Units of j (α) are generally particles cm^{-2} sr^{-1} s^{-1}.

If we consider the case of a population of particles trapped on a single guiding geomagnetic field line (ignore drift motions), it is

possible in/.....

possible in principle to measure j (α) at any point on the field line. However, the function J - the omnidirectional flux-completely describes all the particles on the field line. From the Liouville theorem

$$j_o (\alpha_o) = j (\alpha)$$

where j_o is the directional flux distribution at the equatorial point of the field line

j is the directional flux distribution at any point on the field line.

This allows us to compute J through the expression

$$J = 2 \int_0^{\pi/2} j (\alpha) \; 2\pi \sin \alpha \; d\alpha$$

even though we may only know j (α) for a point not at the equator (Hess (1968)). Omnidirectional fluxes are quoted in units of particles $cm^{-2} s^{-1}$.

One of the first papers to present radiation belt results (Van Allen et al. (1959)) contains a footnote that explains the use of geometric factors.

The unidirectional geometric factor G is defined by:

$$G \; \frac{D}{-} \; \frac{R}{\epsilon j}$$

where: R is the true counting rate of the detector

j is the directional intensity of the radiation in units of cm^{-2} sr^{-1} s^{-1}

ϵ is an efficiency factor for the detector.

Units of G are cm^2 sr.

--- 0 ---

COMPUTER SYSTEM FLOWCHART.

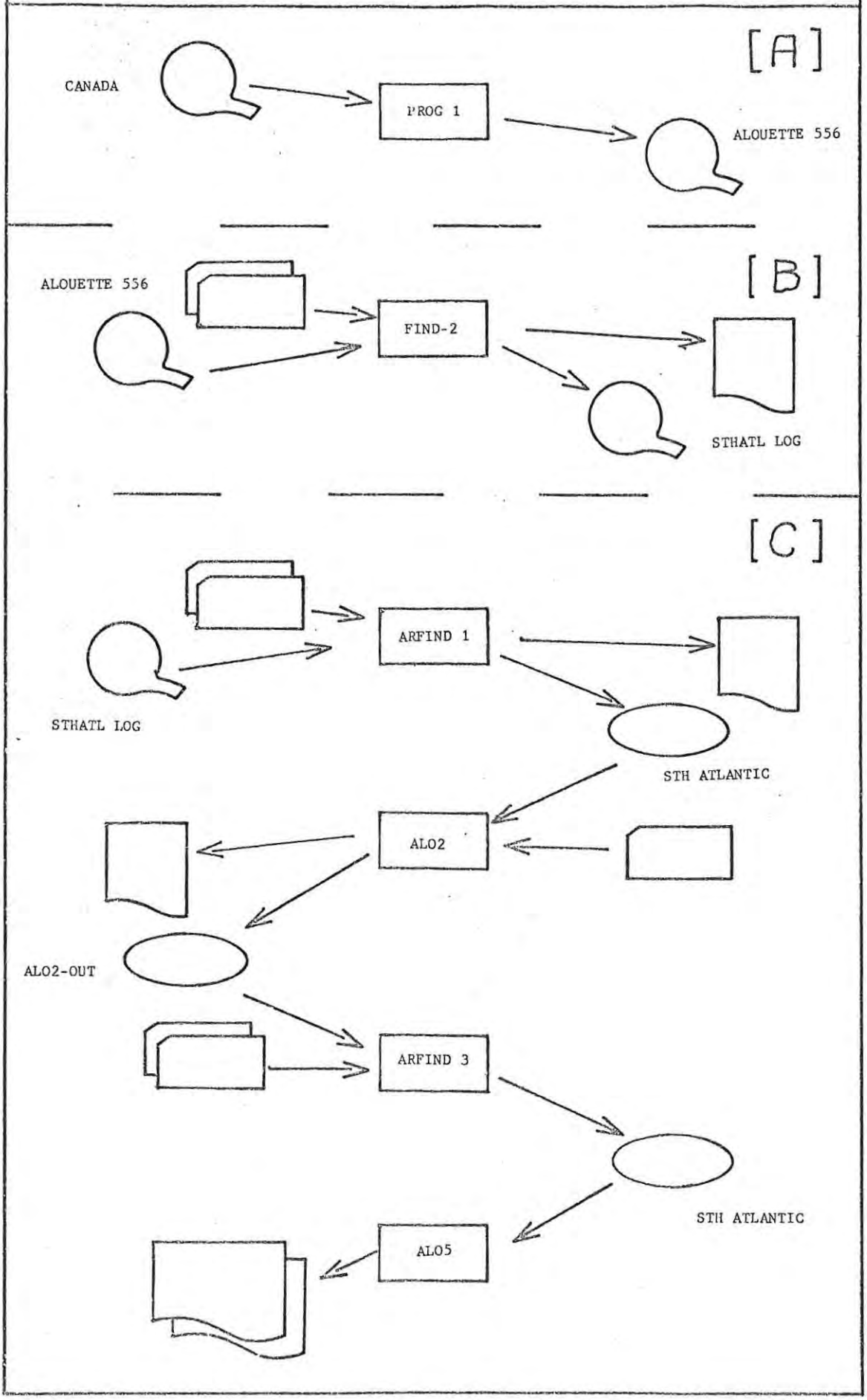

APPENDIX 2

THE COMPUTER SYSTEM

The computational work was almost entirely performed on the I.C.L. 1901A digital computer currently installed at the Rhodes University Computer Centre. All the systems and programs were designed and written by the author. Two high level languages, EMA and 1900 FORTRAN were used. In addition, extensive use was made of an I.C.L. file scan and report package known as FIND - 2.

A description of the computer system is made brief if we refer to the system flowchart opposite. We consider the operations in three sections.

A. Conversion of 9-track EBCDIC code magnetic tape to 7-track BCD code. The program was written by Mr. M.A. Lawrie of Messrs. I.C.L. in Cape Town. The output tape of this operation was labelled ALOUETTE 556.

B. Sorting of ALOUETTE 556 and extraction of records received at South Atlantic station. This operation was carried out by FIND-2. Several parameter cards were required. The output tape was labelled STHATL LOG.

C. This operation was performed by four separate programs.

ARFIND 1 This program scanned the tape STHATL LOG and extracted records that satisfied certain requirements. These requirements were of two types depending on whether the 22 invariant latitude strips were being processed or whether the 27 longitude strips were being processed.

(i) Records with invariant latitude values falling within the limits of the current analysis.

(ii) Ditto longitude.

This Program/...

This program was the I.C.L. FIND-2 package. Several parameter cards were required. Output of the 'hit' records was to a disc file named STH ATLANTIC. An output report listed the number of records that were 'hits'.

ALO2 This program read the records on the file STH ATLANTIC and performed three operations on each record before outputting the changed record to a disc file named ALO2- OUT. The operations were:-

1) Conversion of $\log_{10}$ 223-type count rate and
$\log_{10}$ 302-type count rate to real numbers.

2) Computation of corrected 223-type count rate.

3) Computation of local time value for the record.

The program produced a brief output report verifying that it had read all the input records. The program was written in FORTRAN.

ARFIND 3 This program scanned the records in the file ALO2-OUT and compiled 'hit lists'. These hit lists consisted of counts of the number of records that satisfied certain condition. These conditions comprised the heart of the analysis. Records were 'interrogated' about their corrected 223-type count rate, their pitch angle value, their local time value, their universal time value and their longitude value (in the case of the invariant latitude survey) or their invariant latitude value (in the case of the longitude survey). To each record, the program appended a numerical field which defined which interrogations had scored a 'hit' in that record. These enlarged records were output to the disc file STH ATLANTIC. An output record gave details of 'hit' counts.

APPENDIX 2 (CONTD.)

AL05 This program used the records of STH ATLANTIC as input data. It scanned the appended numerical field to identify those records falling into each analysis group. Within each group this program counted the number of records and the number of records that had suffered 'overcorrection'. Further computation yielded the maximum, minimum, mean and median corrected 223-type count rates in each group. These count rates were multiplied by 2200 to convert to directional flux. An output report contained all these values and formed the basis of the whole survey.

This program was written in two languages : EMA and FORTRAN.

The third operation (C) was carried out 22 times and 27 times for the invariant latitude and the longitude analyses respectively. In addition the system was also run several times to produce the northern hemisphere results from Ottawa and St. Johns.

--- 0 ---

APPENDIX 3

NUMBER DISTRIBUTION OF DIRECTIONAL FLUXES

In this appendix we present the histograms of the number distributions of the directional flux values of electrons with energies greater than 40 keV. The flux range of 0 to ∞ electrons cm^{-2} sr^{-1} s^{-1} is split into 18 non-equal intervals.

1	0	-	10^5	electrons cm^{-2} sr^{-1} s^{-1}
2	1×10^5	-	2×10^5	"
3	2×10^5	-	3×10^5	"
4	3×10^5	-	4×10^5	"
5	4×10^5	-	5×10^5	"
6	5×10^5	-	6×10^5	"
7	6×10^5	-	7×10^5	"
8	7×10^5	-	8×10^5	"
9	8×10^5	-	9×10^5	"
10	9×10^5	-	10^6	"
11	10^6	-	2×10^6	"
12	2×10^6	-	4×10^6	"
13	4×10^6	-	6×10^6	"
14	6×10^6	-	8×10^6	"
15	8×10^6	-	10^7	"
16	10^7	-	5×10^7	"
17	5×10^7	-	10^8	"
18	10^8	-	∞	"

It should be remembered when consulting the histograms that the intervals differ in size. No results or conclusions were drawn directly from these histograms so the choice of interval size was one of convenience.

Two groups/....

Two groups of histograms are presented. The first 22 cover the invariant latitude range $\lambda = 17^{\circ}$ to $\lambda = 61^{\circ}$. The last 27 cover the longitude range 277° East to 331° East.

--- 0 ---

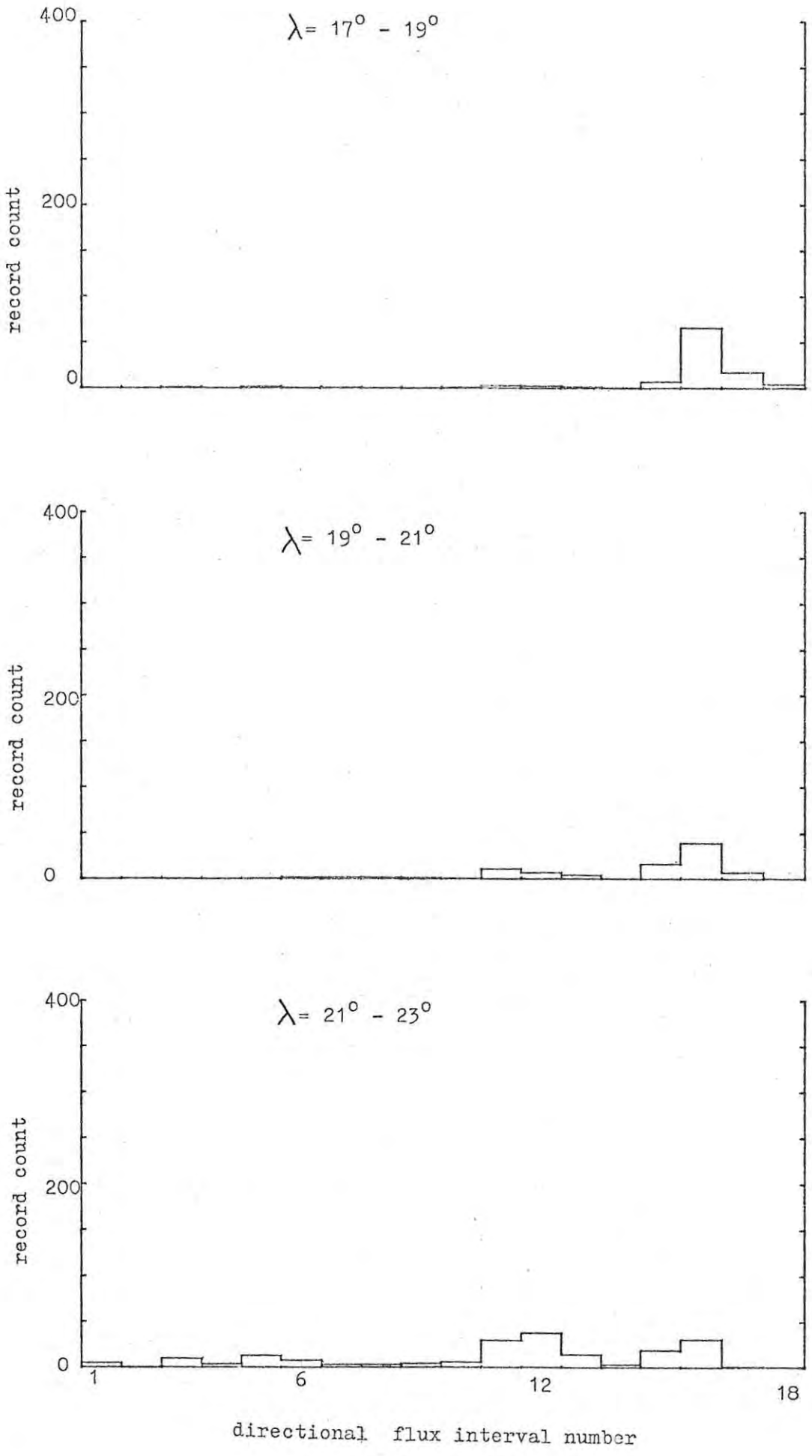
λ= 17° - 19°
λ= 19° - 21°
λ= 21° - 23°
400
200
0
record count
1
6
12
18
directional flux interval number

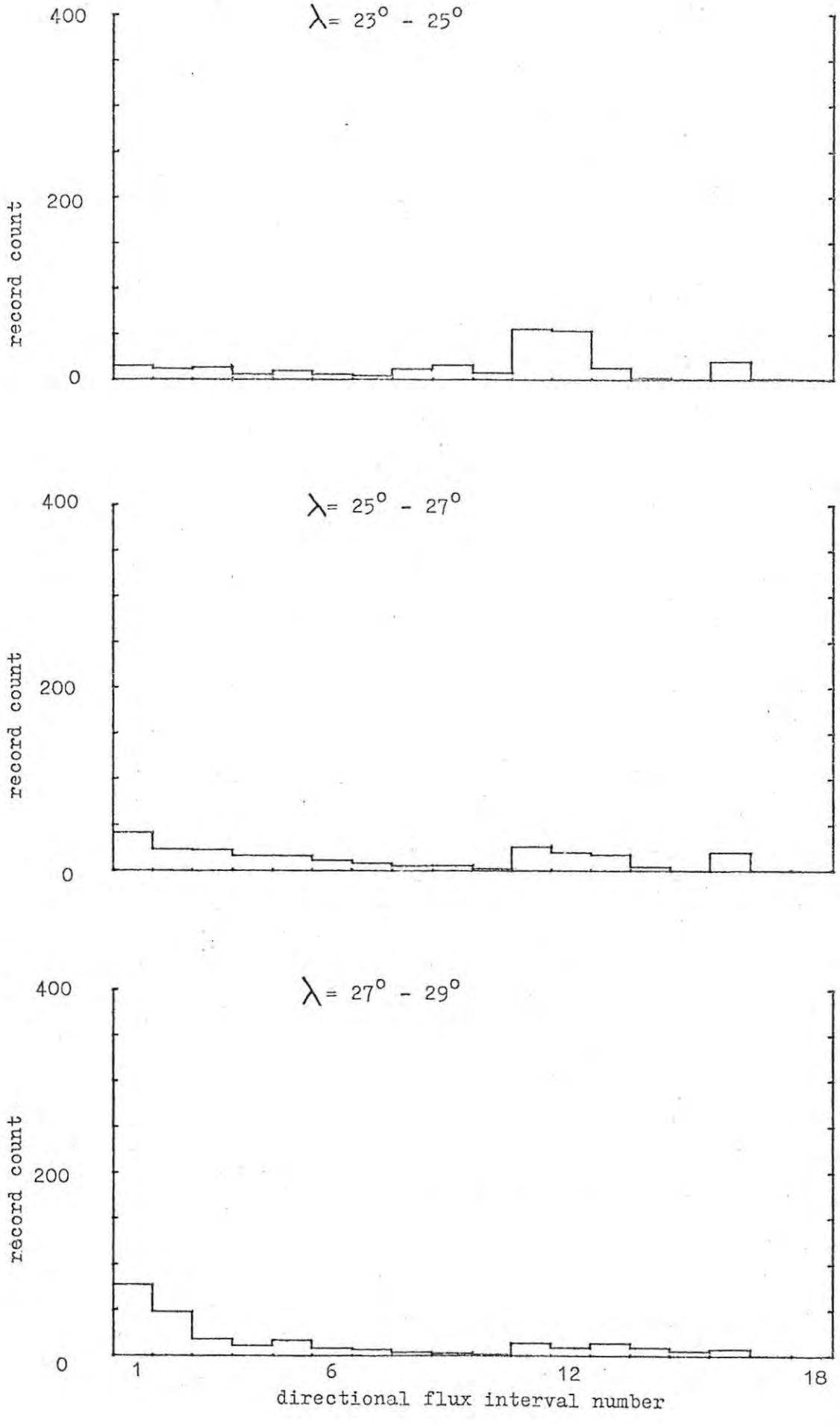
λ= 23° - 25°
λ= 25° - 27°
λ= 27° - 29°
400
200
0
record count
1
6
12
18
directional flux interval number

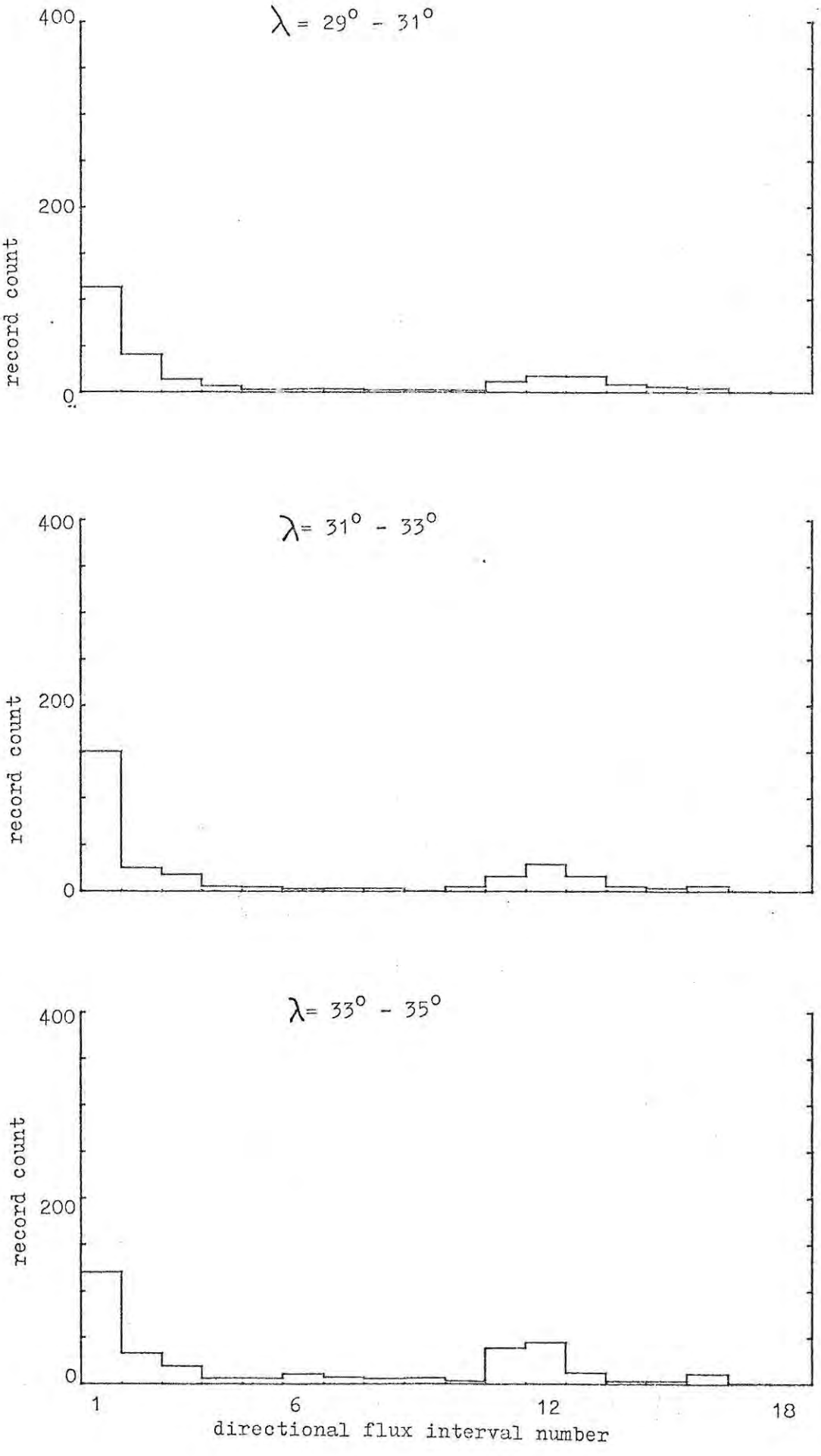
λ = 29° - 31°
400
200
0
record count
λ = 31° - 33°
400
200
0
record count
λ = 33° - 35°
400
200
0
record count
1
6
12
18
directional flux interval number

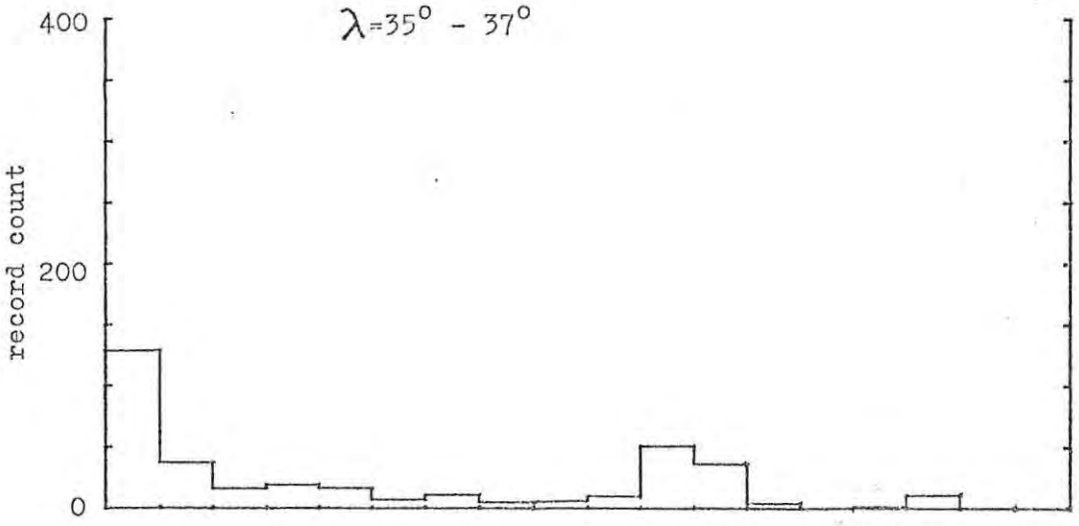
λ=35° - 37°
400
200
0
record count

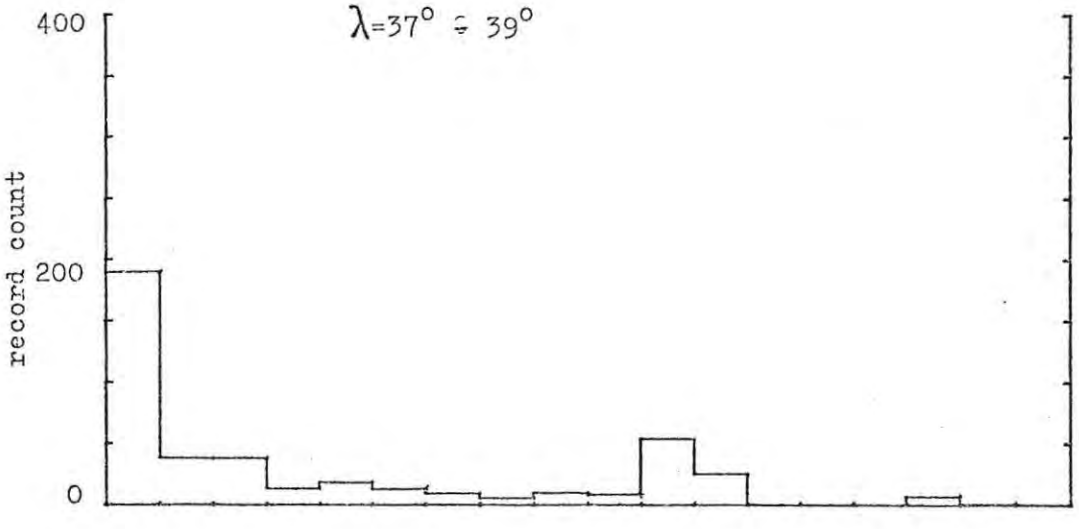
λ=37° - 39°
400
200
0
record count

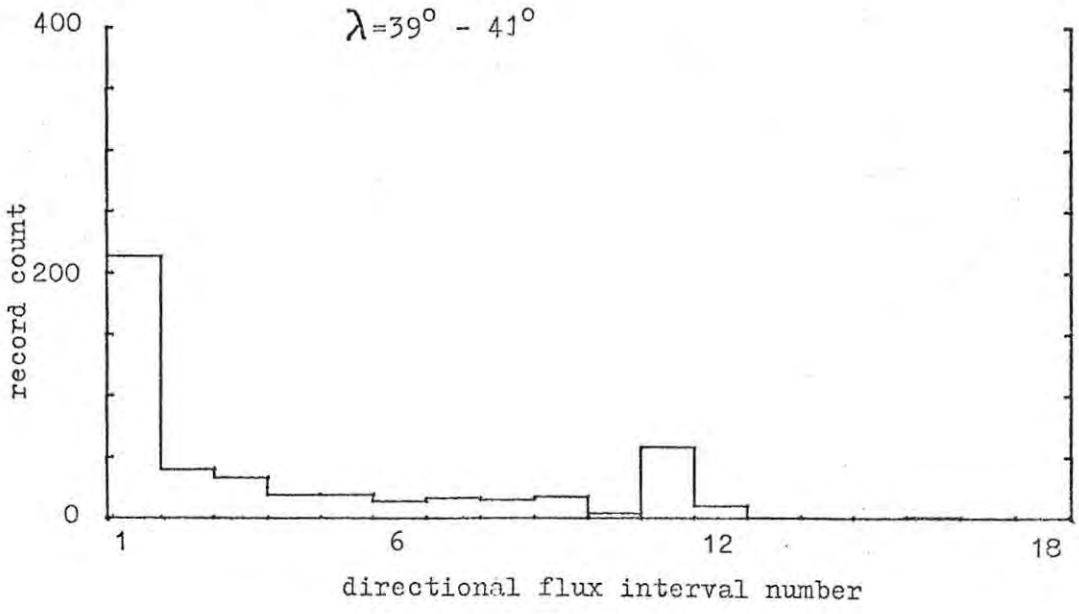
λ=39° - 41°
400
200
0
record count
1
6
12
18
directional flux interval number

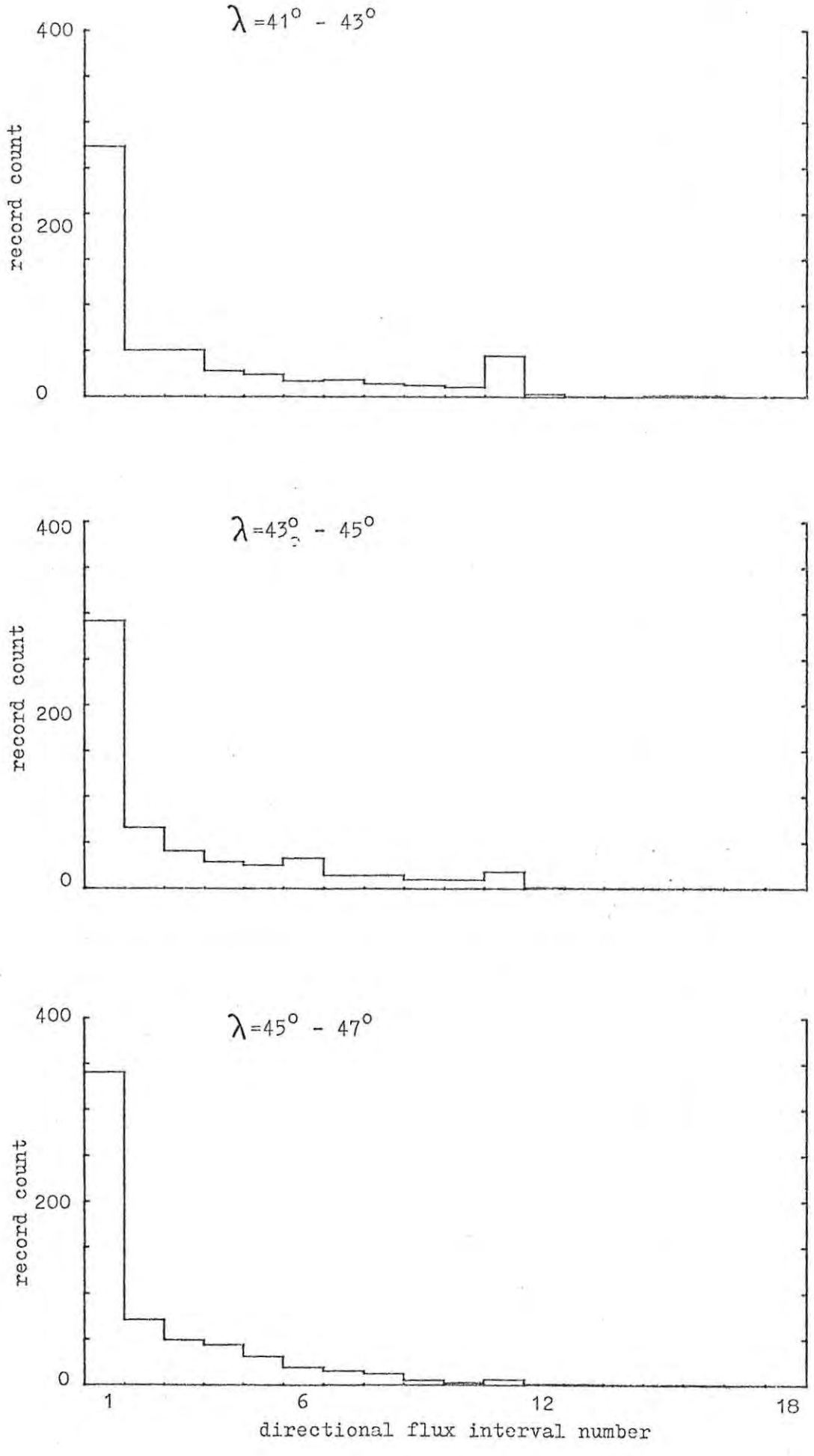
λ=41° - 43°
λ=43° - 45°
λ=45° - 47°
400
200
0
record count
1
6
12
18
directional flux interval number

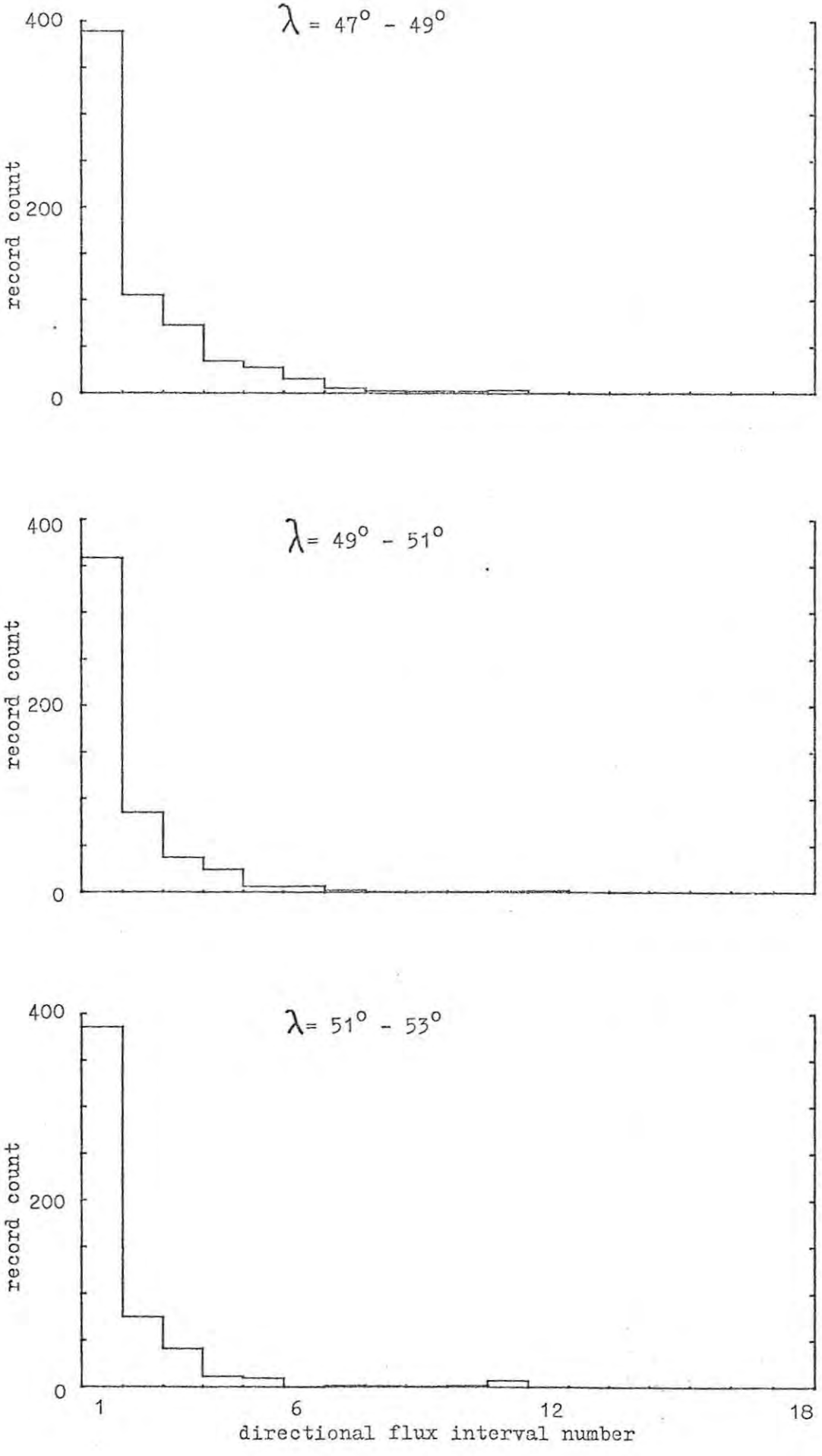
λ = 47° - 49°
λ = 49° - 51°
λ = 51° - 53°
400
200
0
record count
1
6
12
18
directional flux interval number

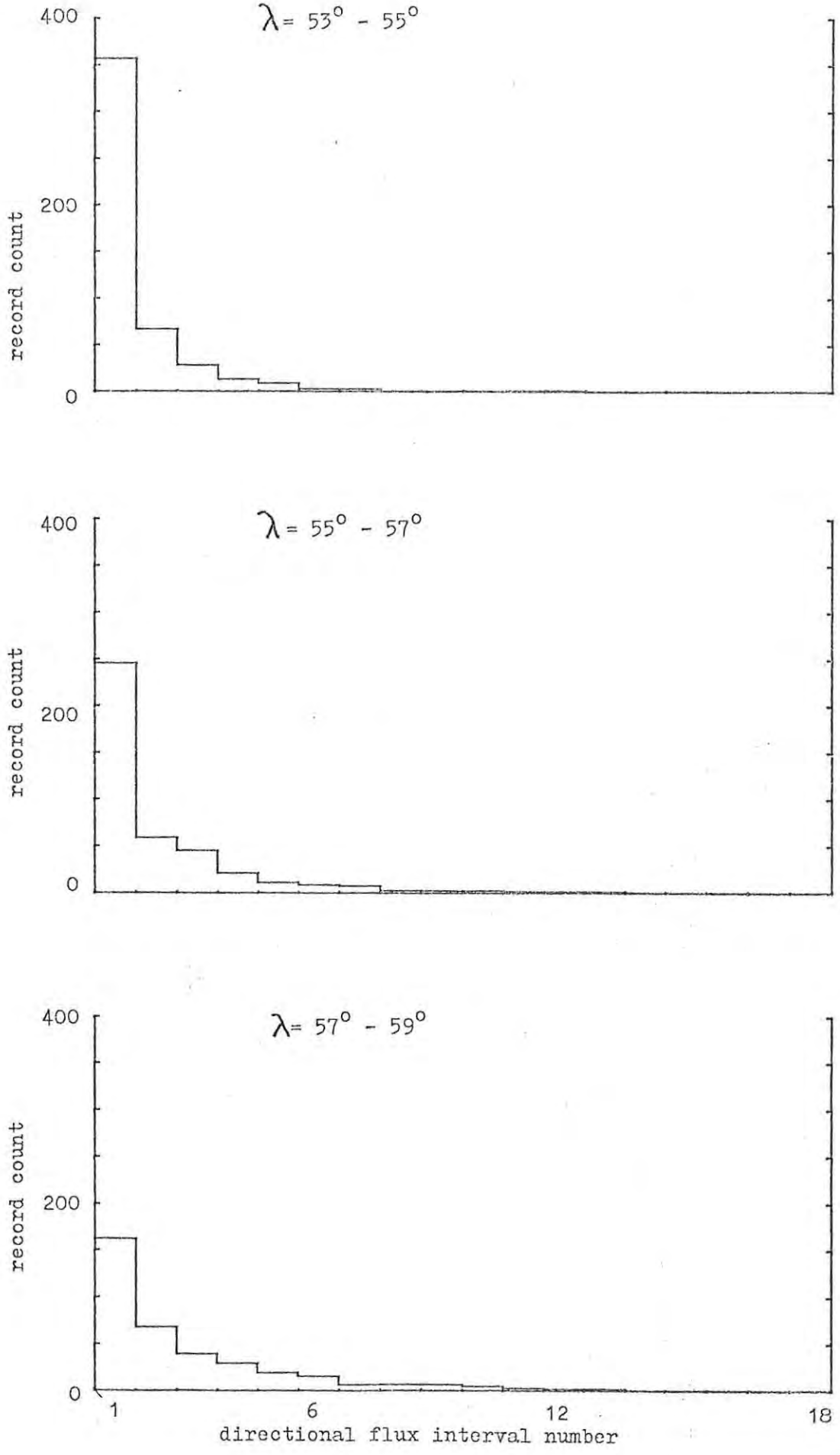
λ= 53° - 55°
λ= 55° - 57°
λ= 57° - 59°
400
200
0
record count
1
6
12
18
directional flux interval number

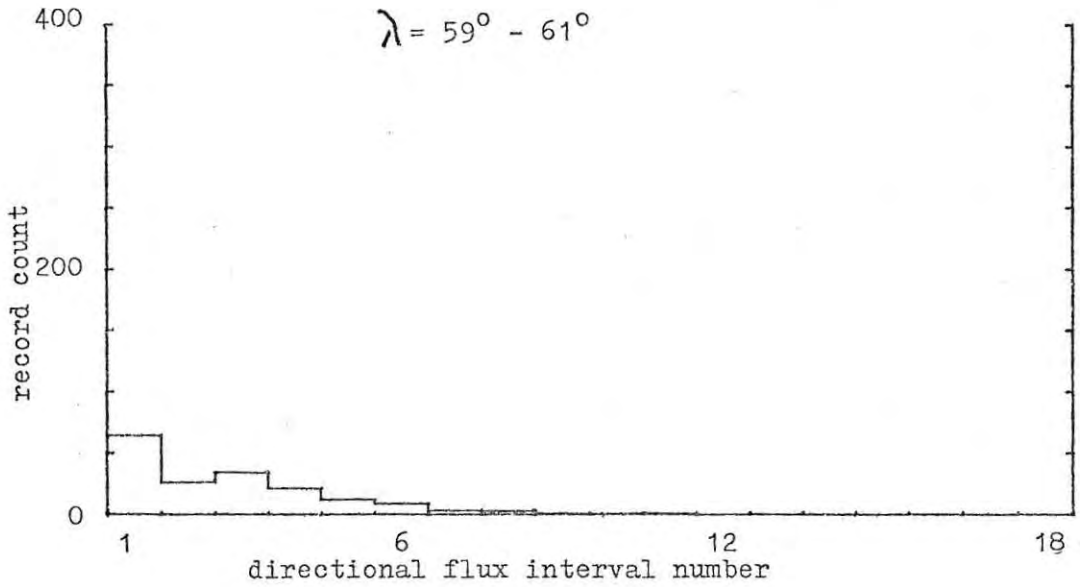
λ = 59° - 61°
400
200
0
record count
1
6
12
18
directional flux interval number

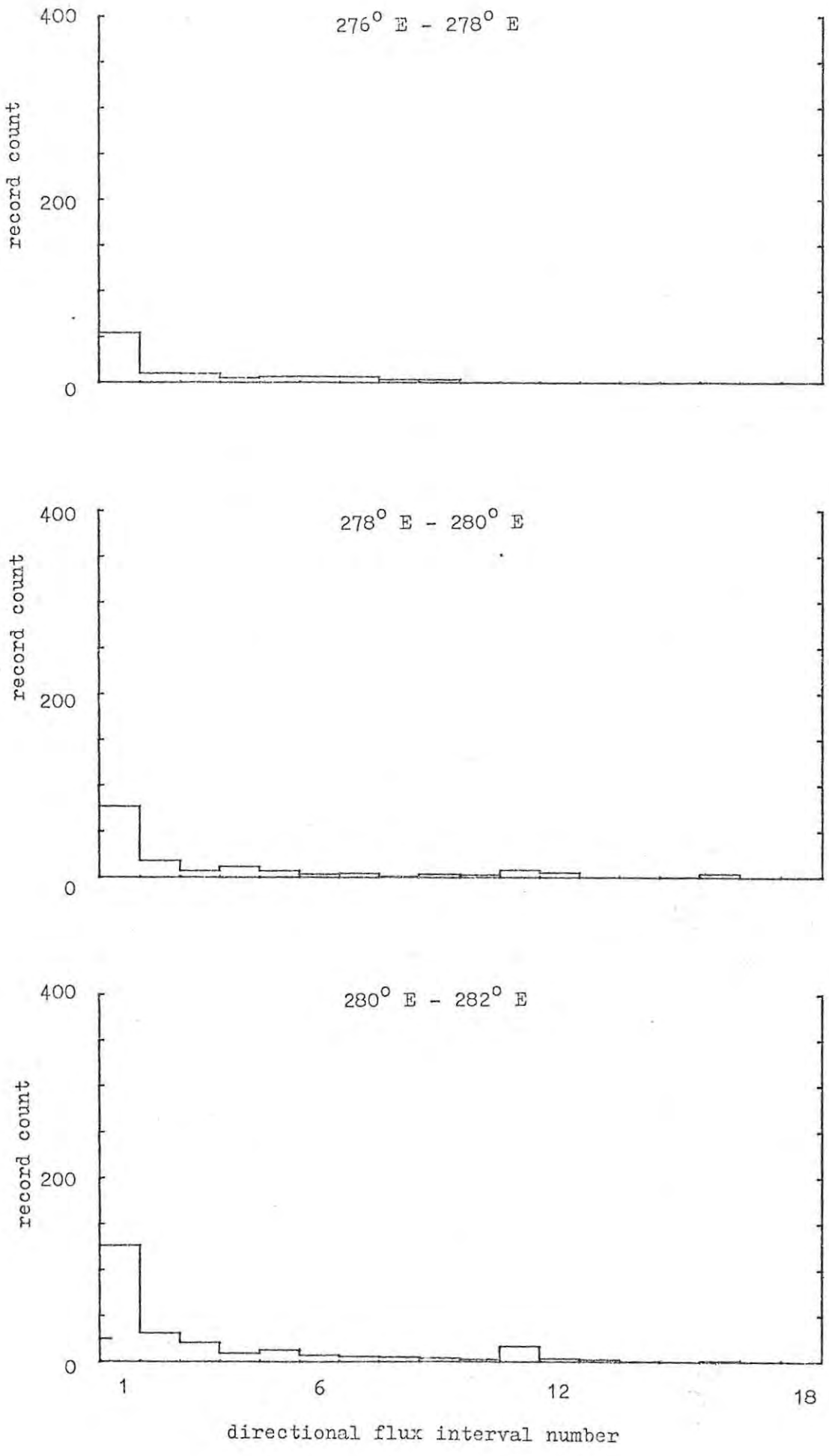
276° E - 278° E
278° E - 280° E
280° E - 282° E
record count
400
200
0
1
6
12
18
directional flux interval number

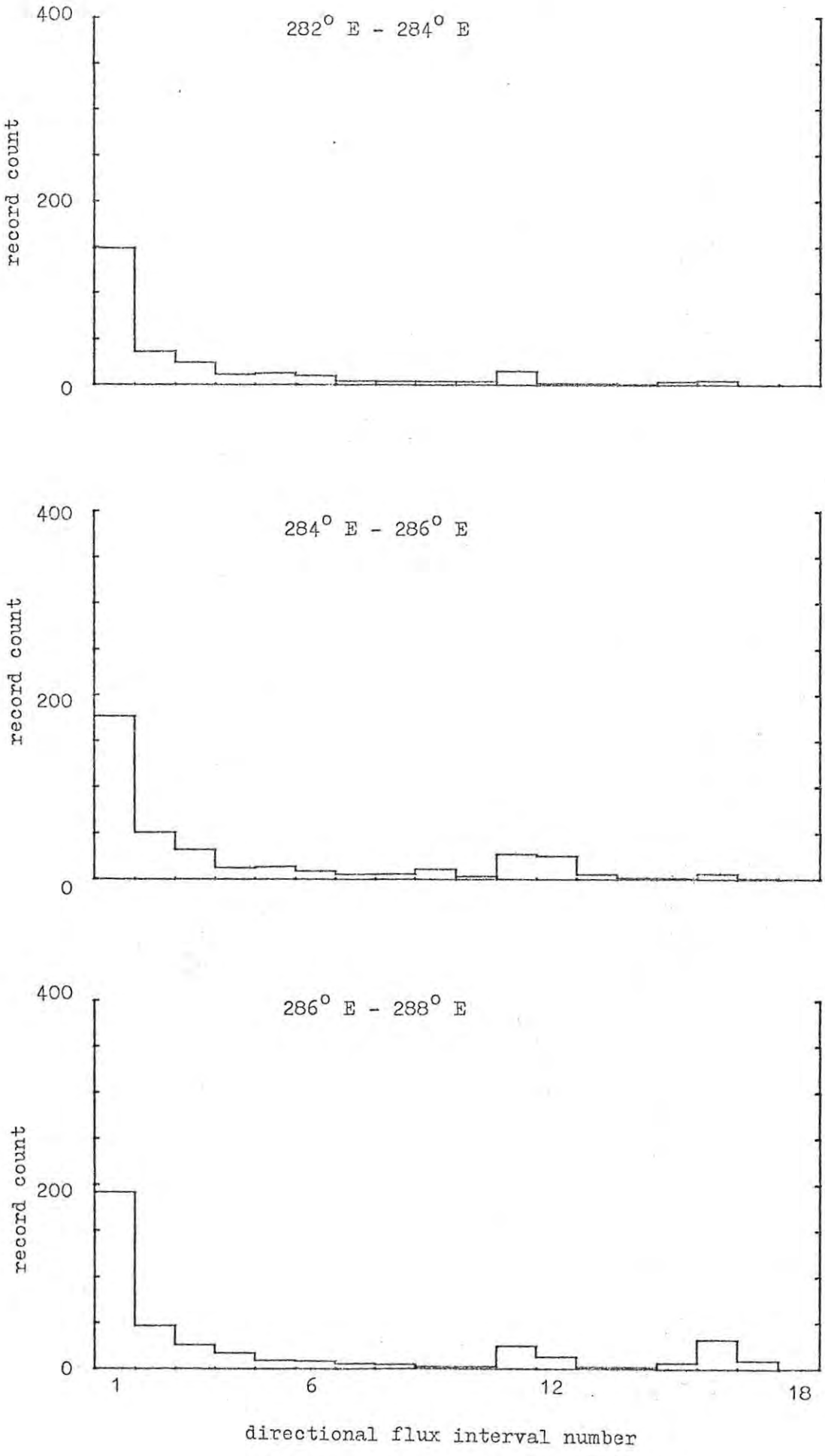
282° E - 284° E
284° E - 286° E
286° E - 288° E
record count
400
200
0
1
6
12
18
directional flux interval number

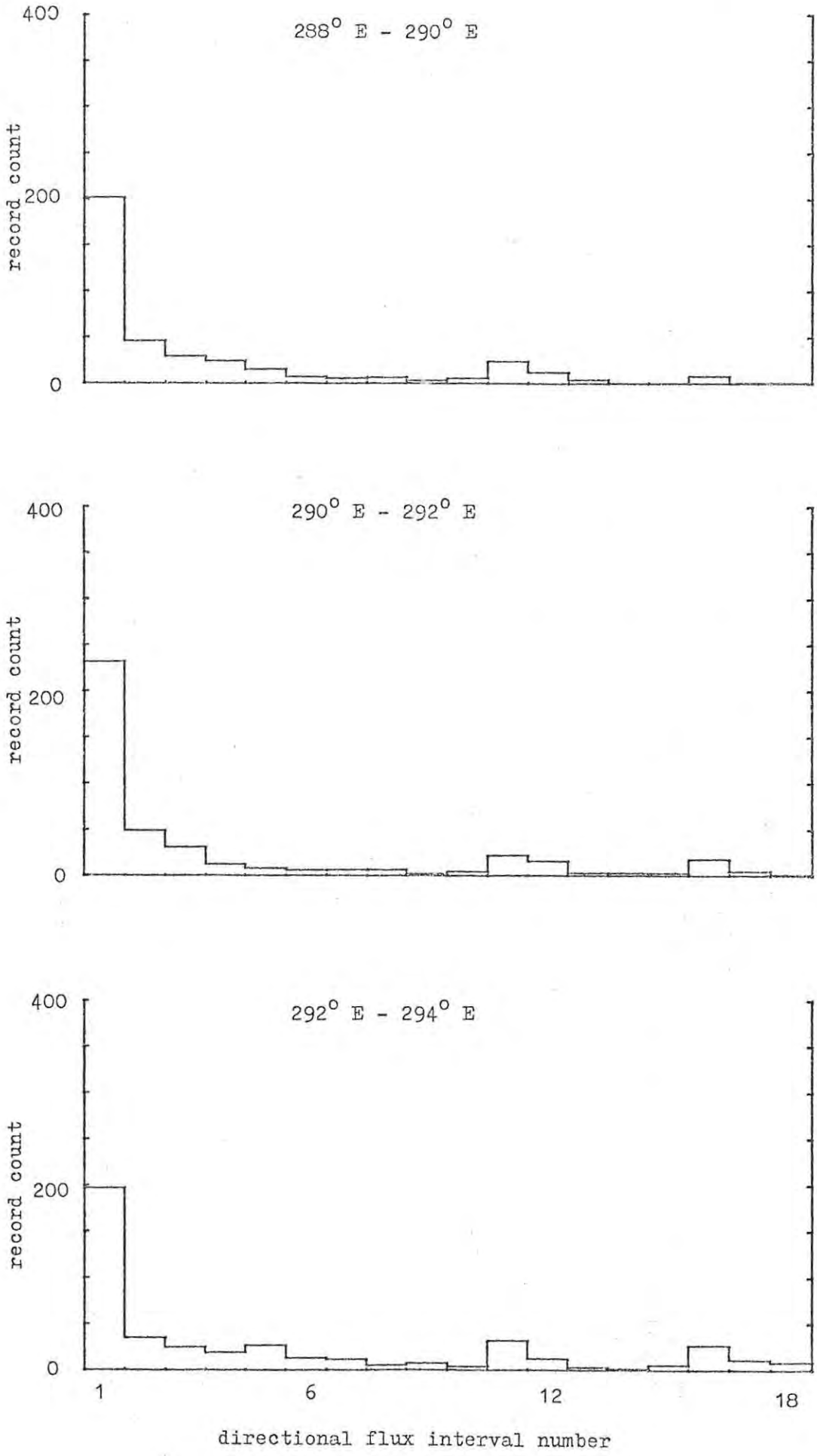
288° E - 290° E
290° E - 292° E
292° E - 294° E
record count
400
200
0
1
6
12
18
directional flux interval number

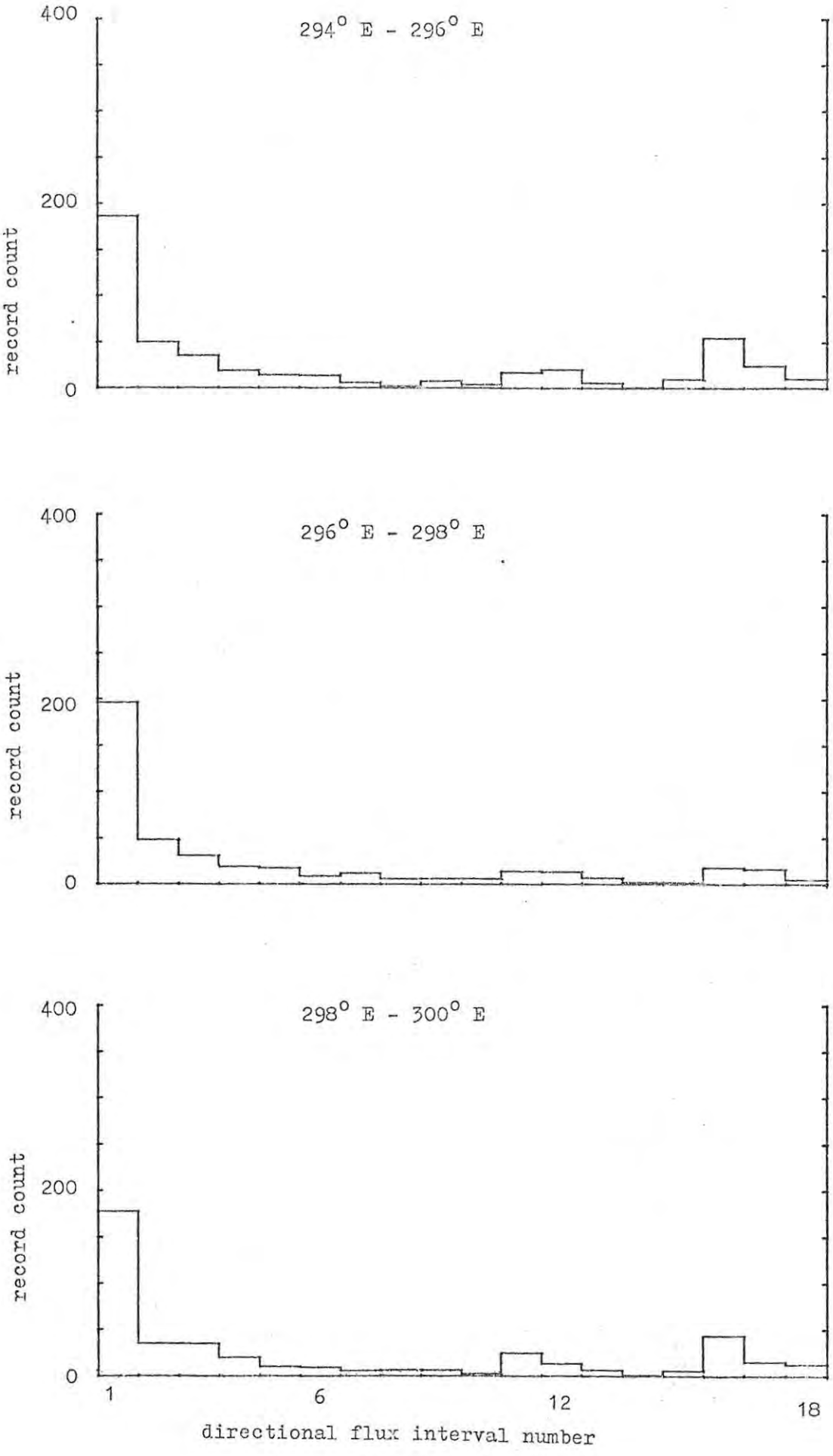
294° E - 296° E
296° E - 298° E
298° E - 300° E
400
200
0
record count
1
6
12
18
directional flux interval number

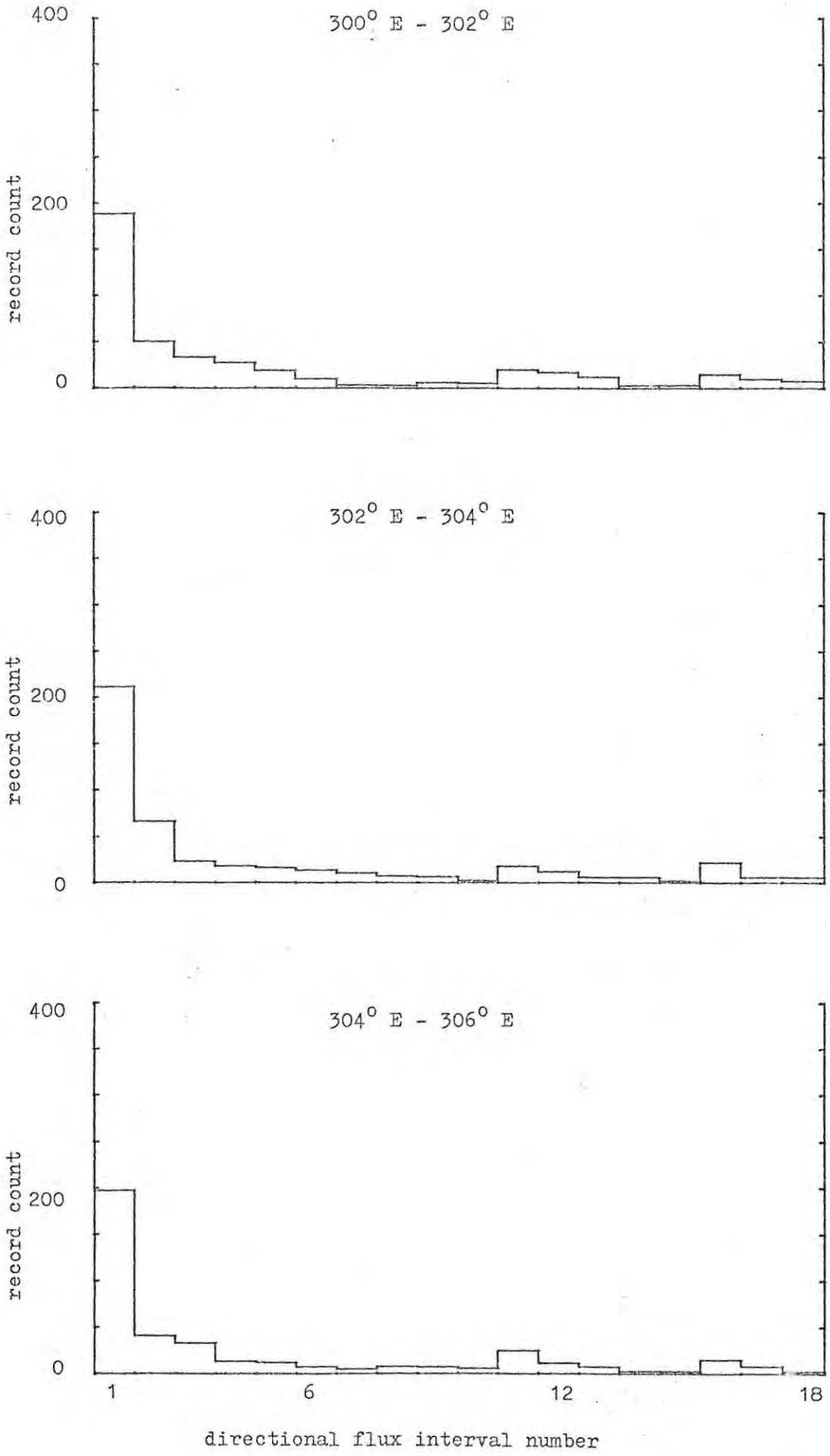
300° E - 302° E
302° E - 304° E
304° E - 306° E
400
200
0
record count
1
6
12
18
directional flux interval number

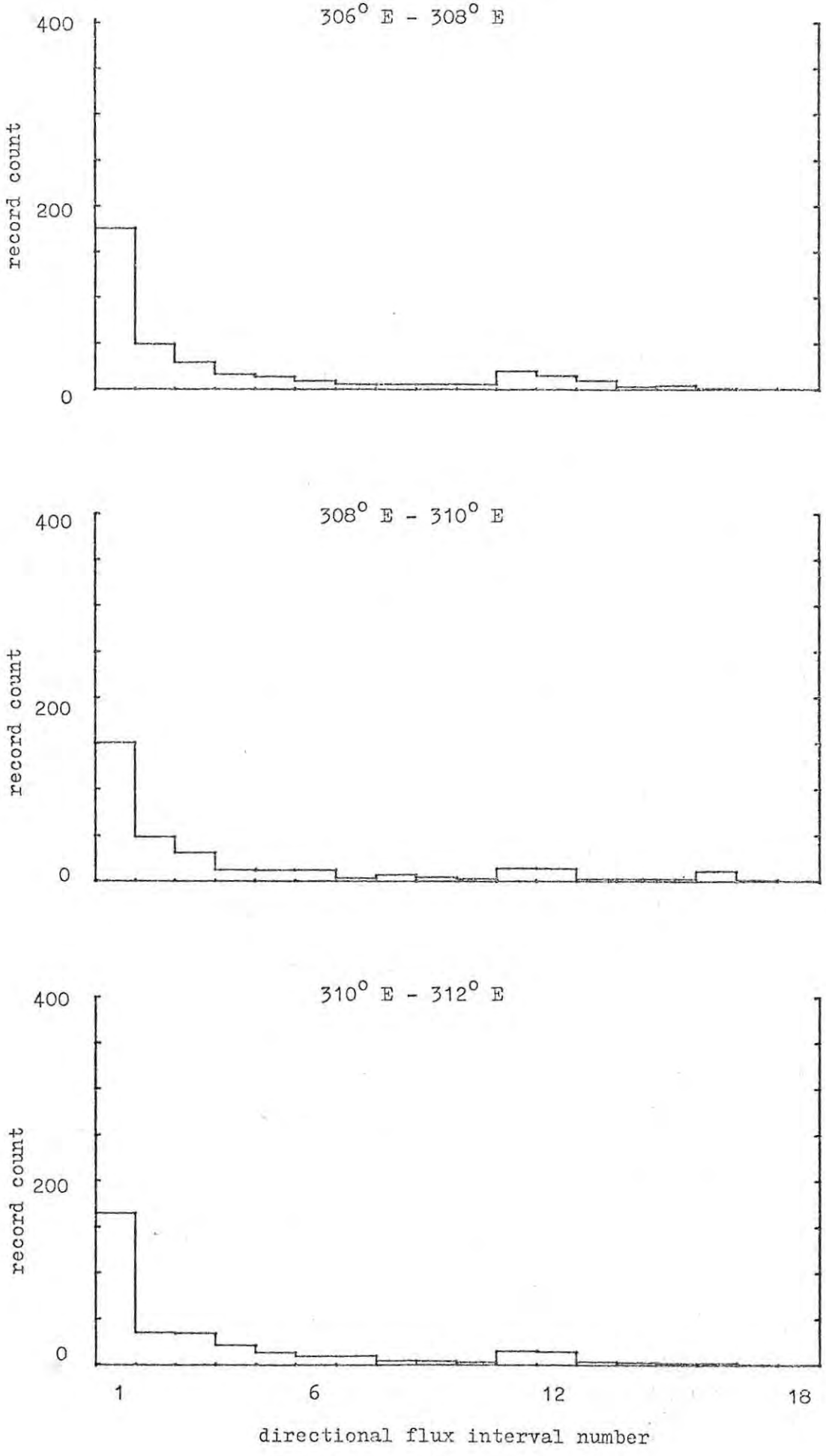
306° E - 308° E
308° E - 310° E
310° E - 312° E
record count
400
200
0
1
6
12
18
directional flux interval number

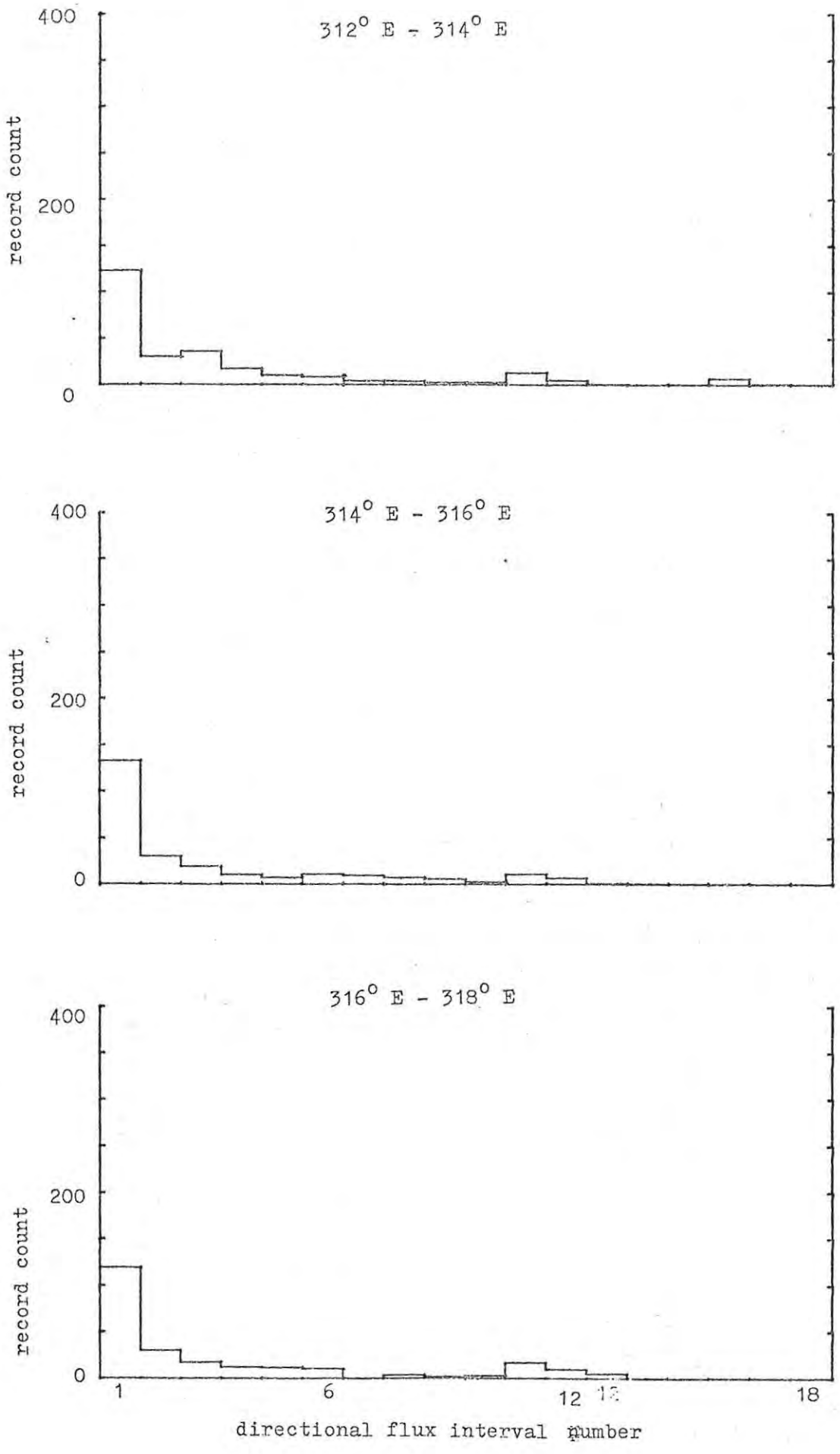
312° E - 314° E
314° E - 316° E
316° E - 318° E
record count
400
200
0
1
6
12
18
directional flux interval number

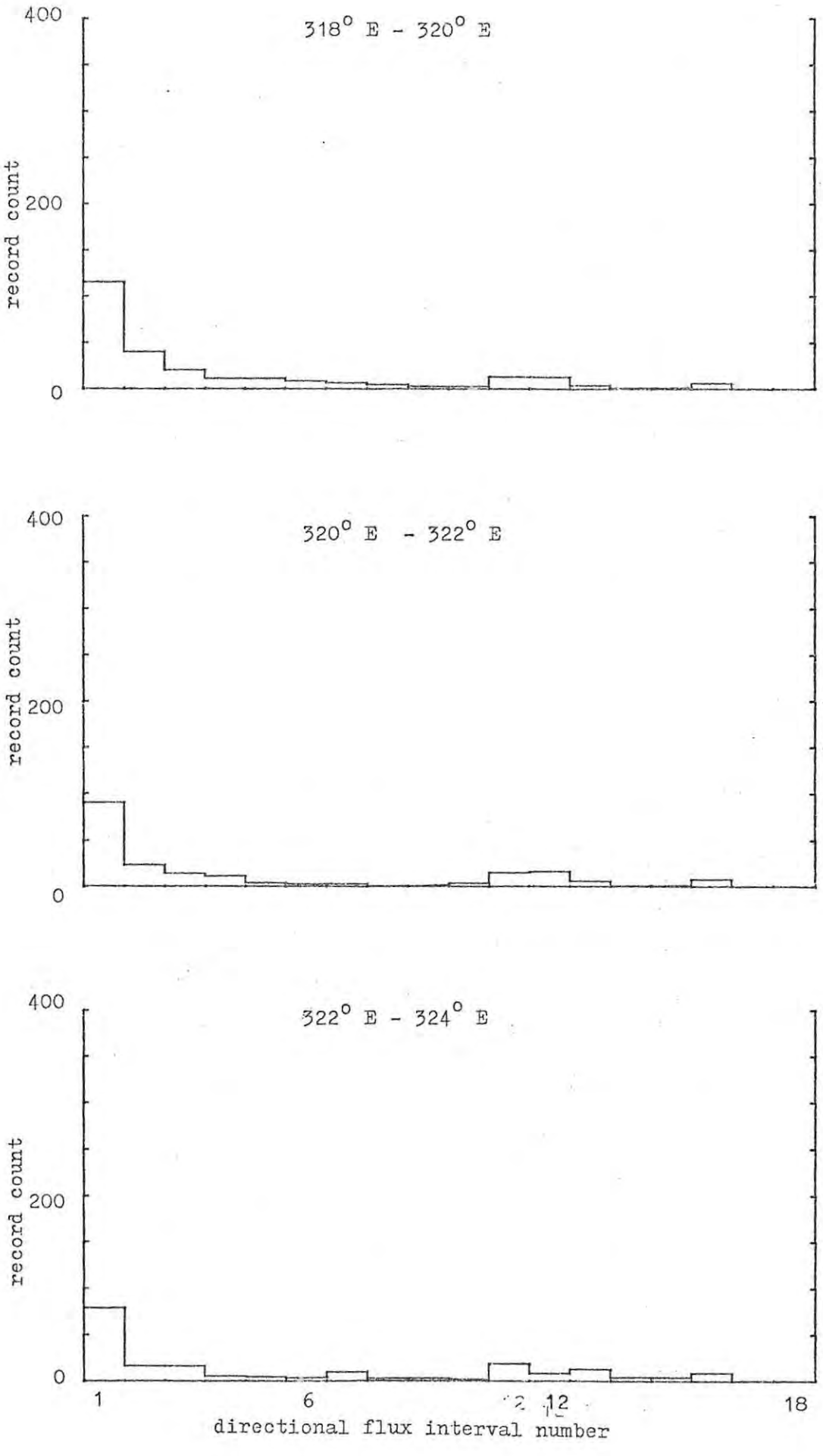
318° E - 320° E
320° E - 322° E
322° E - 324° E
record count
400
200
0
1
6
12
18
directional flux interval number

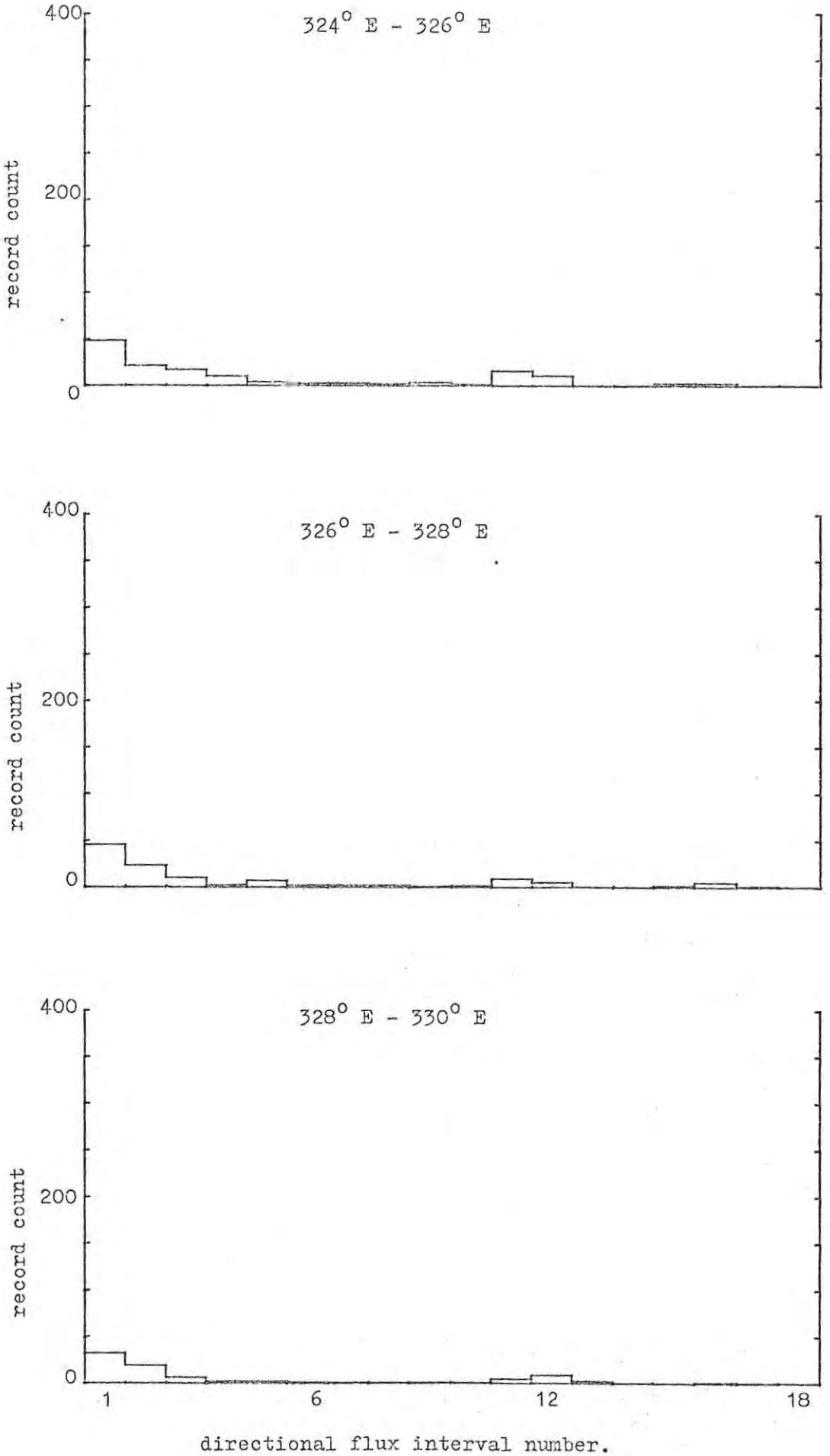
324° E - 326° E
326° E - 328° E
328° E - 330° E
record count
400
200
0
1
6
12
18
directional flux interval number.

APPENDIX 4.

DIRECTIONAL FLUX DISTRIBUTION IN PITCH ANGLE

We present the pitch angle distribution of the flux values in each of the 22 ranges of invariant latitude and the 27 ranges of geographic longitude. In every case the median flux value for the pitch angle range is plotted.

The pitch angle ranges are:

0^{o} - 10^{o}

10^{o} - 30^{o}

30^{o} - 50^{o}

50^{o} - 70^{o}

70^{o} - 90^{o}

The flux scale changes between histograms to accommodate the large changes in directional fluxes between two different spatial regions.

--- 0 ---

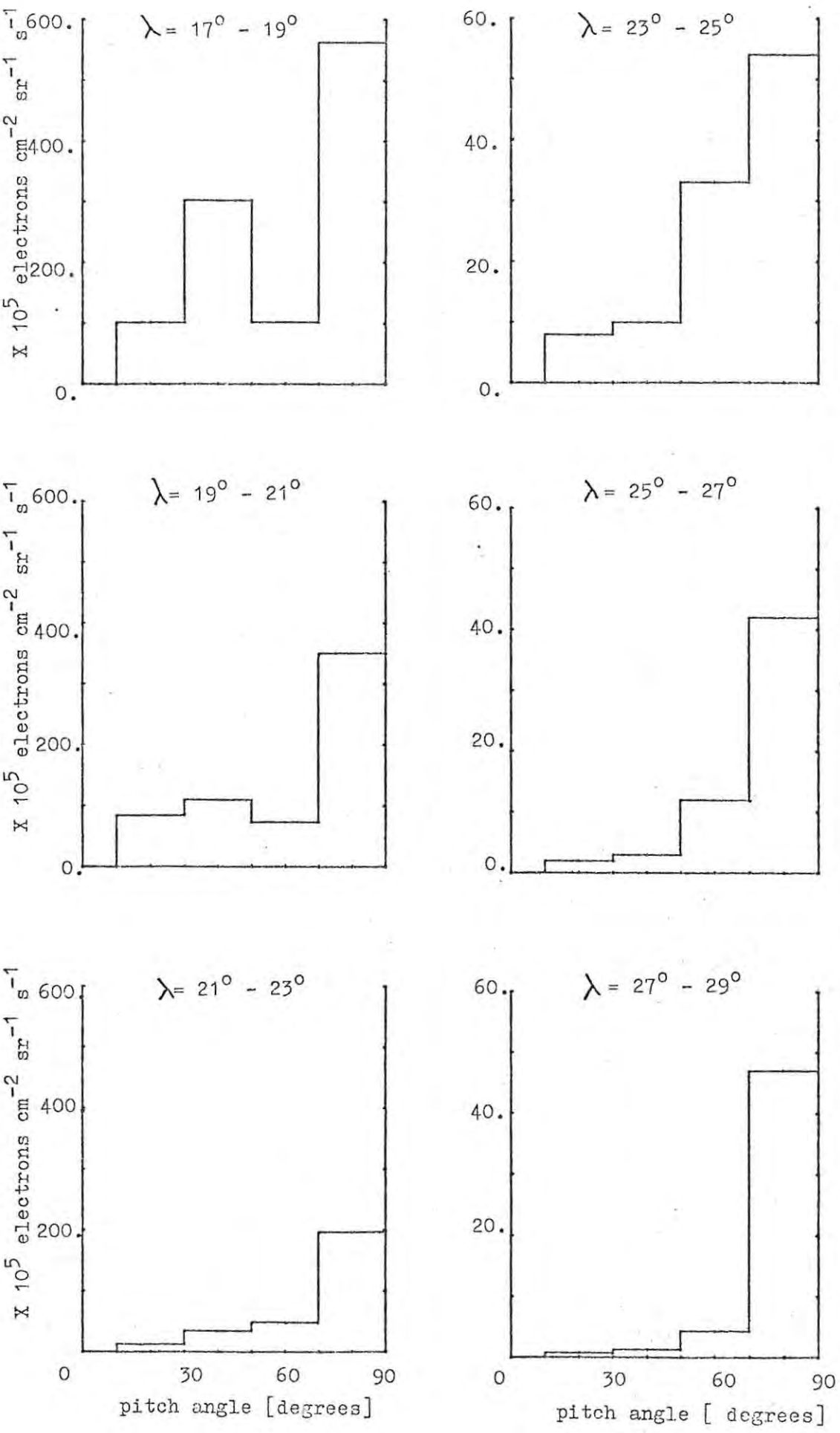
λ = 17° - 19°
λ = 23° - 25°
λ = 19° - 21°
λ = 25° - 27°
λ = 21° - 23°
λ = 27° - 29°
X 10^5 electrons cm^-2 sr^-1 s^-1
600.
400.
200.
0.
60.
40.
20.
0
30
60
90
pitch angle [degrees]
pitch angle [degrees]

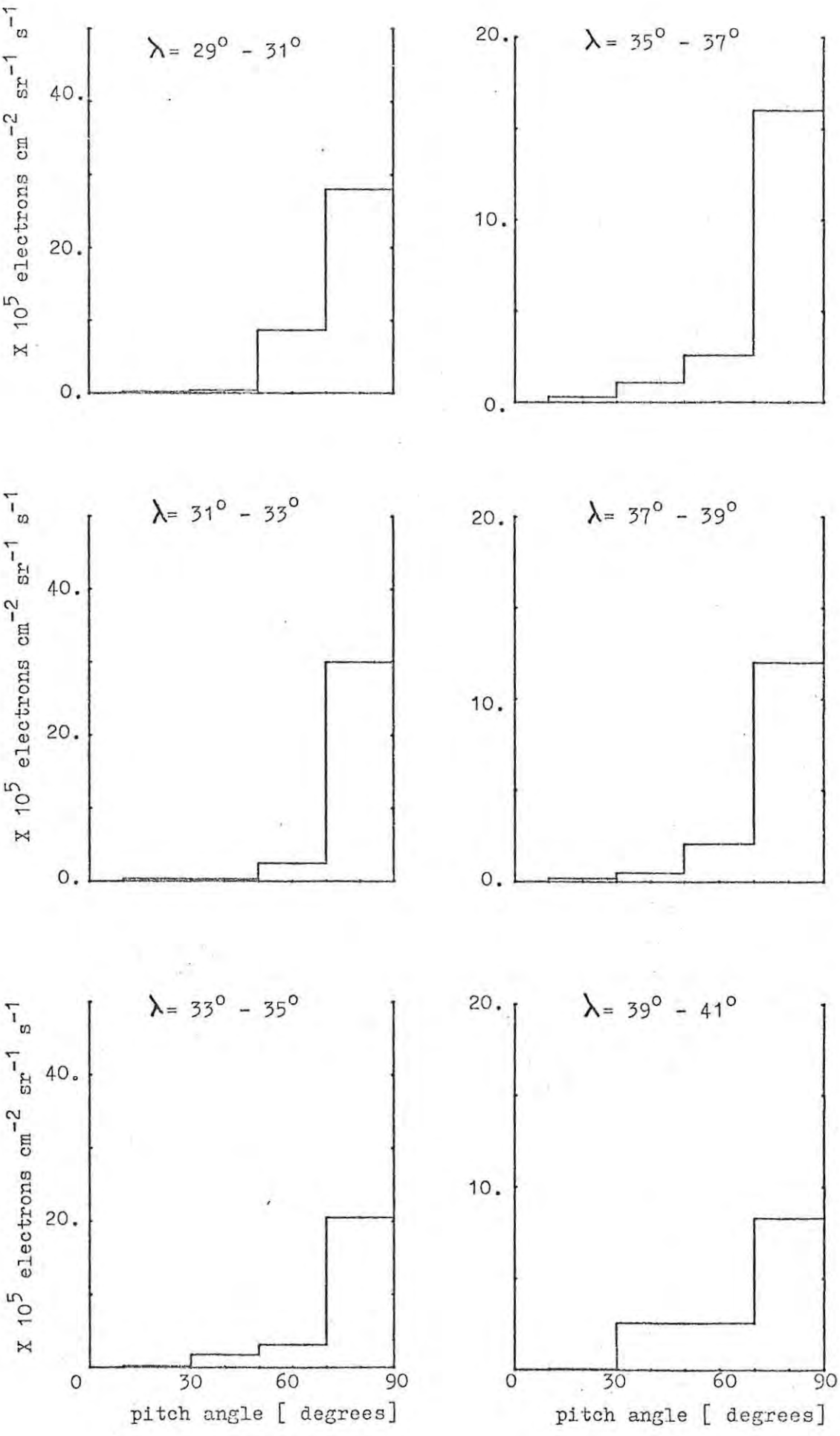
λ = 29° - 31°
λ = 35° - 37°
λ = 31° - 33°
λ = 37° - 39°
λ = 33° - 35°
λ = 39° - 41°
X 10^5 electrons cm^-2 sr^-1 s^-1
0.
20.
40.
10.
0
30
60
90
pitch angle [degrees]

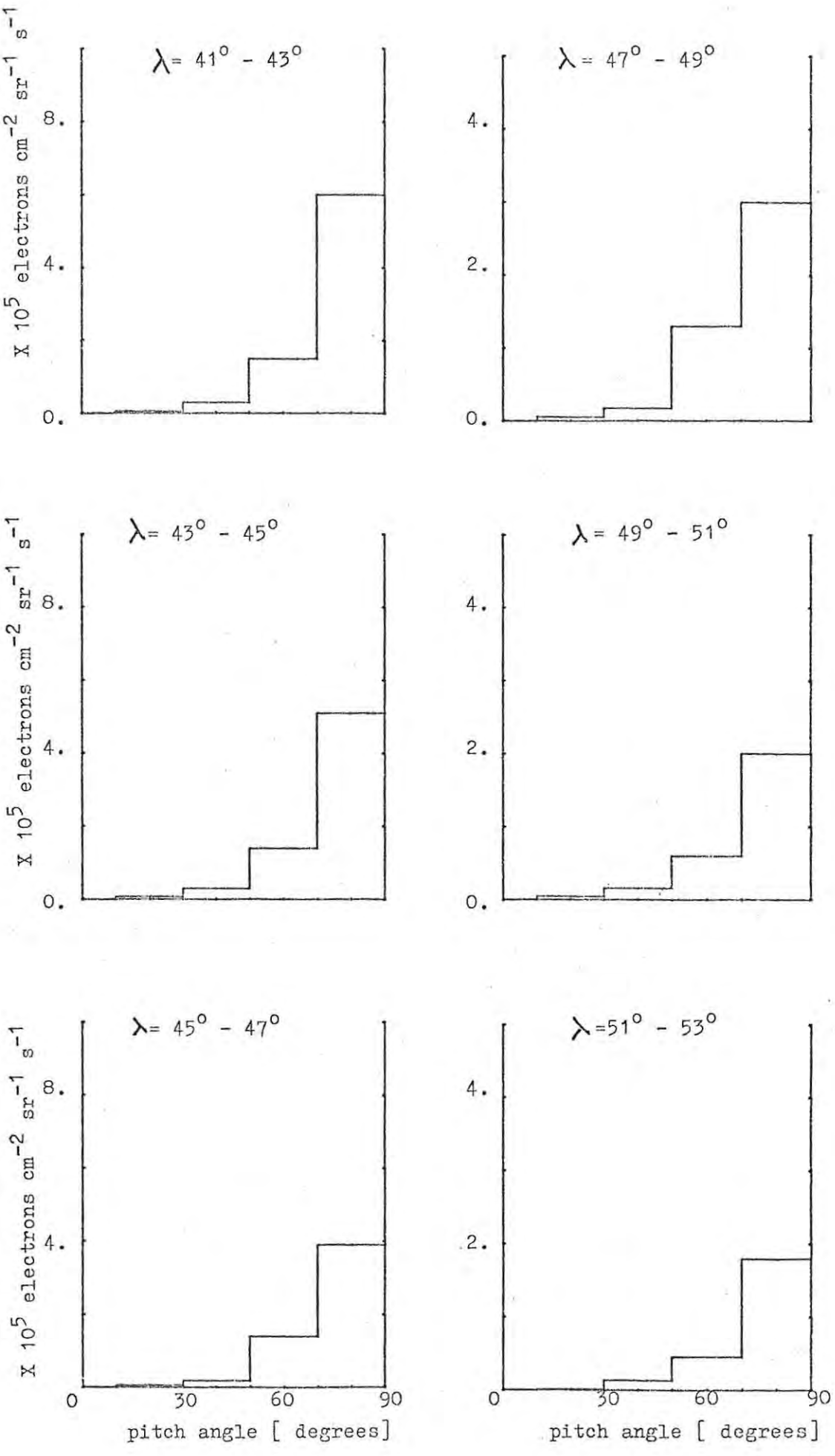
λ= 41° - 43°
λ= 47° - 49°
λ= 43° - 45°
λ= 49° - 51°
λ= 45° - 47°
λ=51° - 53°
X 10^5 electrons cm^-2 sr^-1 s^-1
0.
4.
8.
2.
0
30
60
90
pitch angle [degrees]

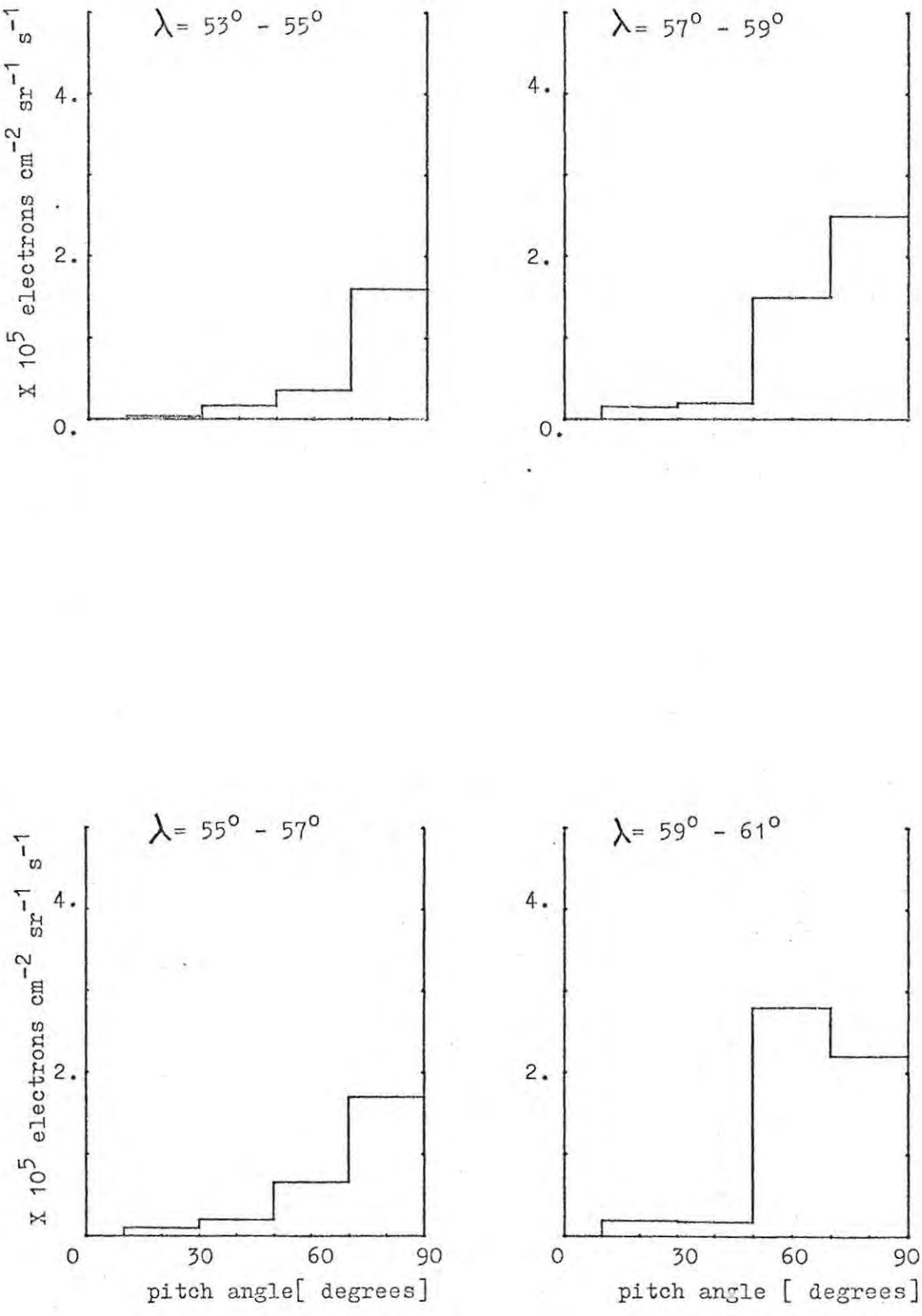
λ= 53° - 55°
λ= 57° - 59°
λ= 55° - 57°
λ= 59° - 61°
X 10^5 electrons cm^-2 sr^-1 s^-1
0.
2.
4.
0
30
60
90
pitch angle[degrees]
pitch angle [degrees]

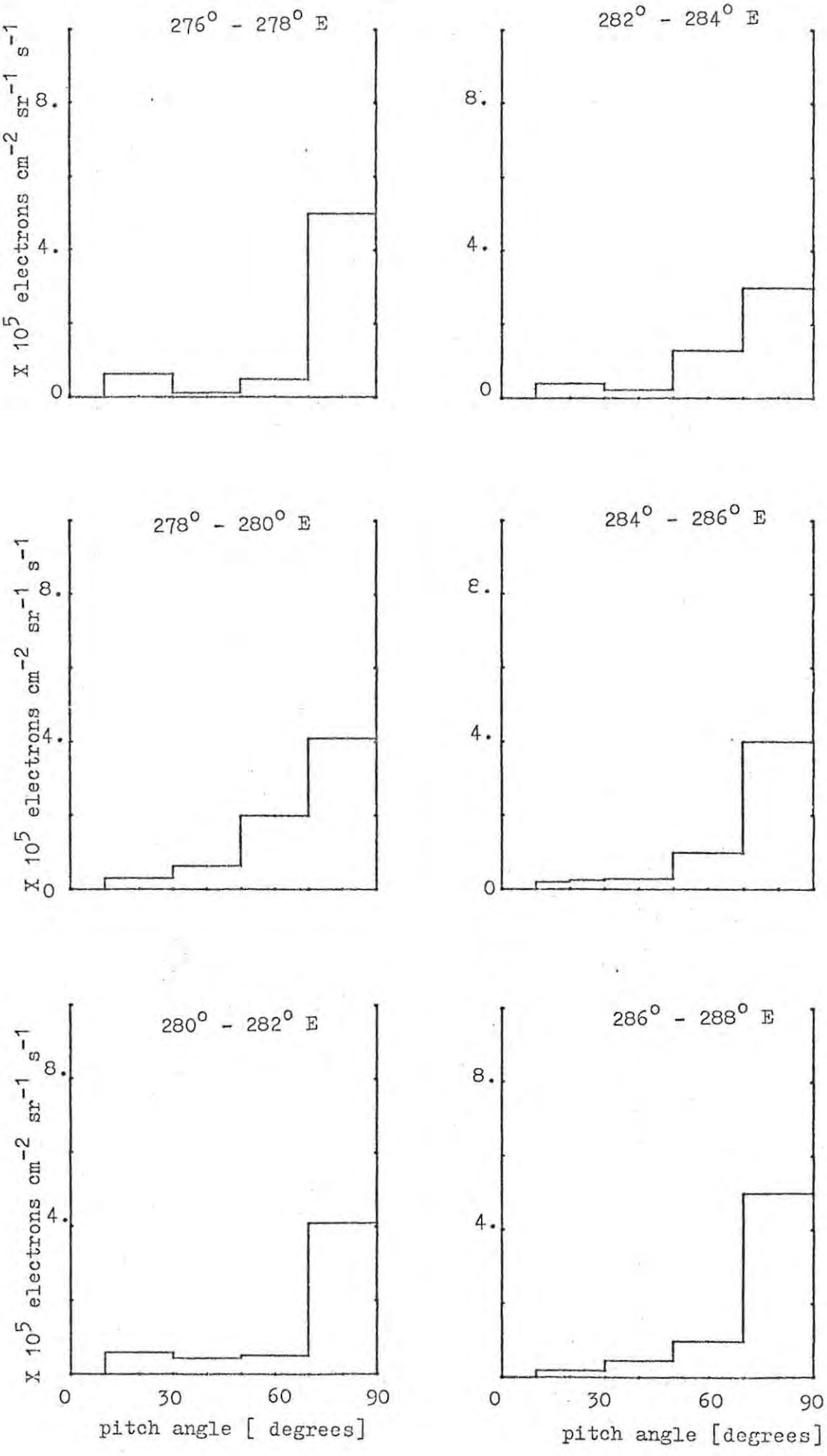
276° - 278° E
282° - 284° E
278° - 280° E
284° - 286° E
280° - 282° E
286° - 288° E
X 10^5 electrons cm^-2 sr^-1 s^-1
0
4.
8.
0
30
60
90
pitch angle [degrees]
pitch angle [degrees]

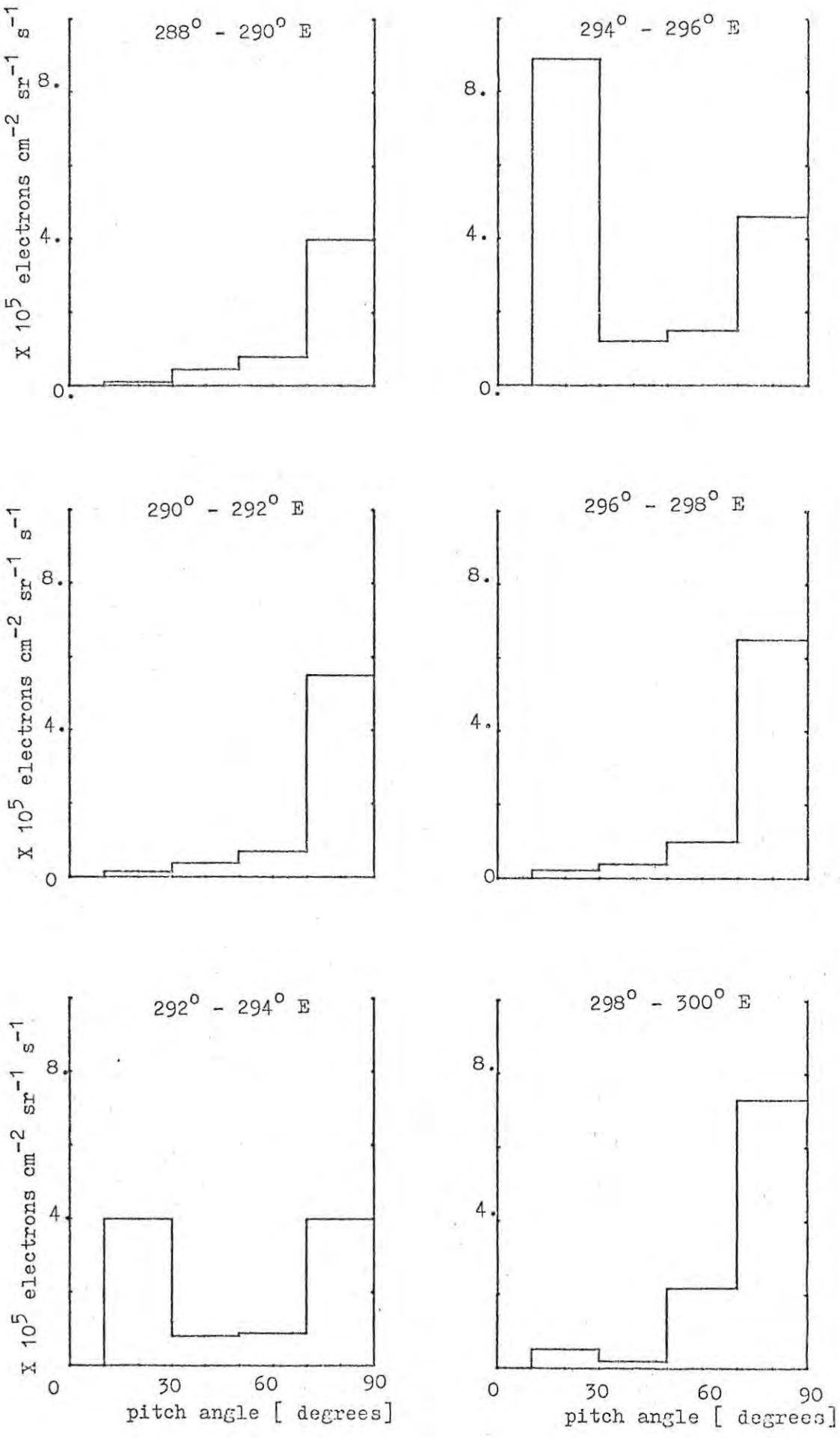
288° - 290° E
294° - 296° E
290° - 292° E
296° - 298° E
292° - 294° E
298° - 300° E
X 10^5 electrons cm^-2 sr^-1 s^-1
0
4.
8.
0
30
60
90
pitch angle [degrees]

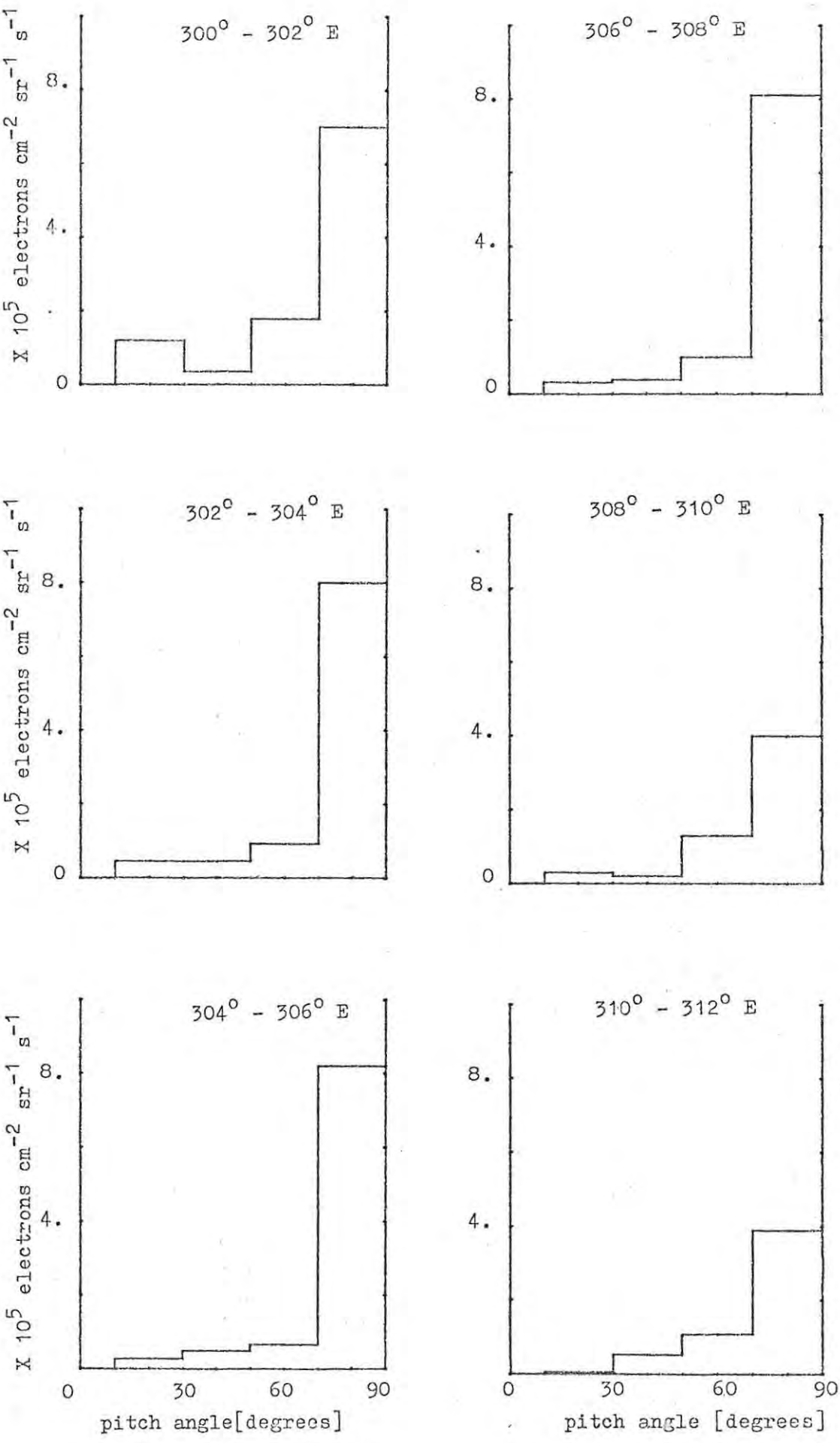
300° - 302° E
306° - 308° E
302° - 304° E
308° - 310° E
304° - 306° E
310° - 312° E
X 10^5 electrons cm^-2 sr^-1 s^-1
0
4.
8.
0
30
60
90
pitch angle[degrees]
pitch angle [degrees]

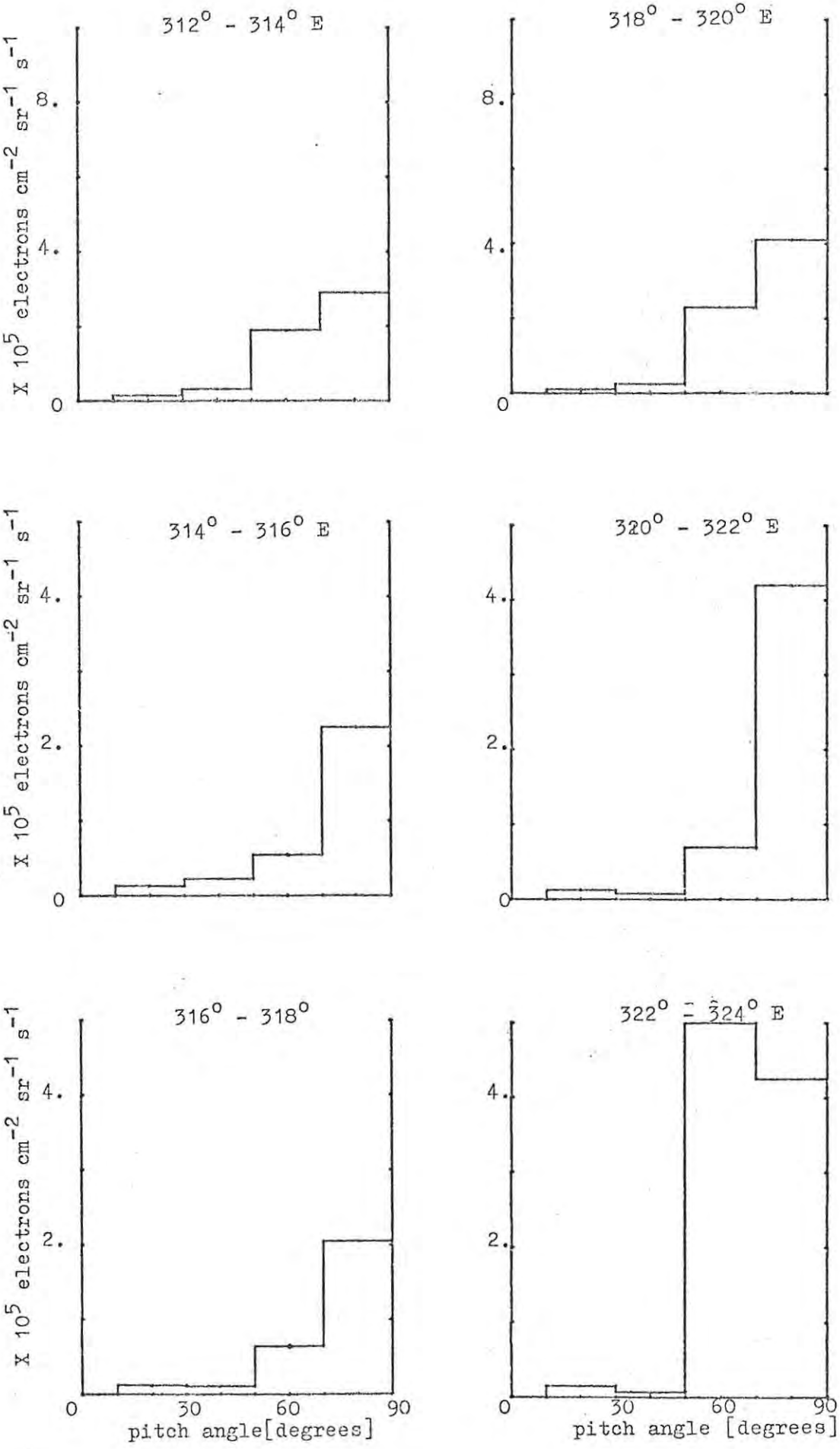
312° - 314° E
318° - 320° E
314° - 316° E
320° - 322° E
316° - 318°
322° - 324° E
X 10^5 electrons cm^-2 sr^-1 s^-1
0
2.
4.
8.
0
30
60
90
pitch angle[degrees]
pitch angle [degrees]

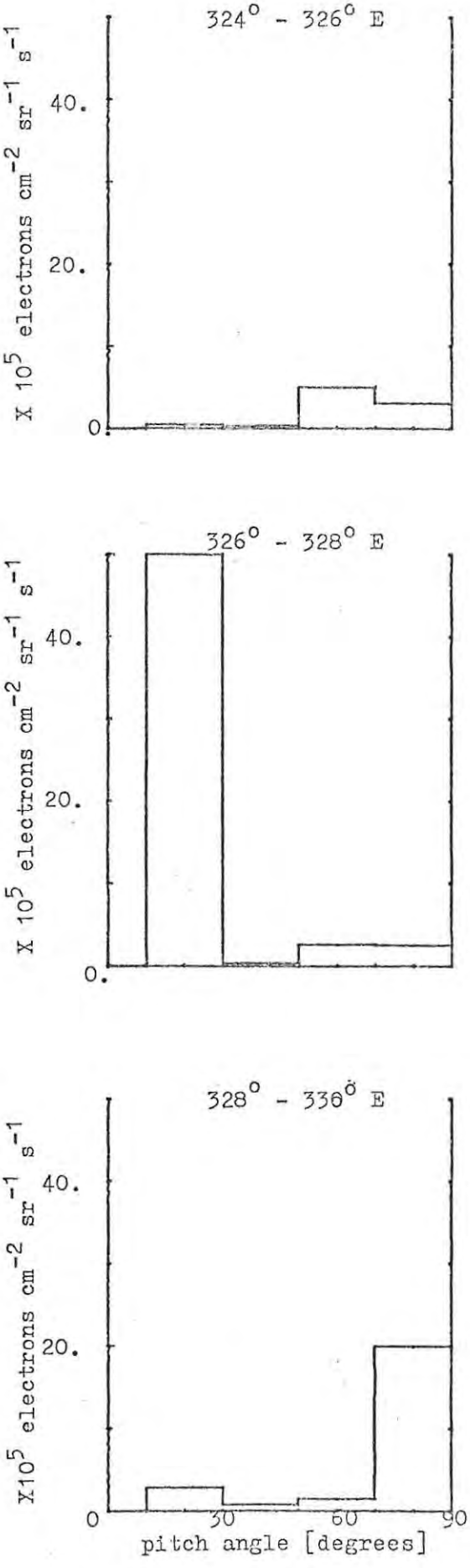
324° - 326° E
326° - 328° E
328° - 330° E
X 10^5 electrons cm^-2 sr^-1 s^-1
40.
20.
0
30
60
90
pitch angle [degrees]

APPENDIX 5

DIRECTIONAL FLUX DISTRIBUTIONS IN LOCAL TIME

The 24 hour range of local time is split into twelve equal intervals. The median flux value of the directional fluxes recorded within each time interval is plotted. The histograms appear in two groups. The first 22 cover the range of invariant latitude. The last 27 cover the range of geographic longitude.

The flux scale changes between histograms to accommodate the large changes in directional fluxes between two spatial regions.

--- 0 ---

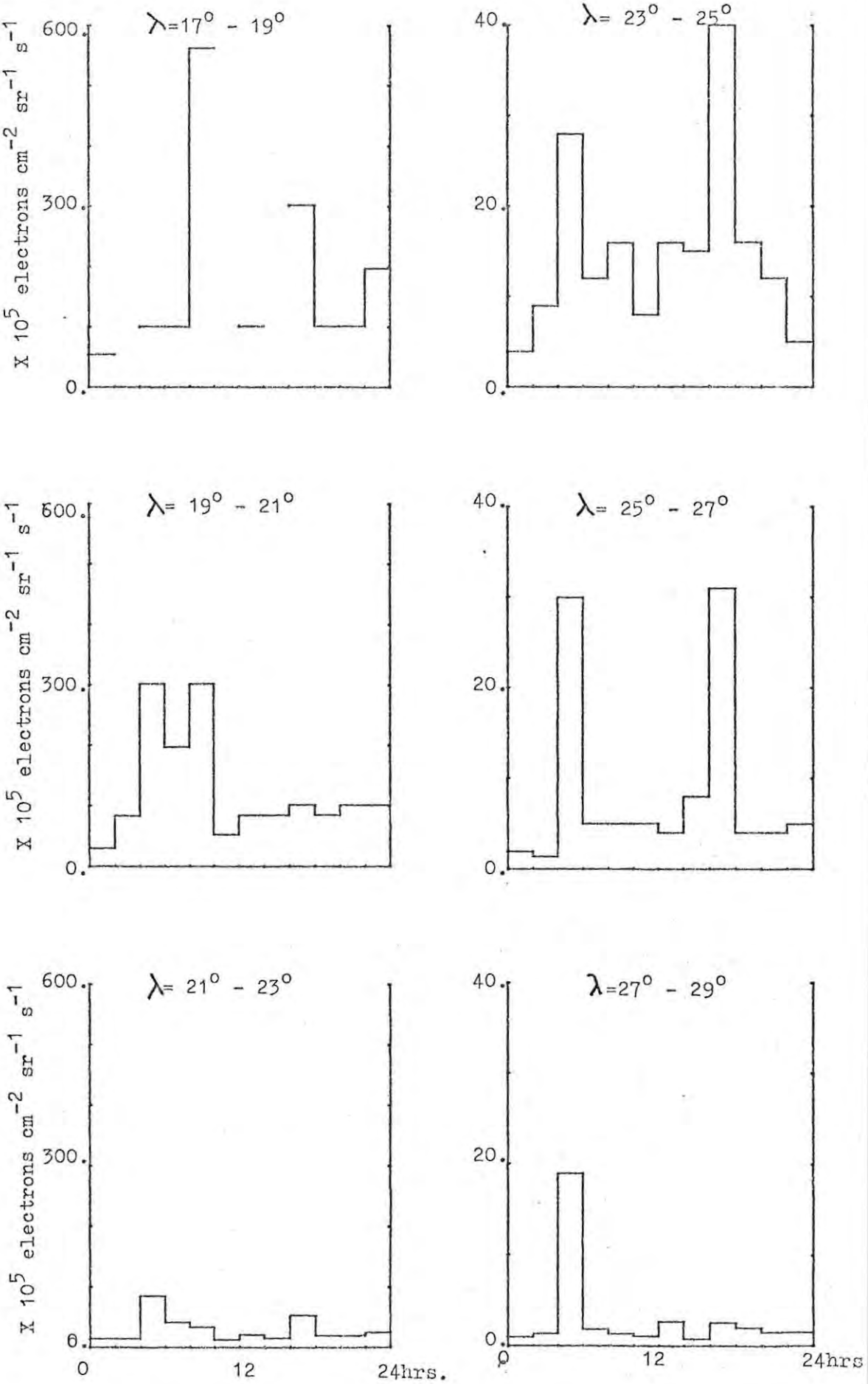
λ=17° - 19°
λ= 23° - 25°
λ= 19° - 21°
λ= 25° - 27°
λ= 21° - 23°
λ=27° - 29°
X 10^5 electrons cm^-2 sr^-1 s^-1
600.
300.
0.
40.
20.
0
12
24hrs.

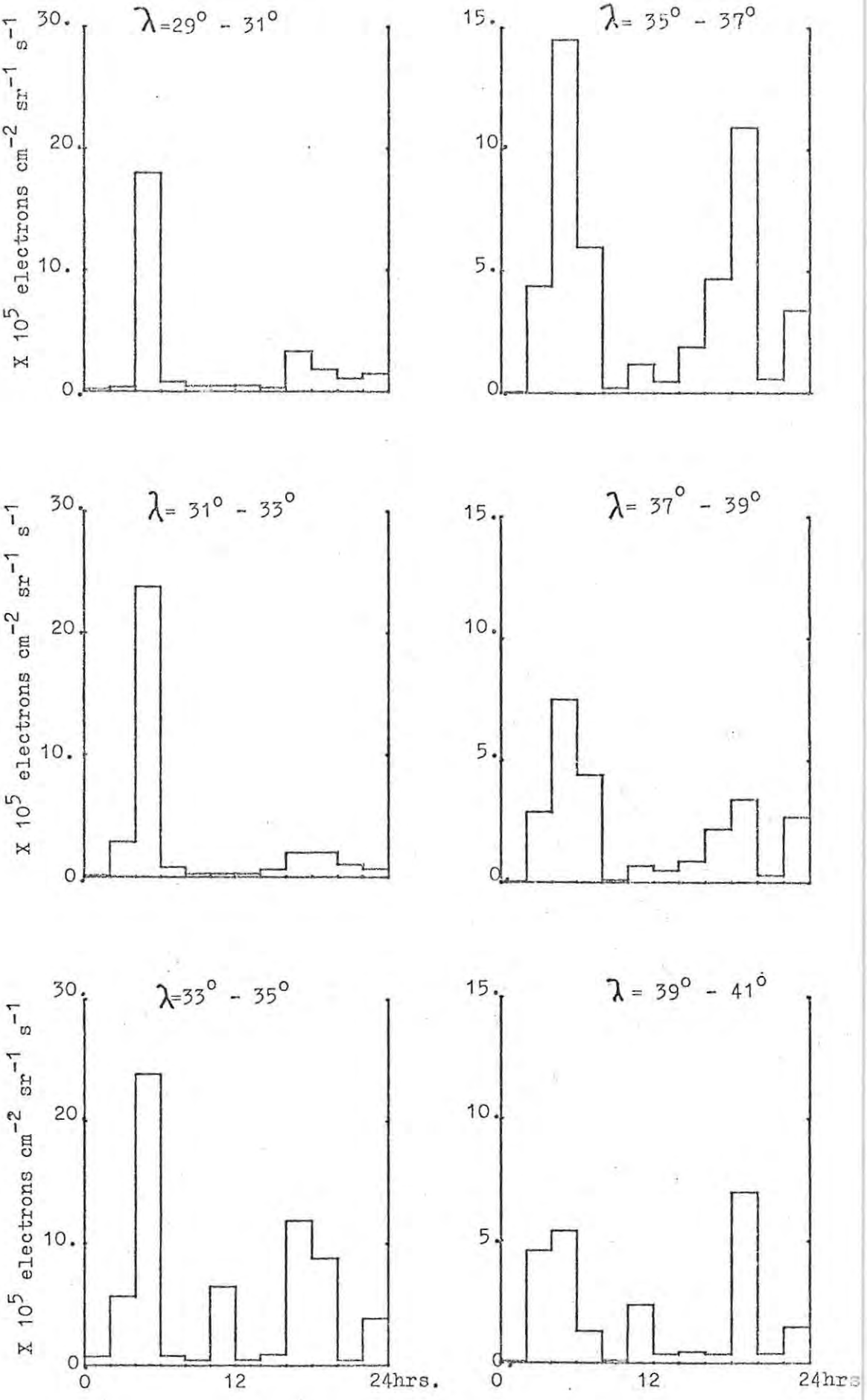
λ=29° - 31°
λ= 35° - 37°
λ= 31° - 33°
λ= 37° - 39°
λ=33° - 35°
λ = 39° - 41°
X 10^5 electrons cm^-2 sr^-1 s^-1
30.
20.
10.
0
15.
10.
5.
0
0
12
24hrs.

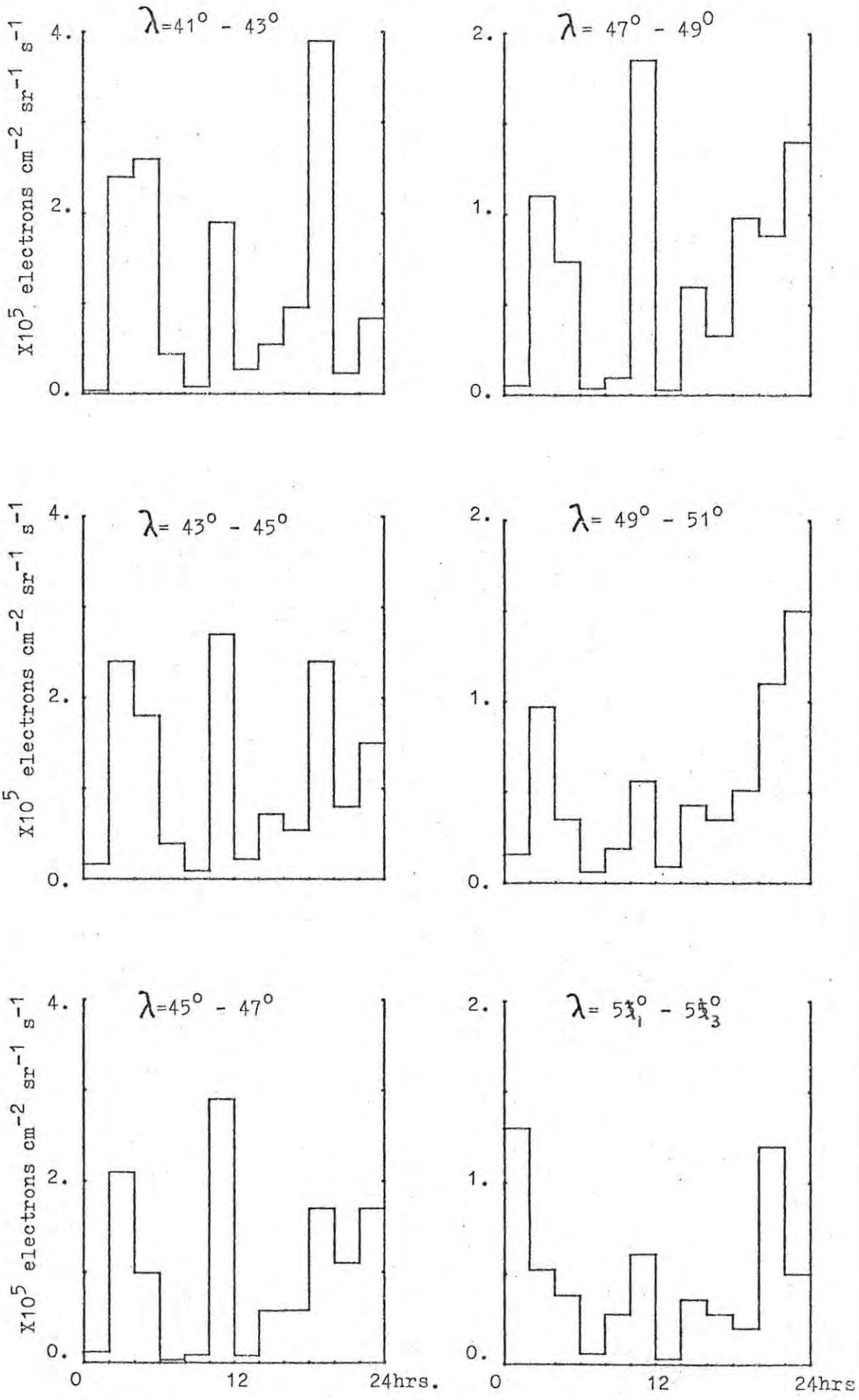
λ=41° - 43°
λ= 47° - 49°
λ= 43° - 45°
λ= 49° - 51°
λ=45° - 47°
λ= 51° - 53°
X10^5 electrons cm^-2 sr^-1 s^-1
4.
2.
0.
1.
0
12
24hrs.

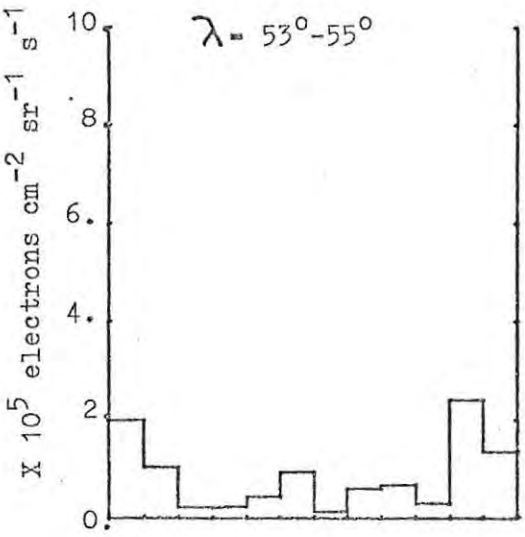
λ = 53°-55°
X 10^5 electrons cm^-2 sr^-1 s^-1
0
2
4
6
8
10

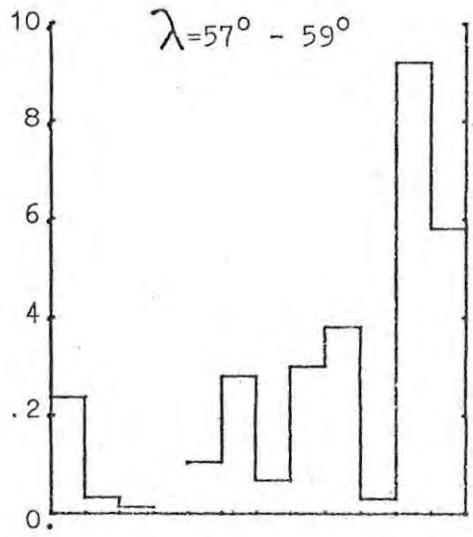
λ=57° - 59°
0
2
4
6
8
10

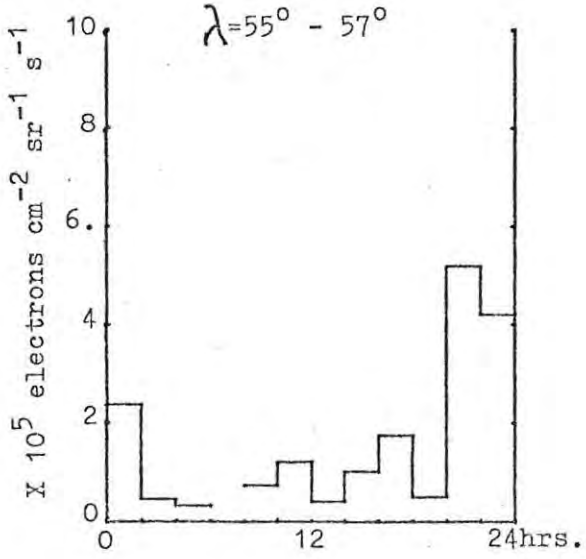
λ=55° - 57°
X 10^5 electrons cm^-2 sr^-1 s^-1
0
2
4
6
8
10
0
12
24hrs.

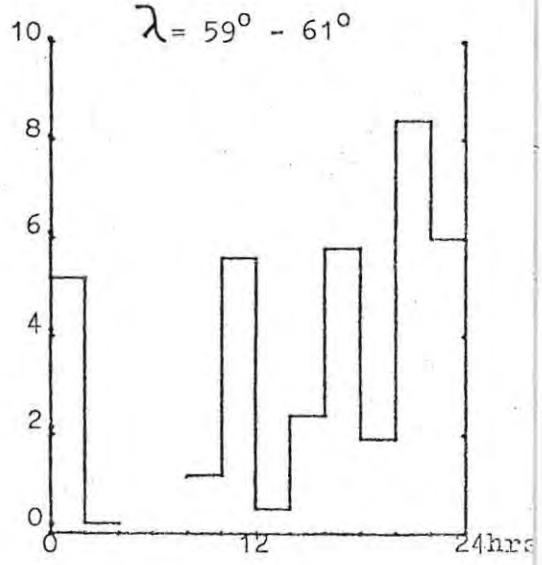
λ= 59° - 61°
0
2
4
6
8
10
0
12
24hrs

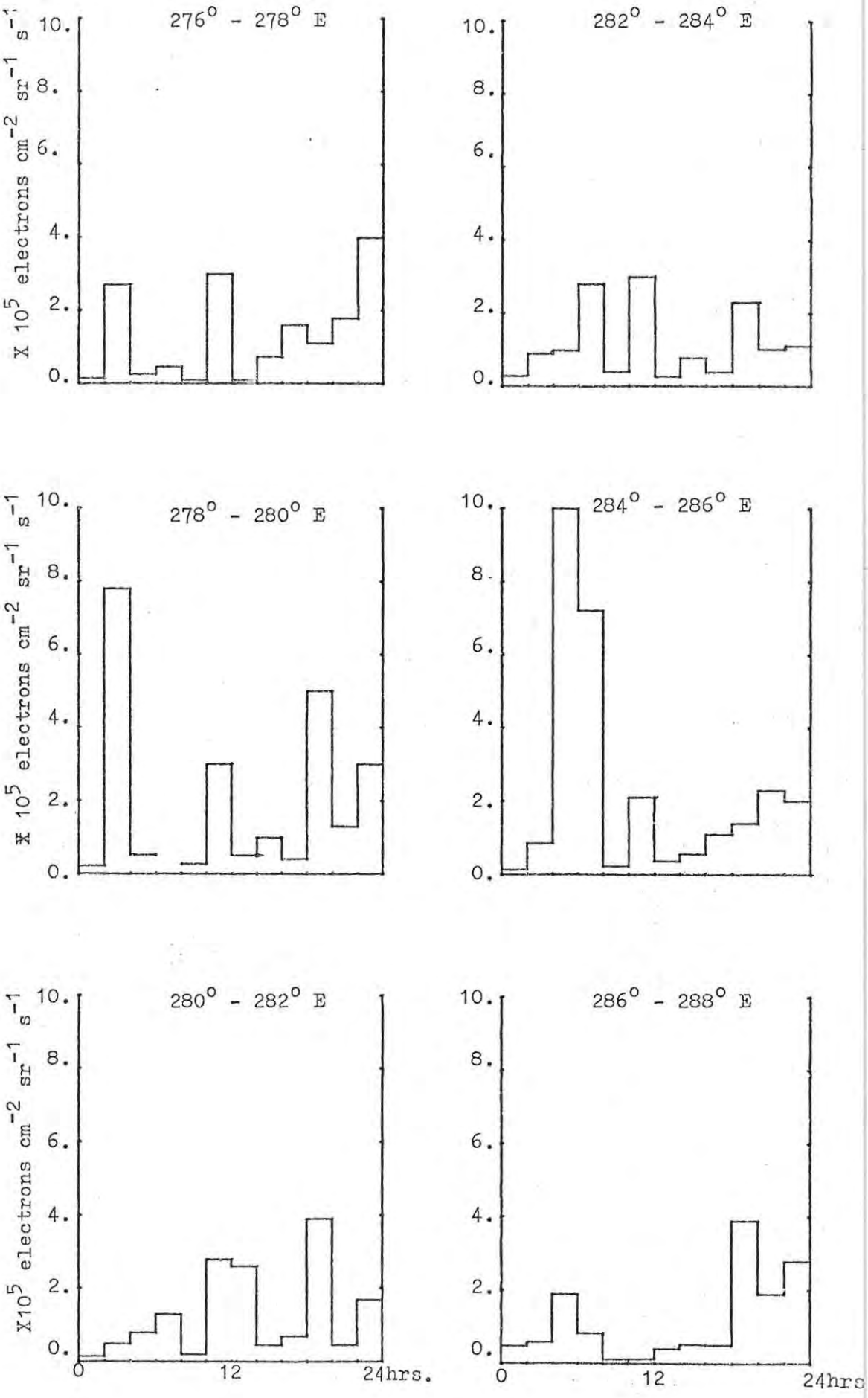
276° - 278° E
282° - 284° E
278° - 280° E
284° - 286° E
280° - 282° E
286° - 288° E
X 10^5 electrons cm^-2 sr^-1 s^-1
0.
2.
4.
6.
8.
10.
0
12
24hrs.

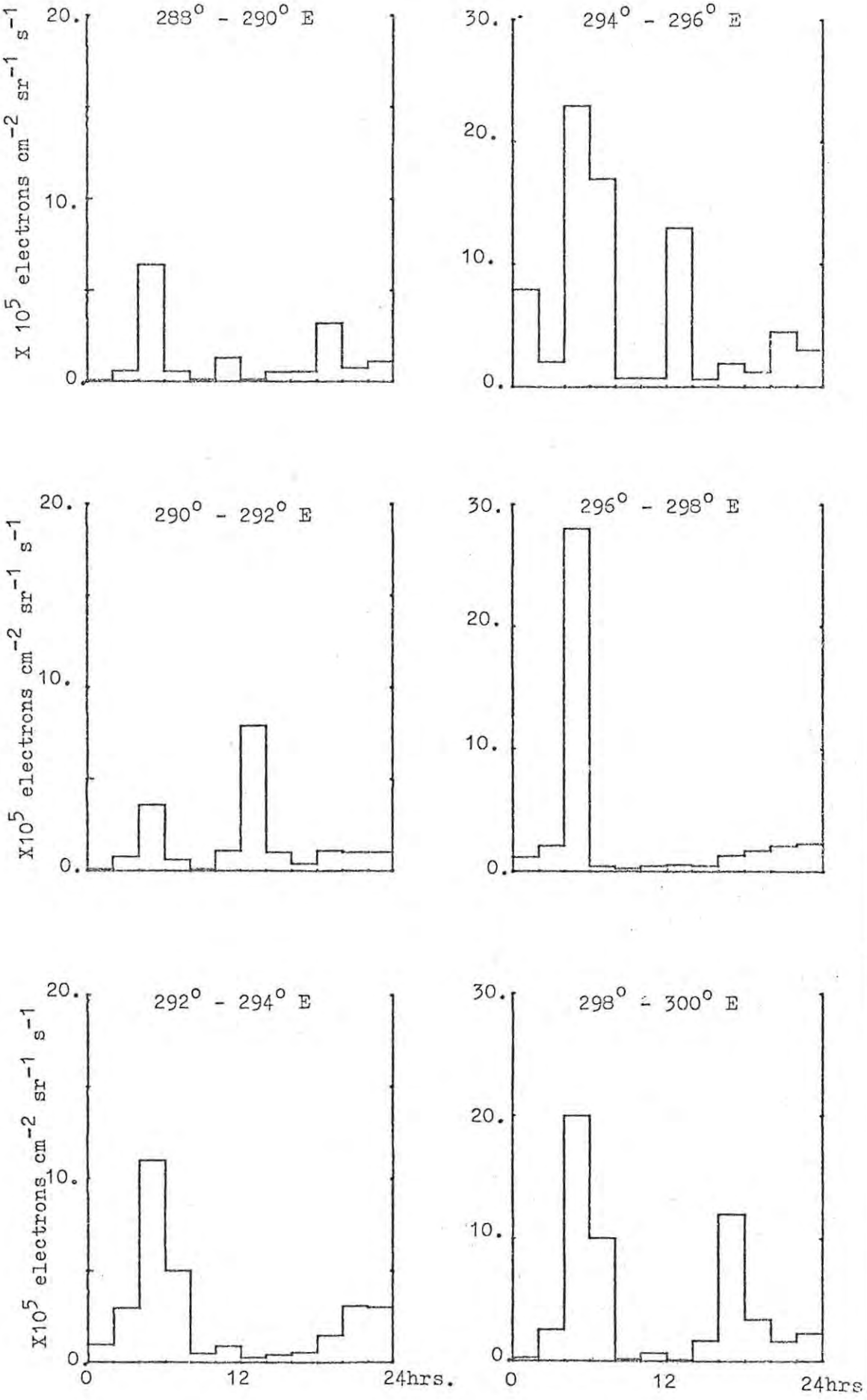
288° - 290° E
294° - 296° E
290° - 292° E
296° - 298° E
292° - 294° E
298° - 300° E
X 10^5 electrons cm^-2 sr^-1 s^-1
X10^5 electrons cm^-2 sr^-1 s^-1
20.
10.
0.
30.
0
12
24hrs.

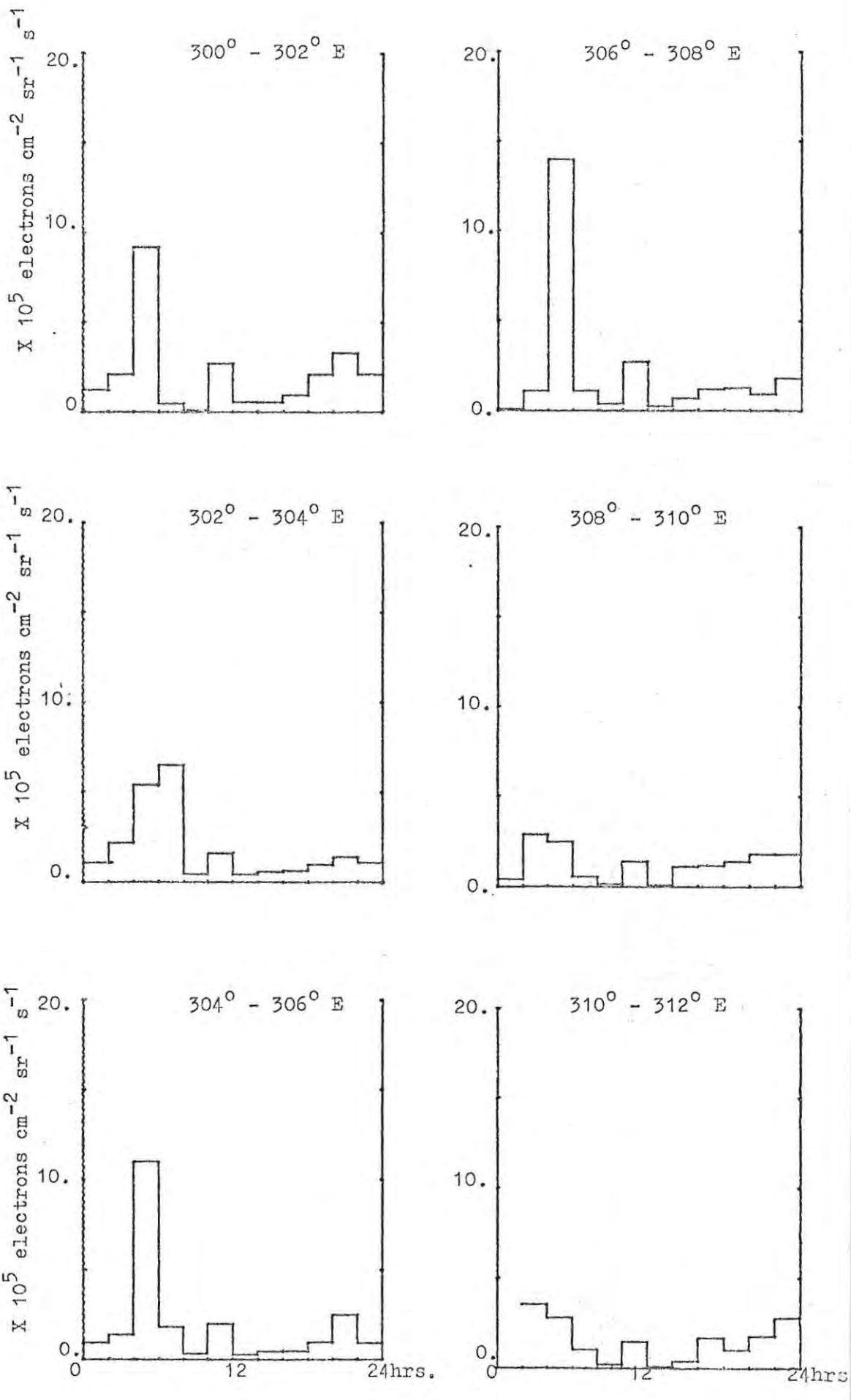
300° - 302° E
306° - 308° E
302° - 304° E
308° - 310° E
304° - 306° E
310° - 312° E
X 10^5 electrons cm^-2 sr^-1 s^-1
20.
10.
0.
0
12
24hrs.

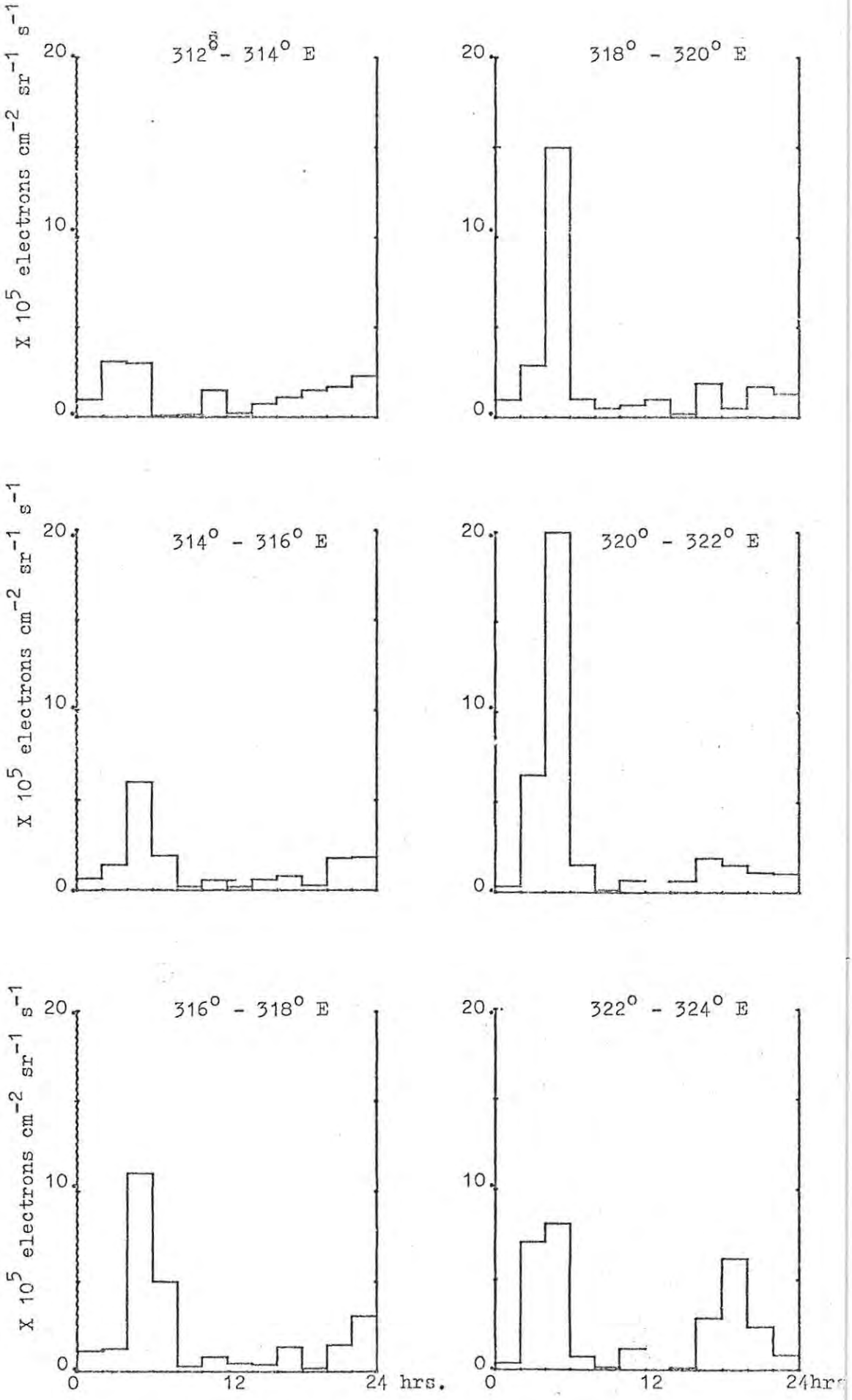
312° - 314° E
318° - 320° E
314° - 316° E
320° - 322° E
316° - 318° E
322° - 324° E
X 10^5 electrons cm^-2 sr^-1 s^-1
20
10
0
0
12
24 hrs.

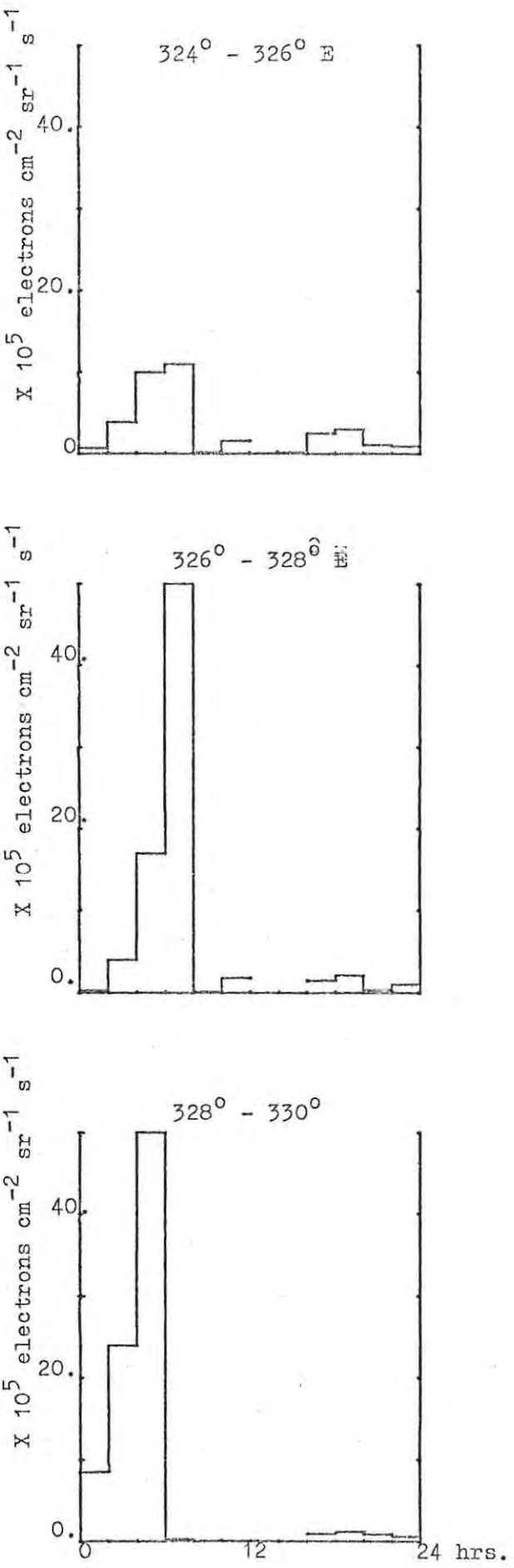
324° - 326° E
326° - 328° E
328° - 330°
X 10^5 electrons cm^-2 sr^-1 s^-1
0
20
40
0
12
24 hrs.

APPENDIX 6.

DIRECTIONAL FLUX DISTRIBUTION

IN

LONGITUDE AND INVARIANT LATITUDE

Within each of the 22 invariant latitude intervals we have sorted the records within each interval according to the longitude value of the records. 10^{o} wide ranges of longitude have been used:-

260^{o} East - 270^{o} East

270^{o} " - 280^{o} "

280^{o} " - 290^{o} "

290^{o} " - 300^{o} "

300^{o} " - 310^{o} "

310^{o} " - 320^{o} "

320^{o} " - 330^{o} "

330^{o} " - 340^{o} "

The median flux value of the records within each block has been plotted in the histogram.

The second set of histograms in this appendix contains the result of the invariant latitude sort that was performed on each of the 27 longitude intervals in turn. 5^{o} wide ranges of invariant latitude were used:-

$\lambda = 10^{o}$ - $\lambda = 15^{o}$

$= 15^{o}$ - $= 20^{o}$

$= 20^{o}$ - $= 25^{o}$

$= 25^{o}$ - $= 30^{o}$

$= 30^{o}$ - $= 35^{o}$

$= 35^{o}$ - $= 40^{o}$

$= 40^{o}$ - $= 45^{o}$

$= 45^{o}$ - $= 50^{o}$

$= 50^{o}$ - $= 55^{o}$

$= 55^{o}$ - $= 60^{o}$

$= 60^{o}$ - $= 65^{o}$

The flux scale changes between histograms to accommodate the large changes in directional fluxes between two spatial regions.

--- 0 ---

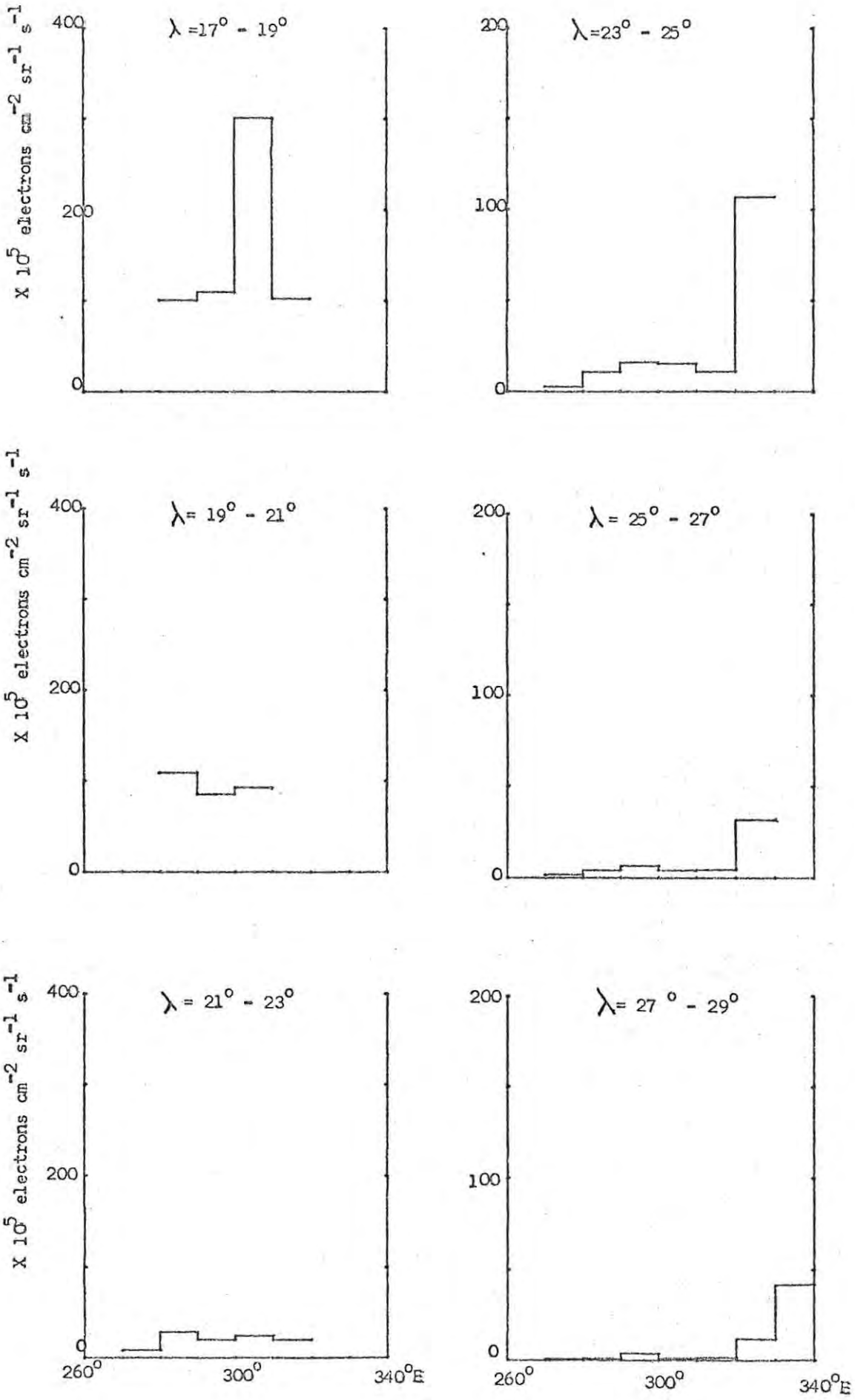
λ =17° - 19°
λ=23° - 25°
λ= 19° - 21°
λ= 25° - 27°
λ= 21° - 23°
λ= 27 ° - 29°
X 10^5 electrons cm^-2 sr^-1 s^-1
400
200
0
100
260°
300°
340°E

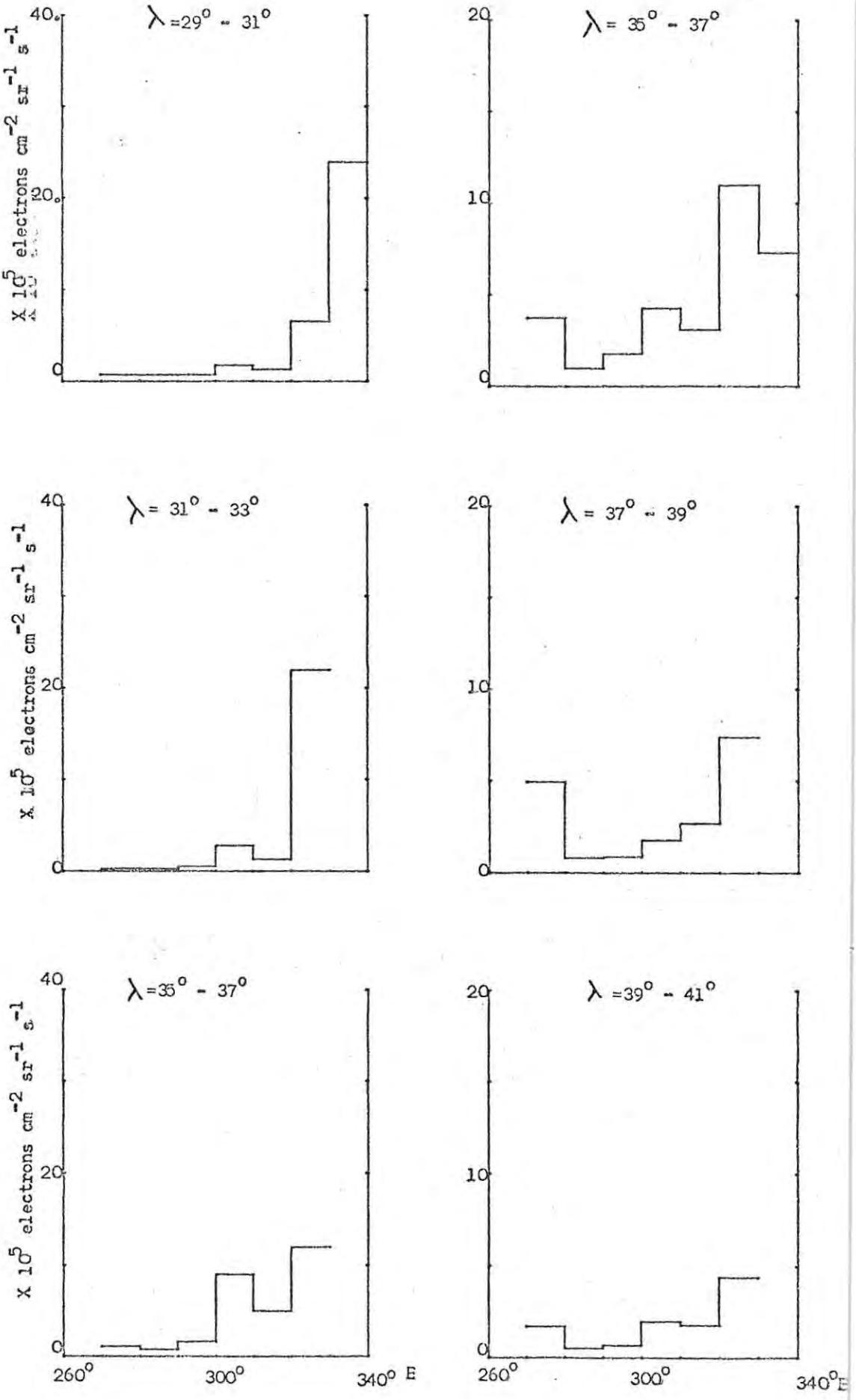
λ =29° - 31°
λ = 35° - 37°
λ = 31° - 33°
λ = 37° - 39°
λ =35° - 37°
λ =39° - 41°
X 10^5 electrons cm^-2 sr^-1 s^-1
40
20
0
10
260°
300°
340° E

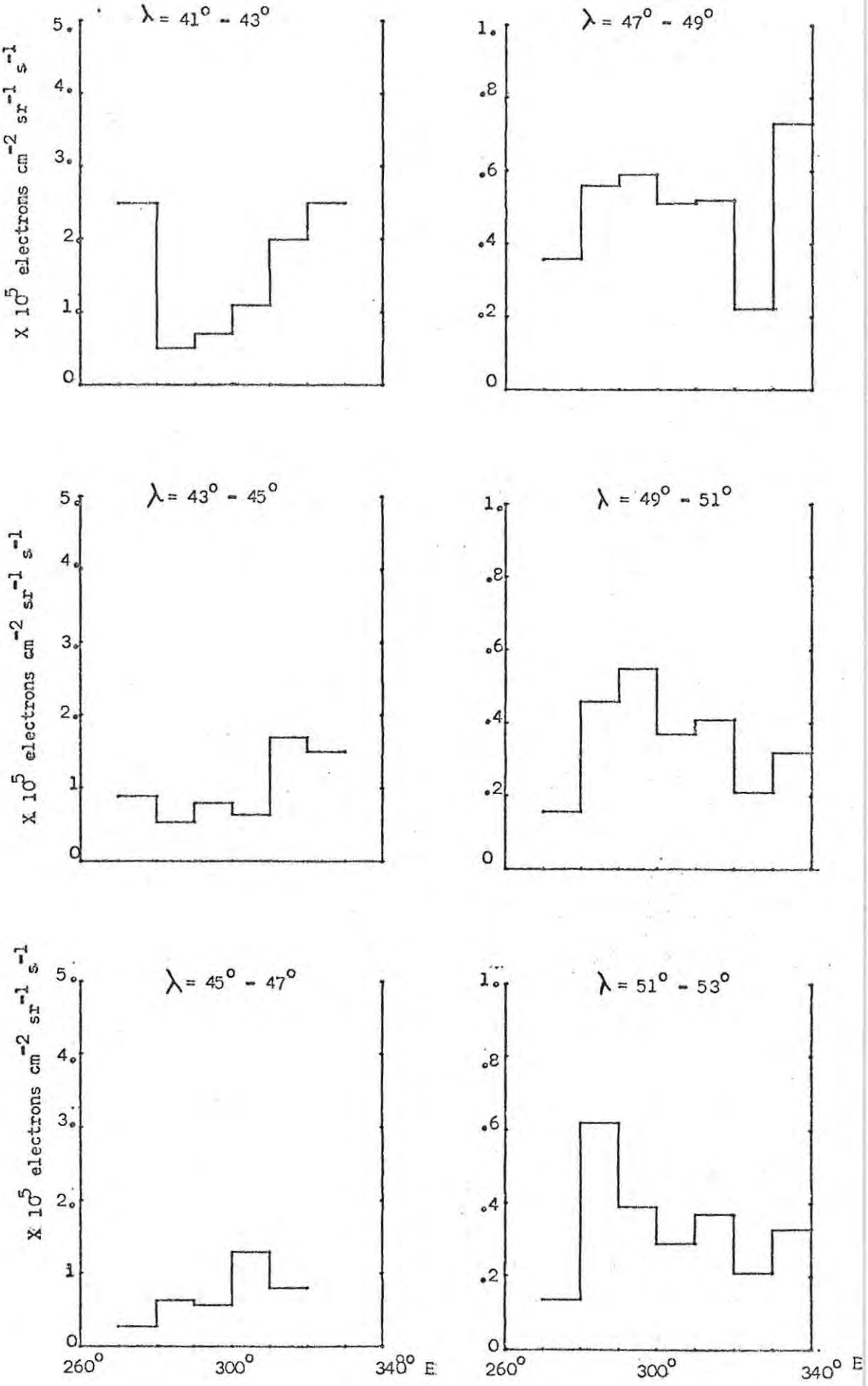
λ = 41° - 43°
λ = 47° - 49°
λ = 43° - 45°
λ = 49° - 51°
λ = 45° - 47°
λ = 51° - 53°
X 10^5 electrons cm^-2 sr^-1 s^-1
0
1
2
3
4
5
.2
.4
.6
.8
1.
260°
300°
340° E

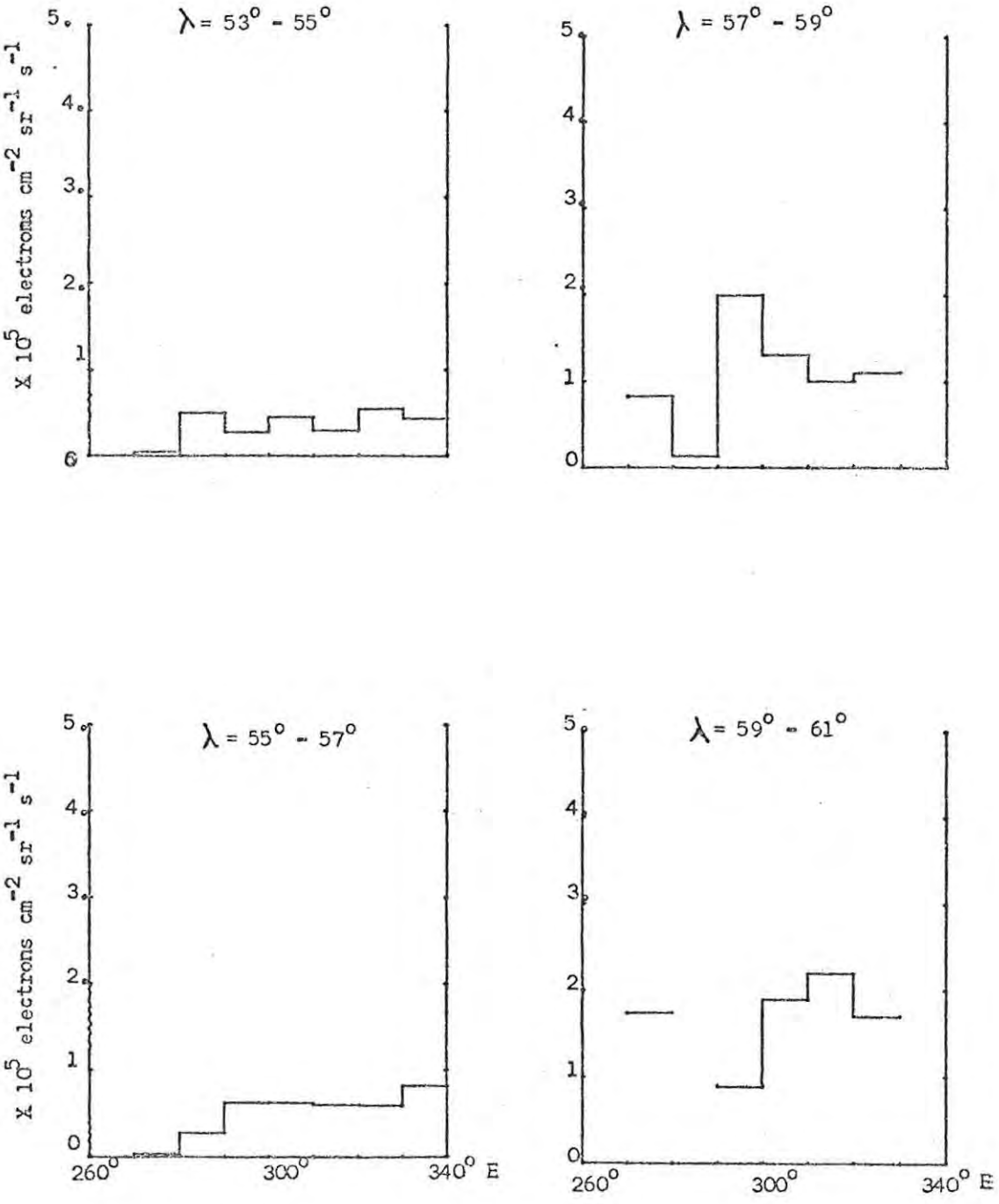
λ = 53° - 55°
λ = 57° - 59°
λ = 55° - 57°
λ = 59° - 61°
X 10^5 electrons cm^-2 sr^-1 s^-1
0
1
2
3
4
5
260°
300°
340° E

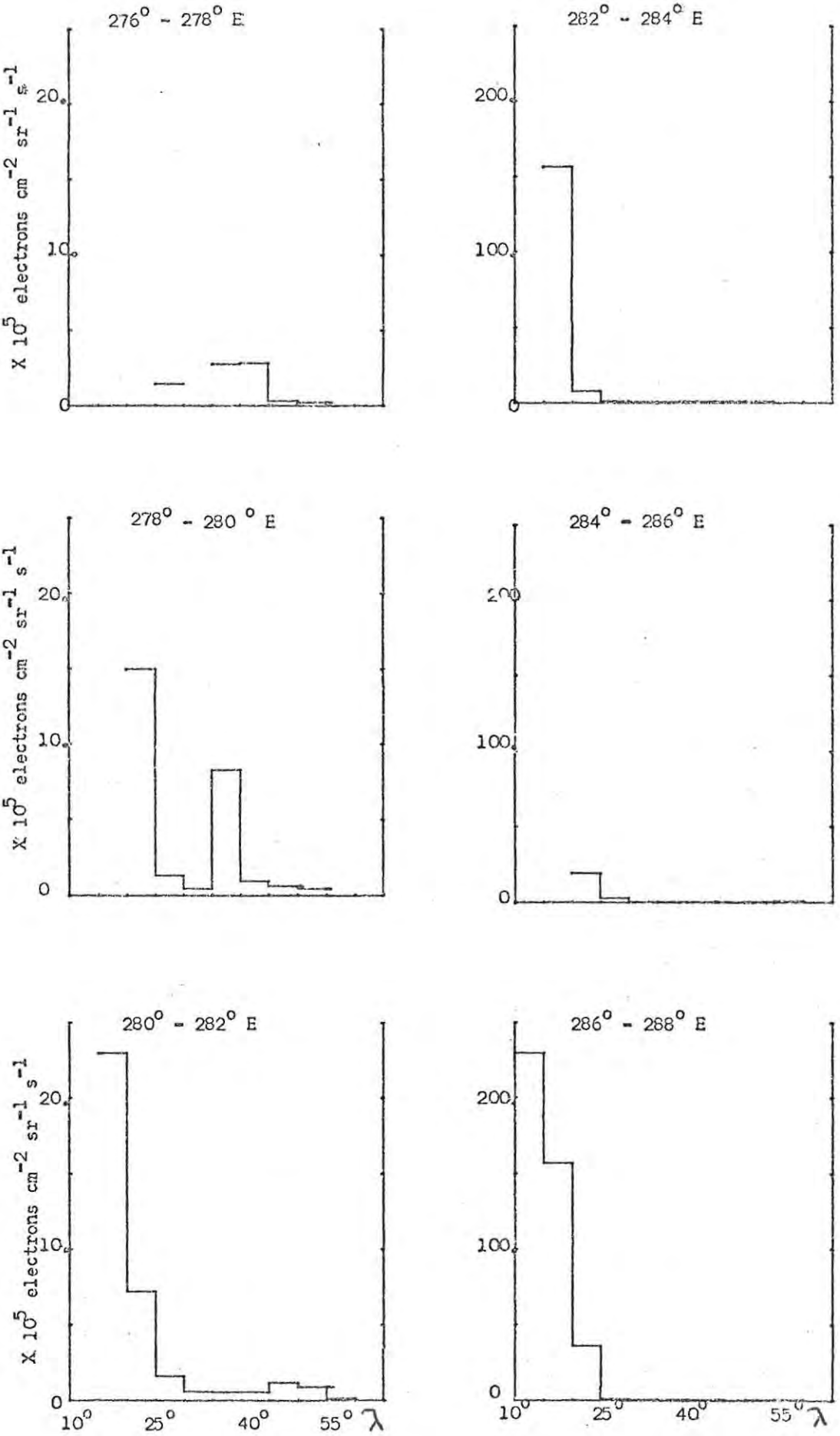
276° - 278° E
282° - 284° E
278° - 280 ° E
284° - 286° E
280° - 282° E
286° - 288° E
X 10^5 electrons cm^-2 sr^-1 s^-1
0
10
20
100
200
10°
25°
40°
55°
λ

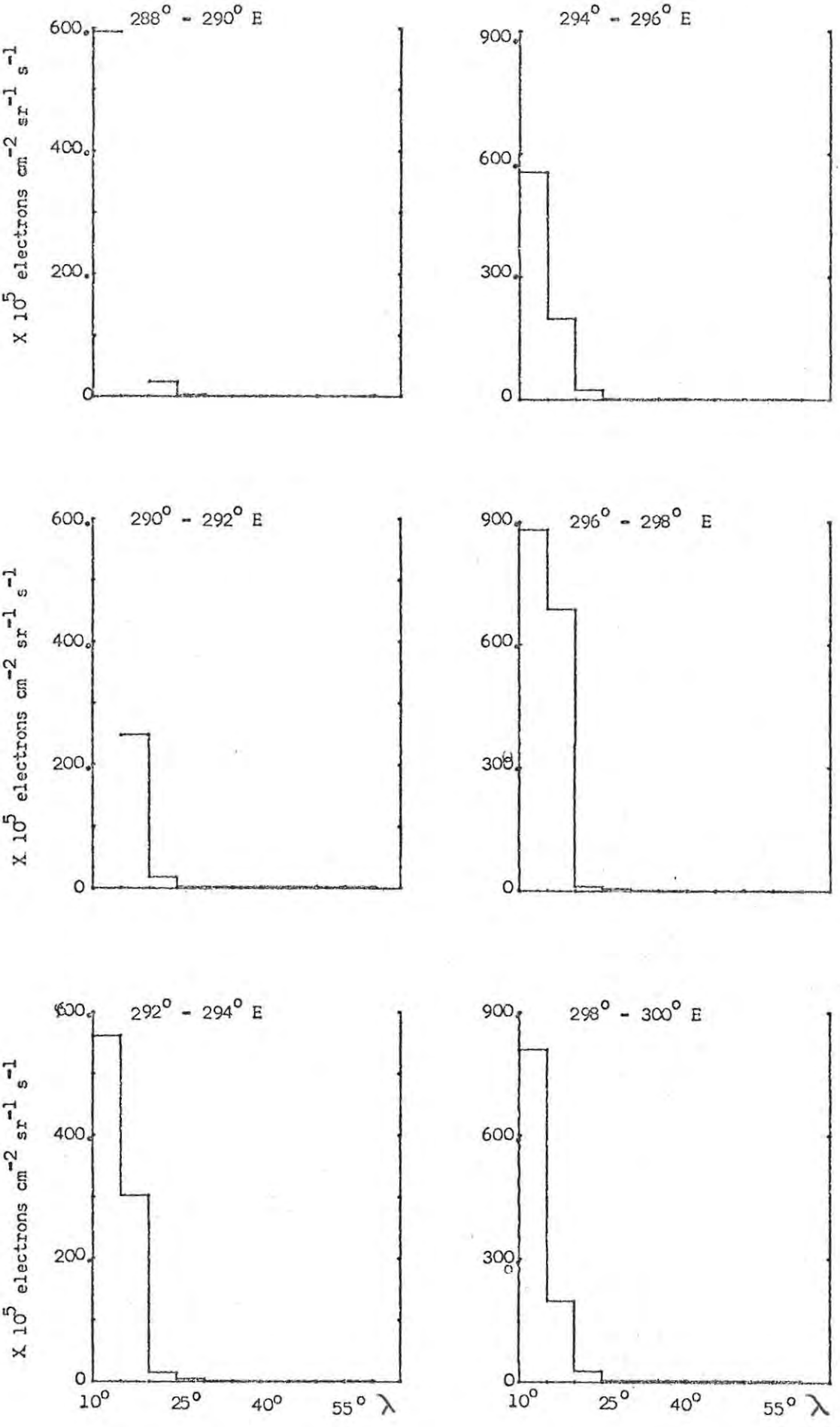
288° - 290° E
294° - 296° E
290° - 292° E
296° - 298° E
292° - 294° E
298° - 300° E
X 10^5 electrons cm^-2 sr^-1 s^-1
600
400
200
0
900
300
10°
25°
40°
55° λ

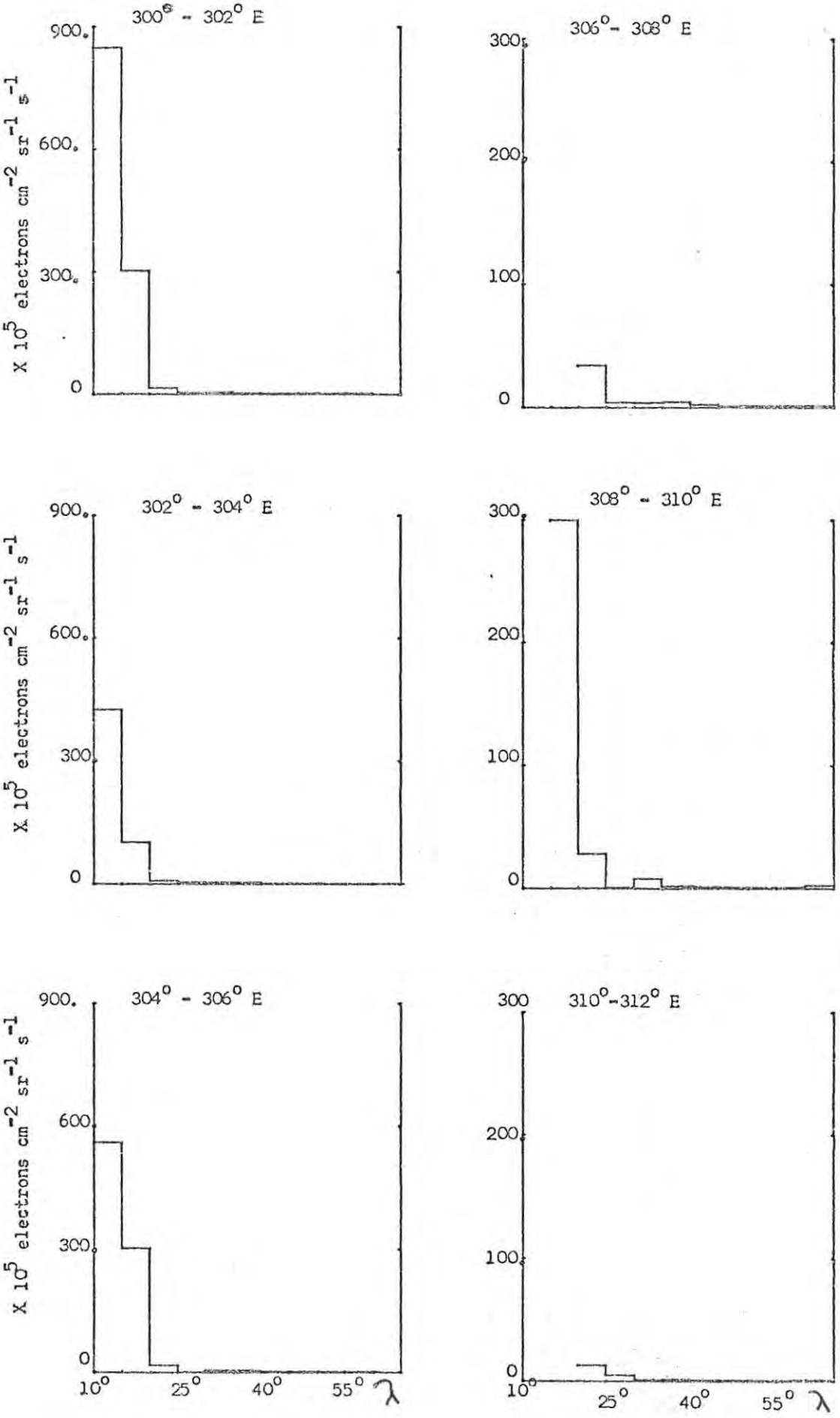
300° - 302° E
306° - 308° E
302° - 304° E
308° - 310° E
304° - 306° E
310° - 312° E
X 10^5 electrons cm^-2 sr^-1 s^-1
900.
600.
300.
0
200
100
10°
25°
40°
55°
λ

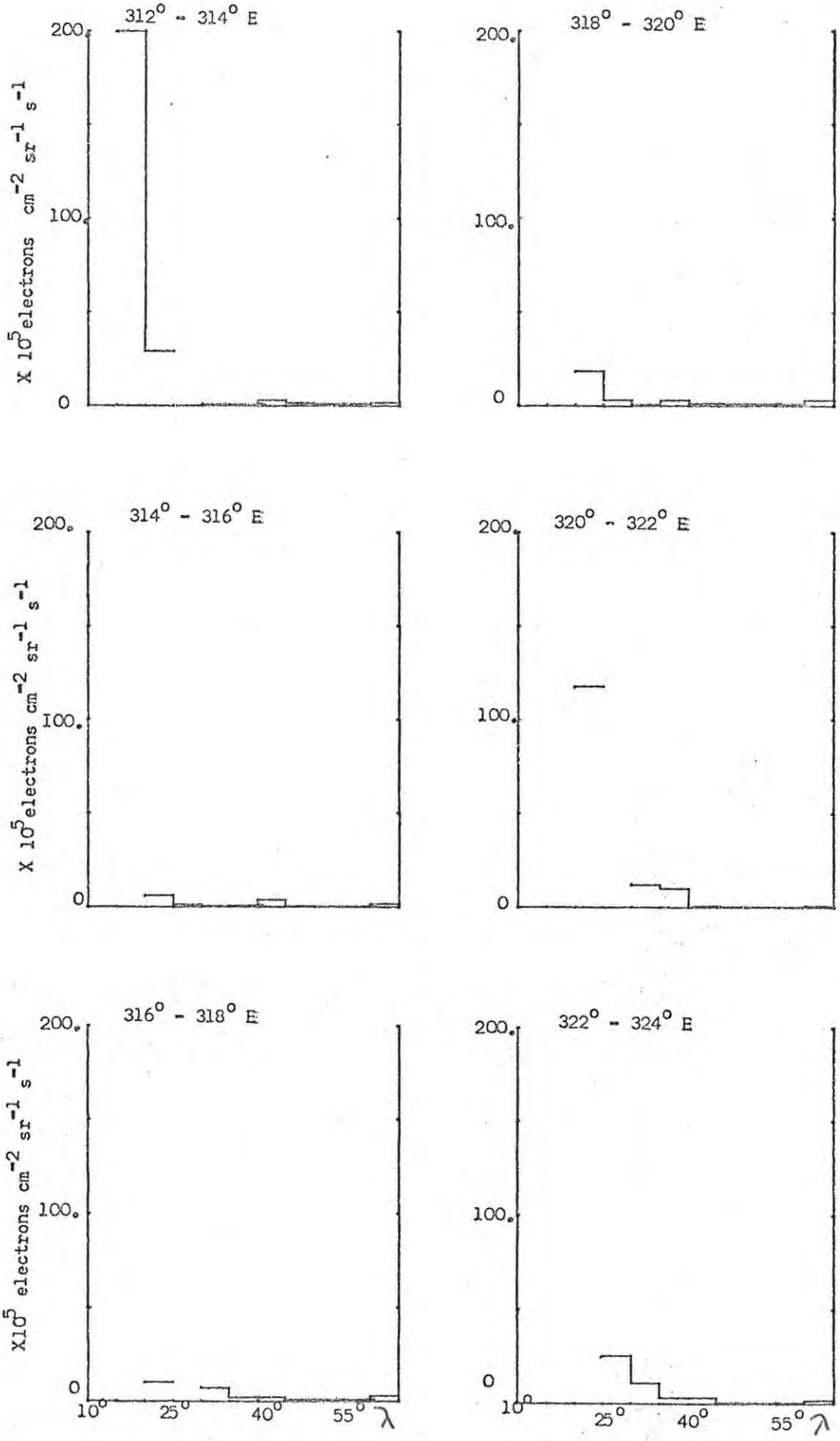
312° - 314° E
318° - 320° E
314° - 316° E
320° - 322° E
316° - 318° E
322° - 324° E
200.
100.
0
X 10^5 electrons cm^-2 sr^-1 s^-1
X10^5 electrons cm^-2 sr^-1 s^-1
10°
25°
40°
55°
λ

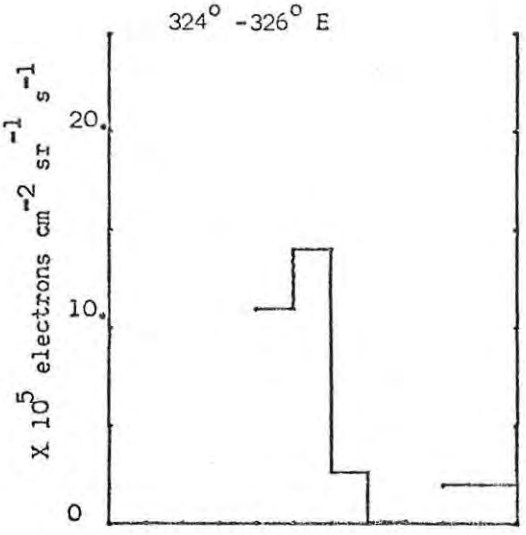
324° -326° E
X 10^5 electrons cm^-2 sr^-1 s^-1
20.
10.
0

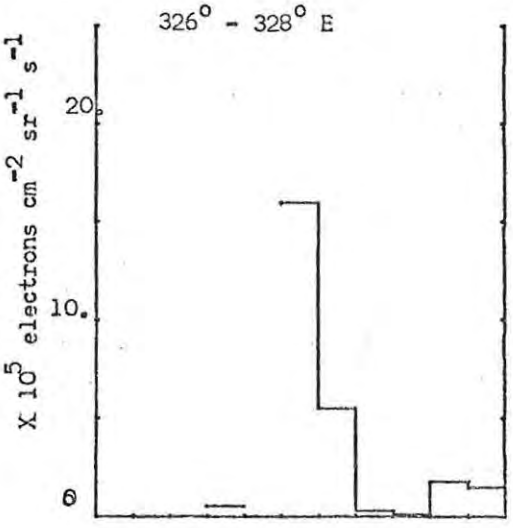
326° - 328° E
X 10^5 electrons cm^-2 sr^-1 s^-1
20.
10.
0

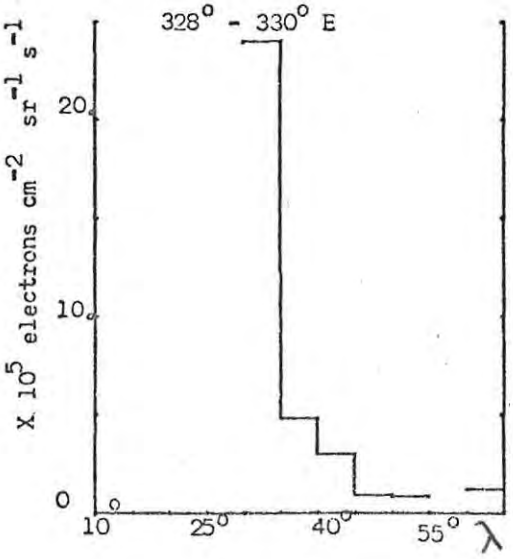
328° - 330° E
X 10^5 electrons cm^-2 sr^-1 s^-1
20.
10.
0
10°
25°
40°
55°
λ

APPENDIX 7

A GRAPH OF L VERSUS λ AT 1000 KM IN THE SOUTH ATLANTIC REGION

We present a curve of values of L versus λ, at 1000 km in the South Atlantic region. The points plotted in this graph were obtained by averaging the L values of the records used in producing the λ grid in the map of section 2.2.

--- 0 ---

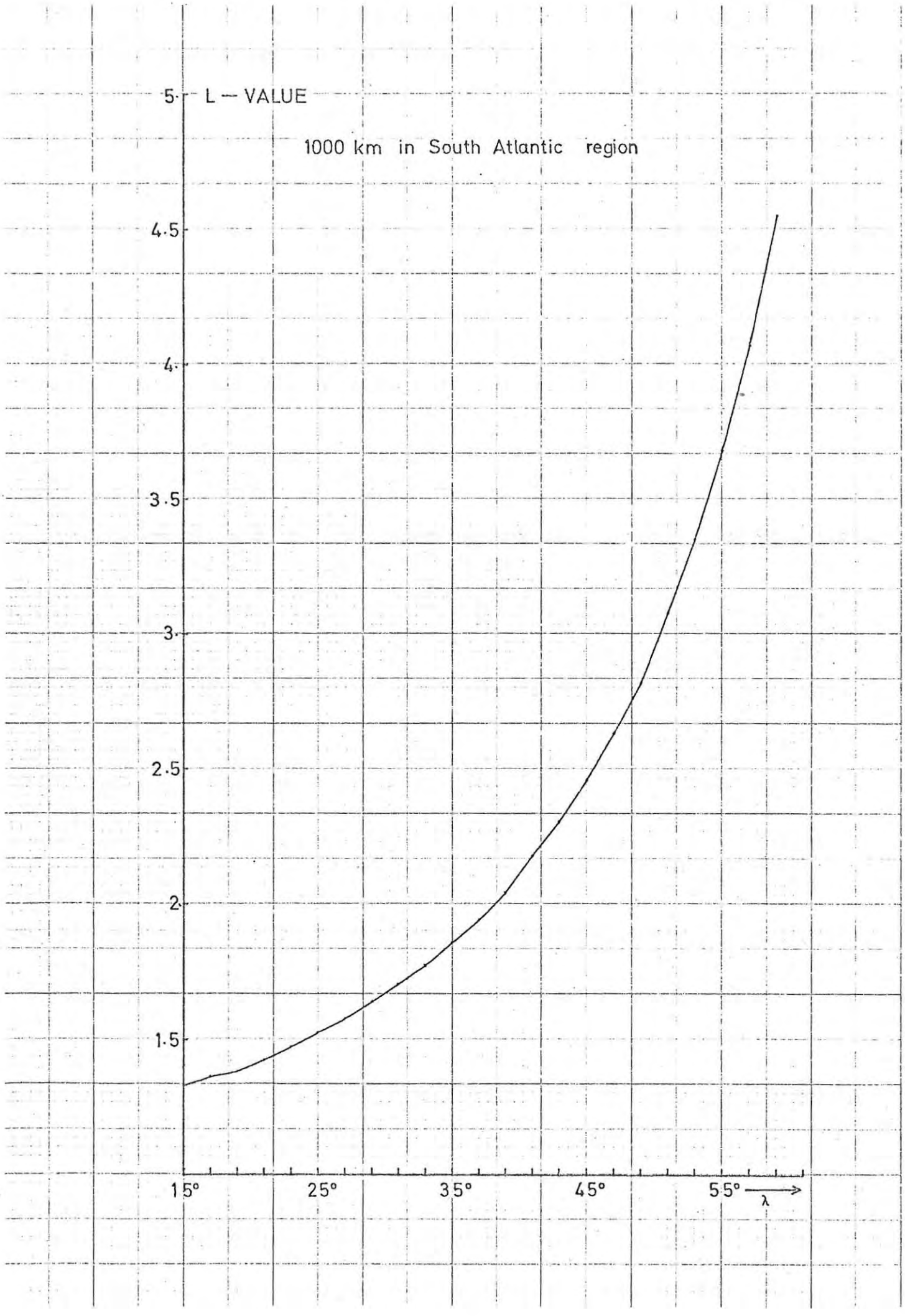
L — VALUE
1000 km in South Atlantic region
5
4.5
4
3.5
3
2.5
2
1.5
15°
25°
35°
45°
55°
λ

REFERENCES

1. Bailey, D.K., Some quantitative aspects of electron precipitation in and near the auroral zone, Rev. Geophys., 6, 289 - 346, 1968.

2. Cumming, W.D., La Quey, R.E., O'Brien, B.J. and Walt, M, Rocket-borne measurements of particle fluxes and auroral light, J. Geophys. Res., 71, 1399 - 1405, 1966.

3. Dungey, J.W., Loss of Van Allen electrons due to whistlers, Planetary Space Sci., 11, 591 - 595, 1963.

4. Frank, L.A., Van Allen, J.A. and Craven, J.D., Large diurnal variations of geomagnetically trapped and of precipitated electrons observed at low altitudes, J. Geophys. Res., 69, 3155 - 3167, 1964.

5. Frank, L.A., A survey of electrons E $>$ 40 keV beyond 6 Earth radii with Explorer XIV, J. Geophys. Res., 70, 1593 - 1626, 1965.

6. Frank, L.A., Relationship of the plasma sheet, ring current, trapping boundary, and plasmapause near the magnetic equator and local midnight, J. Geophys. Res., 76, 2265 - 2275, 1971.

7. Frank, L.A. and Ackerson, K.L., Observations of charged particle precipitation into the auroral zone, J. Geophys. Res., 76, 3612 - 3643, 1971.

8. Frank, L.A. and Ackerson, K.L., Local-time survey of plasma at low altitudes over the auroral zones, J. Geophys. Res., 77, 4116 - 4127, 1972.

9. Gledhill, J.A. and Torr, D.G., Ionospheric effects of precipitated electrons in the South radiation anomaly, Proc. VI th Internat. Symp. on Space Sci., Mar del Plata, 222 - 229, 1966.

10. Hess, W.N., The radiation belt and magnetosphere, Blaisdell, 1968.

11. Huitson, A., The analysis of variance, Charles Griffin & Co., 1966.

12. Kennel, C.F. and Petschek, H.E., Limit on stably trapped particle fluxes, J. Geophys. Res., 71, 1 - 28, 1966.

13. McDiarmid, I.B., Burrows, J.R., Budzinski, E.E: and Rose, D.C., Satellite Measurements in the "Starfish" artificial radiation zone, Can. J. Phys., 41, 1332 - 1345, 1963, a.

14. McDiarmid, I.B., Burrows, J.R., Budzinski, E.E. and Wilson, Margaret D., Some average properties of the outer radiation zone at 1000 km, Can. J. phys., 41, 2064 - 2079, 1963, b.

15. McDiarmid, I.B. and Burrows, J.R., Local time asymmetries in the high latitude boundary of the outer radiation zone for different electron energies, Can. J. phys., 46, 49 - 57, 1968.

16. Mead, G.D. and Beard, D.B., Shape of the geomagnetic field solar wind boundary, J. Geophys. Res., 69, 1169 - 1179, 1964.

17. Mead, G.D., Deformation of the geomagnetic field by the solar wind, J. Geophys. Res., 69, 1181 - 1195, 1964.

18. Northrop, T.G., The Adiabatic motion of charged particles, Interscience, 1963.

19. O'Brien, B.J., Direct observations of dumping of electrons at 1000 - kilometer altitude and high latitudes, J. Geophys. Res., 67, 1227 - 1233, 1962, a.

20. O'Brien, B.J., Lifetimes of outer-zone electrons and their precipitation into the atmosphere, J. Geophys Res., 67, 3687 - 3706, 1962, b.

21. O'Brien, B.J., A large diurnal variation of the geomagnetically trapped radiation, J. Geophys. Res., 68, 989 - 995, 1963.

22. O'Brien, B.J., High latitude geophysical studies with satellite Injun 3, J. Geophys. Res., 69, 13 - 43, 1964.

23. Paulikas, G.A. and Freden, S.C., Precipitation of energetic electrons into the atmosphere, J. Geophys. Res., 69, 1239 - 1249, 1964.

24. Roederer, J.G., Hess, W.N. and Stassinopoulos, E.G, Conjugate intersects to selected geophysical stations, Goddard Space Flight Center publication X - 642 - 65 - 182, 1965.

25. Roederer, J.G., Southern Hemisphere Anomalies, Proc. VI th Internat. Symp. on Space Sci., Mar del Plata, 117 - 129, 1966.

26. Roederer, J.G., Dynamics of geomagnetically trapped radiation, Springer-Verlag, Berlin, 1970.

27. Roederer, J.G., Geomagnetic field distortions and their effects on radiation belt particles, publication of Department of Physics, University of Denver, 1971.

28. Rose, D.C., The Alouette satellite results, Radiation trapped in the Earth's magnetic field, ed. McCormac, B.M., 191 - 214, 1966.

29. Sutcliffe, P.R., Resume of Magnetic Co-ordinate Systems, Internal Report M71 - 1, Department of Physics, Potchefstroom University for C.H.E., 1971.

30. Thomas, J.O. and Andrews, M.K., Transpolar exospheric plasma, J. Geophys. Res., 73, 7407 - 7417, 1968.

31. Tulinov, V.F., Shibaeva, L.V. and Jakovlev, S.G., The ionization of the lower ionosphere under the influence of corpuscular radiation, Proc. IX th Internat Symp. on Space Sci., Tokyo, 231 - 236, 1969.

32. Van Allen, J.A., Mc Ilwain, C.E. and Ludwig, G H., Radiation observations with Satellite 1958€, J. Geophys. Res., 64, 271 - 286, 1959.

33. Van Allen, J.A., Particle description of the magnetosphere, Physics of the magnetosphere, ed. Carovillano, R.L., 147 - 217, 1968.

34. West, H.I., Some observations of the trapped electrons produced by the Russian high-altitude nuclear detonation of October 28, 1962, Radiation trapped in the Earth's magnetic field, ed. McCormac, B.M., 634 - 662, 1966.

35. Data Catalog of Satellite Experiments, Goddard Space Flight Center Publication 71-20, 1971.

--- 0 ---